Spitting image

Image based prevention and measurement of radiation-induced xerostomia

Eleftheria Astreinidou

Colofon:
This text was set using the freely available LaTeX 2_ε typesetting and text formatting system. The line drawings were made using the freely available METAPOST program.

Cover design by Nina Petropoulea
Model: Orpheus Manaris
The background of the cover has been inspired by the music CD of
Manos Hatzidakis: *Dance with my shadow*, Mercury/ PolyGram Records, 1998

Η διδακτορική διατριβή με τίτλο:
"Spitting Image". Βασισμένες στην απεικόνηση πρόληψη και μέτρηση της,
προκαλούμενης από ακτινοβολία, χεροστομίας.
συντάχθηκε από την Ελευθερία Αστρεινίδου,
στην Πανεπιστημιακή κλινική της Ουτρέχτης, στην Ολλανδία.
Η Ελευθερία γεννήθηκε 18 Νοεμβρίου 1970 στην Θεσσαλονίκη, Ελλάδα.

ISBN-10: 90-393-4231-8
ISBN-13: 978-90-393-4231-2
Druk: PrintPartners Ipskamp, Enschede

Spitting Image

Image based prevention and measurement of radiation-induced xerostomia

"Spitting Image"
Beeldgeleide preventie en meting van door stralings geïnduceerde xerostomie
(met een samenvatting in het Nederlands)

Proefschrift ter verkrijging van de graad van doctor aan de
Universiteit Utrecht
op gezag van de Rector Magnificus, Prof. dr. W.H. Gispen
ingevolge het besluit van het College voor Promoties
in het openbaar te verdedigen
op dinsdag 30 mei 2006 des middags te 2:30 uur

door
Eleftheria Astreinidou
geboren op 18 november 1970 te Thessaloniki, Griekenland

promotor:	Prof. dr. ir. J.J.W. Lagendijk Faculteit der Geneeskunde, Universiteit Utrecht
co-promotor:	Dr. C.P.J. Raaijmakers Faculteit der Geneeskunde, Universiteit Utrecht

Het beschreven werk werd verricht op de afdeling Radiotherapie van het Universitair Medisch Centrum Utrecht, participerend in het Image Sciences Institute en de onderzoekschool voor biomedische beeldwetenschappen, ImagO, in een door de Nederlandse Kankerbestrijding gefinancierd project (UU 2001-2468). Deze uitgave is tot stand gekomen met financiële steun van de Nederlandse Kankerbestrijding, het ImagO en Philips Medical Systems BV, Best, the Netherlands.

στους γονείς μου
και
στον παππού μου Θανάση
που είναι πάντα παρέα μου

to my parents
and
to my grandfather Thanasi
who will always be with me

ITHAKA

As you set out for Ithaka
hope the voyage is long,
full of adventure, full of discovery.
Laistrygonians and Cyclops,
angry Poseidon - don't be afraid of them:
you'll never find such things on your way
as long as you keep your thoughts raised high,
as long as wistful emotions
stir your spirit and body.
Laistrygonians and Cyclops,
wild Poseidon - you won't encounter them
unless they dwell your soul,
unless your soul raises them up in front of you.

Hope the voyage is a long one.
May there be many summer mornings when,
with what pleasure and joy, you come into harbors seen for the first time;
may you stop at Phoenician
to buy fine things,
mother of pearl and coral, amber and ebony,
sensual perfume of every kind -
as many sensual perfumes as you can;
and may you visit many Egyptian cities
to gather stores of wisdom from their scholars.

Keep Ithaka always in your thoughts.
Your arrival is your destiny.
But don't ever hurry the journey.
Better if it lasts for years,
so you are old by the time you reach the island,
enriched with what you have gained on the way,
not expecting Ithaka to make you rich.

Ithaka gave you the marvelous journey.
Without her you would have not sailed away.
She has nothing left to give you now.

And if you find her poor, Ithaka won't have fooled you.
This way, wise as you will have become, so full of experience,
you will have understood by then what these Ithakas mean.

K.Kavafis[1]

1. K.Kavafis (1863-1933) a modern poet who lived about hundred years before his age. He was writing directly in modern greek, whereas intellectuals at that time prefered the classical greek language and he focused on critising his own personal passions and weeknesses in a time where everyone was writing lyrics and romance. He is known for his briliant use of historical imagery and his aesthetic perfectionism. He wrote ITHAKA in 1911.

Contents

Chapter 1

General introduction

1.1 Salivary function

In this paragraph some background information is given to highlight the importance of saliva in our lives and to describe briefly how salivary function is currently measured. Consider this paragraph as a prologue to the main subject of this thesis, radiation-induced xerostomia.

1.1.1 Saliva and saliva production

"*Saliva doesn't have the drama of blood, it doesn't have the integrity of sweat and it doesn't have the emotional appeal of tears*" [1]. In contrast to blood, sweat and tears, saliva attracts our attention only when it is not there! The reason is obvious; the perception that saliva is simply water, constantly secreted without any effort, does not make it look very special.
It might be true that saliva is mostly water, 99% of it to be precise, but that last 1%, a combination of proteins, lipids, amino acids and electrolytes, is of such complexity that makes saliva a unique secretory product with an irreplaceable role in a person's well being (Cooper *et al.*, 1995).
Daily normal functions such as mastication of food, swallowing and digesting even talking would have been almost impossible without saliva. The hedonics of tasting and the perception of all flavors would be severely impaired. Saliva moistens the oral cavity, protects the mucosa and teeth and plays an important antibacterial and anti-fungal role. Furthermore, saliva controls the oral pH and protects against demineralization.Therefore lack of saliva predisposes a person to oral disease and discomfort and consequently to deteriorated quality of life (QoL) (Stuchell and Mandel, 1988; Mandel, 2002; Pedersen *et al.*, 2002; Chambers *et al.*, 2004).
The average daily output of saliva in healthy humans is about 1 to 1.5 L, most of

1. quote from Dr Irwin Mandel, professor emeritus at the school of Dental and Oral surgery at Columbia University, USA

which is produced during meals (Lavelle, 1988). In simple words, saliva formation begins in the acinar cells of the salivary glands and then it flows through the minor ducts to finally be secreted by the excretory ducts into the oral cavity (De Rossi, 1987). About 90% of saliva is produced by the three pairs of the major salivary glands, parotid, submandibular and sublingual glands. Only the first two have an elaborate network of functional subunits and a branching network of draining salivary ducts with a single dominant excretory duct (Figure 1.1). It is notable that during exogenous stimulation parotid glands are responsible for more than 60% of the saliva production while in unstimulated state that percentage is due to the submandibular glands. The rest 10% of the total daily salivary flow is produced by the minor salivary glands, which are distributed allover the oral cavity and pharynx. The salivary flow from these glands is continuous throughout the day (Milne and Dawes, 1973; Lavelle, 1988).

1.1.2 What is xerostomia and how do we measure it

Decreased salivary flow due to reduced salivary function is called hyposalivation and the symptom of oral dryness is called xerostomia. Occasionally, xerostomia may be subjective, with no evidence of altered salivary flow. In that case it is associated with psychological factors such as stress (Bergdahl, 2000). The main causes of xerostomia due to hyposalivation include advert reactions to some drugs, systemic disorders, particularly Sjörgens syndrome (SS), chemotherapy, treatment of thyroid cancer with radioactive iodine and external radiation therapy (RT) of other head-and-neck tumors (Porter *et al.*, 2004; Rostron *et al.*, 2002). This last cause is the main topic of this thesis and will be treated extensively.
Measuring the severity of xerostomia is not a simple and straightforward task. A combination of subjective and objective methods is required for the best assessment of xerostomia with regard to the pattern of patient's complaints and the effects of various therapies on these complains (Vissink *et al.*, 2003).
Subjective methods include clinical examination and questionnaires that the patients themselves have to answer. Questions like *do you sip liquid to aid in swallowing dry food?*, or *Does the amount of saliva in your mouth seem to be too little, too much or you do not notice it?* are used to assess the patient's subjective rating of oral symptoms and the influence of those symptoms to patient's QoL (Jensen *et al.*, 2003; Duncan *et al.*, 2005).The European Organization for Research and Treatment of Cancer, EORTC, has developed a special questionnaire that is used as a scoring system for the radiation-induced morbidity of the salivary glands (Cox *et al.*, 1995).
Objective methods involve the measurement of stimulated and unstimulated or *rest secretion*, salivary flow rates (De Rossi, 1987). Unstimulated salivary flow measurements, thus without any gustatory stimulus, are time consuming because the saliva production rate is very low. The most common methods used to measure the salivary flow, especially in case of radiation-induced xerostomia, are saliva

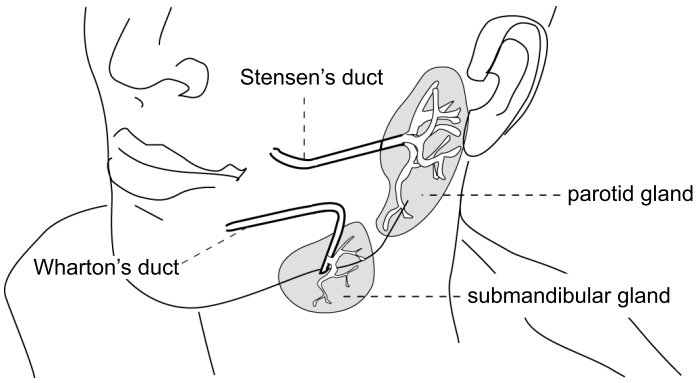

Figure 1.1: Schematic overview of the parotid gland and the submandibular gland. A branching network of draining salivary ducts converge from within the glands to a single dominant excretory duct that opens up into the oral cavity. The excretory duct of the parotid is called Stensen's duct and that of the submandibular Wharton's duct.

collection from the salivary glands after gustatory stimulation and salivary gland scintigraphy.

Stimulated salivary flow measurements

Stimulation is achieved by applying a very small quantity of citric acid solution to the mobile part of the tongue. Stimulation is repeated every minute and saliva is collected for a period of 10 minutes. The mouth of the patient is during the measurement open. Saliva is collected from both parotid glands simultaneously by placing collecting cups, most commonly the Lashley cups, over the intra-oral opening of the parotid ducts, Stensen's ducts (Figure 1.1) (Roesink *et al.*, 2001). Mixed submandibular and sublingual saliva is collected from the floor of the mouth by a pipette (Fox *et al.*, 1985). This method is quite straightforward in measuring saliva and evaluating the capacity of the salivary glands to produce saliva.
However, the time of the day and the time interval between the measurement and the last gustatory stimulus are influencing the amount of saliva produced. Even if salivary flow measurements are performed on different days under similar conditions a variability of about 30% has been observed on healthy persons (Blanco *et al.*, 2005).
This method is commonly used to measure radiation-induced xerostomia. Salivary flow measurement are performed to patients before the initiation of the radiation treatment and after the end of the treatment at various time intervals, such as

6 weeks, 6 months and 1 year. It is commonly used to regard reduction of salivary flow to <25% of the before radiotherapy value as an endpoint for radiation-induced xerostomia, or grade 4 toxicity according to RTOG/EORTC scoring system (Eisbruch *et al.*, 2001b; Roesink *et al.*, 2001).

Radioisotope study of the salivary glands

Another method measuring the salivary function is scintigraphic imaging of the head-and-neck and subsequently of the salivary glands using a gamma camera. The patient is lying in supine position and the camera is positioned for an anterior head-and-neck projection. Dynamic image acquisition starts immediately after intravenous injection of ^{99m}Tc pretechnatate and continues for 30 minutes after injection. ^{99m}Tc pretechnatate is actively trapped and concentrated in the intralobular ductile cells with subsequent ductal epithelium secretion and discharge into the excretory ducts. At 15 minutes after injection, salivary stimulation is induced by the ingestion of citric acid while the frame acquisition continues. Regions of interest are drawn over the individual salivary glands on the planar images and the time-activity curves are analyzed. The secretion fraction provides information about the secretory capacity of the glands (De Rossi, 1987; Roesink *et al.*, 2004). Lately, single photon emission computerized tomography (SPECT) and ^{11}C-methionine positron emission tomography (PET) have been used to measure salivary function 3 dimensionally after radiotherapy of head-and-neck(Bussels *et al.*, 2004; Buus *et al.*, 2004).

1.2 Radiation-induced xerostomia

1.2.1 Etiology

Radiation-induced xerostomia has been observed ever since radiation is used as therapeutic modality for head-and-neck tumors in the beginning of last century (Bergonie and Speder, 1911; Cooper *et al.*, 1995). Nevertheless, the exact mechanism of the radiation injury to the salivary glands is still not fully understood. That is partly due to the enigmatic radio-sensitivity of the salivary glands (Konings *et al.*, 2005a). The salivary glands are highly specified organs and their cells are well differentiated with low mitotic index. Therefore reproductive death due to DNA damage as it happens to the tumor cells during and shortly after irradiation is unlikely to happen to the salivary cells (Jensen *et al.*, 2003).
Histopathological studies, mostly performed on animals, have shown degenerative changes of the serous acinar cells while the mucous acinar cells and the ductal cells were unaffected in the acute phase. In the long-term phase, loss of serous acinar cells, inflammation, fibrosis and atrophy were found. However, salivary flow reduction and changes in the composition of the saliva occur even after the first week

of irradiation, indicating that the gland tissue is acutely radiosensitive at least in the functional aspect (Kashima *et al.*, 1965; Mossman, 1994; Stephens *et al.*, 1896; J, 1991; Guchelaar *et al.*, 1997; Coppes *et al.*, 2001; O'Connell, 2000).
Lately Konings *et al.* (2005a) have shown evidence that the most probable mechanism of action, explaining the enigmatic high radiosensitivity for early effects, is selective radiation damage to the plasma membrane of the secretory cells, disturbing signal transduction primarily affecting watery secretion. Later damage is mainly due to classical mitotic cell death of progenitor cells, leading to a hampered replacement capacity of the gland for secretory cells, but is also caused by damage to the extracellular environment, preventing proper cell functioning.
Sialochemistry shows that both the acinar and ductal functions are affected by radiation (Dreizen *et al.*, 1976; Mossman *et al.*, 1981; Valdez *et al.*, 1993). It has been suggested that edematous stenosis of the major salivary ducts that takes place progressively during the treatment leading to symptoms of acute sialadenitis with an excretory obstacle (De Rossi, 1987). However, the salivary duct system has never been systematically investigated in humans after radiotherapy.

1.2.2 Prediction

Salivary function continues to decline for up to several months after radiation therapy. Depending on the dose received by the salivary glands and the volume of the glands included in the irradiation fields, xerostomia may become an irreversible life-long problem. There is general agreement that fully irradiated parotid glands receiving doses higher than 60 Gy suffer permanent radiation-injury without recovery in function. Recovery can be expected when the glands are partially irradiated and receive modest doses, for example from 30 Gy to 50 Gy. An effort should be made to avoid long-term xerostomia or reverse it as soon as possible because as the treatment of head-and-neck tumors improves and the number of disease free years is increasing, the QoL of the patients after treatment is getting more and more important.
Several studies have been performed to assess dose-response relationships between the salivary output and the dose received by the parotid glands. Mainly the methods described in paragraph 1.1.2 have been used to measure stimulated salivary flow from the salivary glands before radiotherapy and at various time intervals such as 6 weeks, 6 months and 1 to 5 years after the end of the treatment (Braam *et al.*, 2005). Based on salivary gland scintigraphy, Maes *et al.* (2002) suggested that the mean dose to the parotid glands should be $\leq$20 Gy to have a good chance ($\geq$70%) for preserving salivary function 1 after radiotherapy. Chao *et al.* (2001c) measure whole mouth saliva output and reported that stimulated saliva flow 6 months after RT was reduced exponentially at a rate of 4%/Gy of the mean parotid dose. At a mean dose of 32 Gy, the stimulated saliva was predicted to drop to 25% of baseline (RTOG/EORTC grade 4 complication).
Mathematical models that are used to describe and predict the normal tissue

complication probability (NTCP) for xerostomia use this endpoint. A commonly used NTCP model is that of Lyman-Kutcher (Kutcher GJ, 1989). This model assumes that the probability of complications after uniform irradiation of a specific volume of an organ follows a sigmoid dose-response relationship. This curve is characterized by the steepness, parameter m, the tolerance dose (TD_{50}) for 50% complication rate and the 'volume effect' parameter n. The parameter n is relatively high for parallel organs, which means that a small fraction can be damaged without a significant effect on the function of the whole organ, and relatively low when the organ is serial, which means that the tolerance of the whole and partial volumes are similar.
Eisbruch *et al.* (2001a) and Roesink *et al.* (2001) fitted the parotid saliva output, measured with the method described in 1.1.2, to the Lyman-Kutcher NTCP model. Using as an endpoint xerostomia 1 year after radiotherapy Eisbruch *et al.* (2001a) found a steep sigmoid dose-response curve and TD_{50} =28.4 Gy. On the contrary, Roesink *et al.* (2001) found a less steep curve and a TD_{50} =39 Gy . Both studies agree, however, that the parotid glands are parallel organs and the mean dose to the whole organ could be used as predictor for xerostomia.
Furthermore, Roesink *et al.* (2005) have shown that subjective patient scoring for xerostomia does not correlate with the mean parotid dose as the salivary flow measurements do. This might be due to the fact that NTCP modeling for xerostomia is based only to the function of the parotid glands. The patient's subjective feeling for xerostomia, however, results most probably from the reduced salivary function of the whole salivary gland system that includes the submandibular glands, the sublingual glands and the minor salivary glands spread in the oral cavity (Eisbruch *et al.*, 2001a). Therefore for the best assessment of xerostomia with regard to the pattern of patient's complaints an effort should be made to measure and investigate the salivary dysfunction of the whole salivary gland system after radiotherapy.

1.2.3 Management

In order to provide symptomatic relief of the oral dryness saliva substitutes are prescribed to the patients after radiotherapy. Saliva substitutes duplicate the properties of normal saliva but provide only temporary relief (Guchelaar *et al.*, 1997). The fact that there is not one commercial product that mimics 100 % the normal saliva demonstrates how complex saliva is.
Another option is the use of sialogogic agents to stimulate saliva production from remaining intact salivary gland tissue. Pilocarpine is currently the only sialogogic agent approved by the Food and Drug Administration (FDA) for radiation-induced xerostomia (Chambers *et al.*, 2004). Preliminary results suggest that that there is some improvement in objective saliva measurements in patients receiving pilocarpine during radiotherapy compared with patients receiving placebo (Warde *et al.*, 2003). Thus it is possible that patients with parotid glands receiving between 25 Gy to 50 Gy may benefit from treatment with pilocarpine (Roesink *et al.*,

1999; Roesink, 2005).
Other investigators investigate the possibility of gene transfer technology (Nagler and Baum, 2003). Surgical transfer of the submandibular gland to avoid irradiation has also been suggested (Seikaly *et al.*, 2001) .
The best way managing xerostomia is preventing it by reducing the volume of the salivary glands involved in the irradiation fields and the dose delivered to the glands. That could be possible by implementing conformal radiotherapy techniques (Maes *et al.*, 2002; Eisbruch *et al.*, 1998) and especially intensity-modulated radiotherapy (IMRT) which will be described in 1.3.1.
Using IMRT is possible to deliver more conformal doses to the target volumes and consequently spare more of the parotid gland tissue than in conventional techniques (Chao *et al.*, 2001c; Van Asselen *et al.*, 2002). IMRT produces high dose gradients within the glands compared to the more homogeneously distribution to the whole gland delivered by conventional irradiation techniques. Recent experiments in animals, however, have indicated regional differences in the radiosensitivity of the parotid glands (Konings *et al.*, 2005a,c, 2006). It is concluded that the observed region-dependent volume effect for late function loss in the rat parotid gland after partial irradiation is mainly caused by secondary events in the shielded lateral lobe. The most probable first step in the development of this secondary damage is radiation exposure to the hilus region . By injuring major excretory ducts and supply routes for blood and nerves in this area, the facility system necessary for proper functioning of the non-exposed lateral lobe is seriously affected (Konings *et al.*, 2006). This hypothesis should be investigated in humans as it might influence the IMRT planning strategies. In the following paragraphs the IMRT technique and delivery will be presented.

1.3 Radiotherapy for head-and-neck cancer

Radiation therapy is today, together with surgery, the treatment of choice for head-and-neck cancer. The incidence of cancer to the oral cavity, larynx, naso- and oropharynx accounts for about 6% of all the malignancies (excluding skin) worldwide (GLOBOCAN 2000).
The head-and-neck area is an anatomically complex area. In most of the cases not only the primary tumor or the surgical bed of the tumor has to be irradiated (70 Gy, 2 Gy per fraction is the conventional fractionation scheme) but the cervical lymph nodes should be included in the irradiation fields as well. Even if there is no sign of macroscopic disease to the lymph nodes they should be irradiated electively (50 Gy, 2 Gy per fraction) to treat possible microscopic disease. Therefore, the volume of the area to be irradiated with curative intention, thus high dose, increases considerably.
The dose-limiting factor is the tolerance of the adjacent normal tissues more specifically that to the spinal cord and brain because dose >50 Gy increases the risk

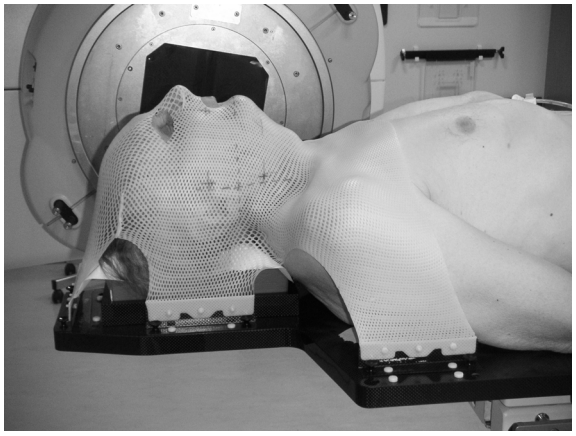

Figure 1.2: Patient positioned at the linac table using the immobilization mask.

of radiation myelitis, irreversible damage to the central nervous system. Other advert reactions to radiation that should be avoided include osteoradionecrosis of the mandible bone and as we have already described xerostomia.

1.3.1 IMRT in head-and-neck cancer

Advances in the radiation delivery technology in combination with parallel advances in anatomical and biological imaging and computers have changed the clinical routine of radiotherapy. Radiotherapy has evolved from therapy based on 2 dimensional (2D) X-ray images to 3D image based conformal RT (Bucci *et al.*, 2005). Most of the linear accelarators today are equipped with multileaf collimators (MLC). MLC consists of thin blades that can be individually manipulated to create irregularly shaped beams that conform to the shape of the target volumes. IMRT is an advanced form of conformal RT. It allows manipulation of beam intensity across each treatment field, providing a dose distribution that conforms more accurately to the 3D configuration of the target volume than conventional 3D-CRT (Stein *et al.*, 1997; Mackie *et al.*, 1999; Webb, 2001). Most commonly the IMRT treatment is delivered by using a multileaf collimator (MLC). The obvious advantages for an anatomically complex area such as the head-and-neck have pushed IMRT in the standard treatment of this site faster than other cancer sites (Figure 1.3).
IMRT delivers higher dose per fraction and the dose to all targets, primary tumor and lymph nodes can be delivered simultaneously in 30 fractions (Butler *et al.*, 1999). That offers an improved biological therapeutic ratio compared to the con-

ventional techniques in which the total dose is delivered in 35 fractions.
Furthermore, matching photon and electron beams in order to spare the spinal cord, with the risk of under-dosage and over-dosage at the areas where the fields intersect, is not necessary anymore.
Moreover, it has been shown that most recurrences occur in the site of the original tumor which suggests that dose escalation should be considered in order increase the tumor control probability (TCP). That would be possible using IMRT because the spinal cord is spared considerably compared to the conventional techniques (Withers *et al.*, 1995; Chao *et al.*, 2002; Dawson *et al.*, 2000; Withers *et al.*, 1995).

Volume delineation

Accurate volume delineation is of great importance for IMRT. First of all, treatment planning is based on optimization of dose constraints assigned to predefined volumes. That requires meticulous delineation of the primary tumor, lymph nodes and all organs at risk. Secondly, IMRT produces sharp dose gradients around the target volumes and not *everything* is included in the irradiation fields as in conventional RT (Figure 1.3).
Inaccurate target volume delineation could result in missing part of the tumor or on the other hand overestimate the target volume. In the first case, that could result in under-dosage of the tumor and in the second case, overdose of the adjacent normal tissues. In both cases, however, the benefits of using IMRT would have been lost. Imaging is without doubt the key to achieve the required delineation accuracy.
Computerized tomography (CT) is the standard imaging modality used for the volume delineation and is necessary for the dose calculation. Magnetic resonance imaging (MRI) provides higher soft tissue contrast than CT and positron emission tomography (PET) provides information on the tumor metabolism. Combined information from all these imaging modalities has been used lately not only for the diagnosis and staging of the disease but for volume delineation as well. The use of the RT immobilization mask every time the patient is scanned and the fact that in head-and-neck area there are no significant organ movements, contributes to successful image registration between the various imaging modalities. The influence of the multi-imaging volume delineation to the outcome of IMRT treatment planning is under investigation by various groups.
For the same reasons, next to the primary tumor delineation the delineation of the lymph nodes requires more attention as well. Gregoire *et al.* (2000) and Nowak *et al.* (1999) have proposed some guidelines for standardizing the target definition of the cervical lymph nodes on CT. However, there are some discrepancies in the delineation approaches especially in the cranial direction of the Level II lymph nodes. The cranial part of Level II lymph nodes are adjacent to the parotid

glands. Therefore, it should be investigated whether those difference in the delineation strategies affect dose received by the parotid glands.

Set-up errors and margins

Clinical evaluation of treatment plans in radiotherapy is based on dose distributions, calculated on a static representation of the anatomy of the patient, with respect to the radiation beams. The unavoidable geometrical uncertainties are taken into account by adding a margin to the clinical target volume (CTV). The dose to this geometrical volume which is called planning target volume (PTV) is assumed to be representative of the dose to the CTV (ICRU Report No. 62, 1999; ICRU Report No. 50, 1993). Defining the optimal PTV margins is very important in order to treat the tumor adequately and at the same time reduce the damage to healthy tissues (Van Asselen *et al.*, 2002). Therefore the geometrical uncertainties of a particular treatment site and technique, and their influence on the dose distributions should be known (Hunt *et al.*, 1993; Mageras *et al.*, 1999; Stroom and Heijmen, 2002).
The geometrical uncertainties originate from the treatment preparation and machine related errors, the day-to-day patient positioning variations and internal organ motion. An error present throughout the whole treatment, causing a displacement of the dose distribution with regard to the intended one, is called a systematic error. Day-to-day variations, causing dose coverage differences to the CTV between fractions, are random errors (Van Herk *et al.*, 2000; Stroom *et al.*, 1999).
The introduction of electronic megavoltage imaging (EPID) in combination with fiducial markers and immobilization devices enabled an accurate detection of these errors (Figure 1.2). By using off-line correction procedures, it became possible to reduce the systematic deviations. On-line correction procedures enabled a further reduction of both systematic and random deviations. (Gilbeau *et al.*, 2001; Bel *et al.*, 2000; van Lin *et al.*, 2003; De Boer *et al.*, 2001; Dehnad *et al.*, 2003; Nederveen *et al.*, 2001; Pisani *et al.*, 2000; Stroom *et al.*, 1999; Van Asselen *et al.*, 2003; Bel, 2003). However, even for well fixated head-and-neck patients (Hurkmans *et al.*, 2001) residual set-up errors remain present. The margin *recipes* currently used to account for the geometrical errors, are derived from geometrical models and they are verified on conformal dose distributions and mainly for prostate irradiation. Therefore the margins might not properly address the complexity of head-and-neck IMRT dose distributions. For that reason they should be evaluated on clinical head-and-neck IMRT cases.

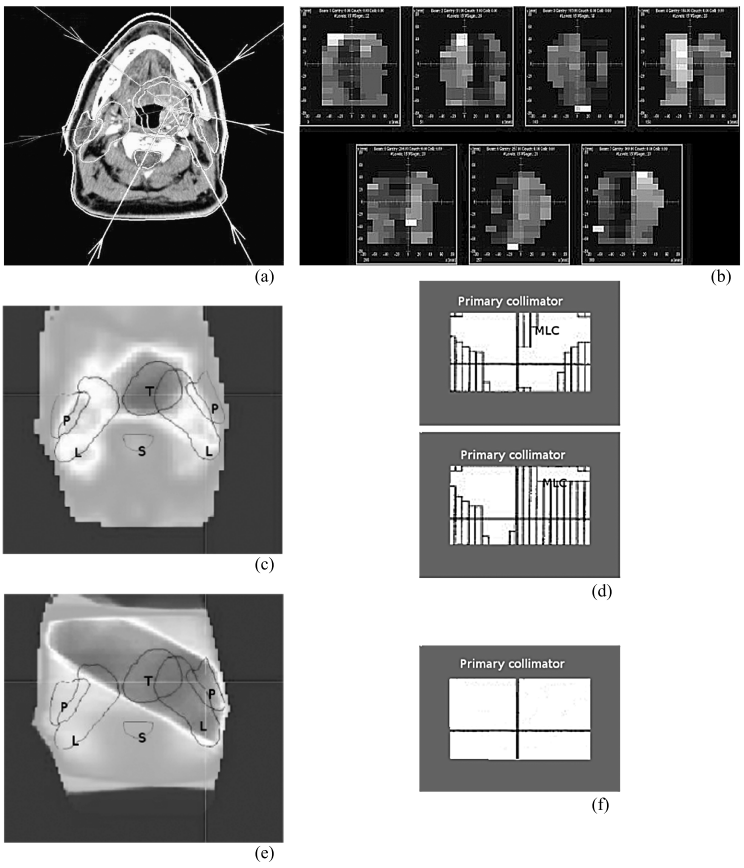

Figure 1.3: (a)A transverse slice of the treatment planning CT of a head-and-neck patient. For IMRT treatment multiple beam entries are used, typically 5 to 9, and in this example 7. The intensity fluence map of each beam portal is given in (b). The intensity fluence of each beam is modulated from high intensity (white areas) to gradually (grey areas) no intensity (black areas). That is possible because each beam consists of multiple segments (typically 10 to 20). Each segment is an irregular shaped field created by a multi-leaf collimator, MLC (d). As a result of that the dose distribution conforms the target volumes (c) more than in the conventional treatment (e) in which open beams are used (f). The dark gray area represents the high dose area. The contour lines are the delineated organs. T=the primary tumor, L=lymph nodes, P=parotid glands and S=spinal cord.

1.4 Purpose of this thesis

This thesis addresses the following questions related to radiation-induced xerostomia:
1. How can we reduce the dose delivered to the salivary glands?
2. Is the planned dose actually the delivered dose?
3. How the delivered dose affects the salivary glands and the salivary function? Can we actually *see* that?Can we measure it? Does that have implications for our IMRT planning strategy regarding salivary function sparing?

The first question was dealt in **chapter 2**. We performed a treatment planning study and compared two different planning techniques and two different target delineation strategies. The goal was to quantify how much is the dose reduction to the parotid glands when our IMRT class solution is used instead of the conventional 3D-CRT, while maintaining the same target dose coverage. Next to that but equally important goal was to quantify the dose reduction to the parotid glands when the cranial border of the adjacent Level II cervical lymph nodes was delineated up to the cervical vertebra C2 instead of C1. The rationale behind this study derives from the empirical fact that the cervical vertebra C2 is often the anatomical cranial boarder in case of surgical dissection. The evaluation of the results was done not only comparing the absolute gain in dose but also the NTCP for xerostomia 1 year after radiotherapy.
In **chapter 3** we tried to answer question 2. We compared head-and-neck IMRT dose distributions as they are conventionally calculated with those calculated including the translational and rotational setup errors, which unavoidably occur during fractionated radiotherapy. This possibility of simulating the setup errors in the treatment planning has been implemented for the first time in a commercial planning system. In this study we evaluated whether the planned dose is the dose that is actually delivered and whether the current margin *recipies* account sufficiently for the random setup errors. The motivation of this study is that the current margins have been developed using geometrical models and they are mostly evaluated on clinical prostate cases and for conventional 3D-CRT dose distributions. Therefore it should be investigated whether those margins are sufficient for complex anatomical sites such as head-and-neck and complex dose distributions such as IMRT dose distributions.
Question(s) 3 is not a trivial question to answer. In order to investigate how dose affects the salivary gland and duct systems we have developed an MRI protocol that we first evaluated on healthy volunteers. Then we performed a pilot study on a group of patients to investigate and evaluate the technical and clinical feasibility of such a protocol. The MRI was performed before RT, 6 weeks and 6 months after the end of the treatment. At the same time intervals we performed salivary flow measurement as described in 1.1.2. The MR protocol included T_1- and T_2-weighted imaging of the head-and-neck that was used to delineate the salivary

glands and 3D MR sialography. MR sialography is a heavily T_2-weighted sequence that allows the imaging of the salivary ducts because the containing saliva appears hyperintense and the surrounding tissue hypointense.
In **chapter 4** we compared the volumes of the salivary glands before radiotherapy to those after radiotherapy and we tried to evaluate whether the observed volume differences were correlated to the 3D dose distribution or to the salivary output.
The development and the evaluation of the 3D MR sialography protocol on healthy volunteers are described analytically in **chapter 5**.
In **chapter 6** the results of the feasibility study of the MR sialography protocol on patients are presented. The use of this method as a novel tool to investigate radiation-induced xerostomia is evaluated. This 3D MR sialography sequence is to our knowledge for the first time used to investigate radiation-induced xerostomia. The rationale behind this effort is that this method is the only 3D imaging modality that has the potential to provide spatial information on the salivary function using saliva itself as contrast medium and furthermore can be registered to the 3D dose distribution, in contrast to the methods described in 1.1.2.
General conclusions and suggestions for future work are presented in **chapter 7**.

Chapter 2

Level II lymph nodes and radiation-induced xerostomia

This chapter has been published as: E. Astreinidou, H. Dehnad, C.H. Terhaard, and C.P Raaijmakers. 2004. Level II lymph nodes and radiation-induced xerostomia *Int J Radiat Oncol Biol Phys*. **58(1)** 124-31.

Abstract

Purpose: To investigate the influence of the cranial border of the elective irradiated level II lymph nodes on xerostomia, in patients with oropharyngeal cancer, using three dimensional conformal and intensity-modulated radiation therapy techniques (3D-CRT and IMRT).**Methods and Materials**: The target volumes and the organs at risk were delineated on planning CT scans of 12 patients. Two elective target volumes were delineated. The first had the transverse process of the atlas C1 and the second had the transverse process of the axis C2, as cranial border of the level II lymph nodes. The 3D-CRT and IMRT planning were performed for both elective volumes, resulting in two plans per patient and technique, that will be called C1 and C2 plans respectively. Irradiation of the ipsilateral elective volume up to C1 and the contralateral up to C2 was also performed for the IMRT technique. The normal tissue complication probability (NTCP) for xerostomia one-year after radiotherapy was calculated using the parotid mean dose. **Results**: The average mean dose ($\pm$1 standard deviation, SD) to the contralateral parotid gland was reduced from 33$\pm$5 Gy for the IMRT C1 plans to 26$\pm$4 Gy for the IMRT C2 plans and from 51$\pm$6 Gy to 49$\pm$7 Gy for the 3D-CRT C1 and C2 plans respectively. The associated NTCP ($\pm$1 standard deviation, SD) for xerostomia was 38$\pm$10% for IMRT C1 plans and 24$\pm$6% for IMRT irradiation up to C2 on the contralateral side regardless of which cranial border was irradiated on the ipsilateral side. For the 3D-CRT C1 and C2 plans, NTCP values of 74$\pm$12% and 71$\pm$15% were obtained respectively. The NTCP for xerostomia of the ipsilateral parotid gland was 53$\pm$17% and 45$\pm$20% for the IMRT C1 and C2 plans and 89$\pm$11% and 87$\pm$12% for the 3D-CRT C1 and C2 plans respectively. **Conclusion**: Lowering the cranial border of the level II lymph nodes from C1 to C2, in case of bilateral elective neck irradiation could be considered on the contralateral side when the risk of metastasis on that side is very low. Especially when IMRT irradiation

is used since the relative reduction of NTCP for xerostomia one-year after radiotherapy could be up to 68% compared to the conventional conformal radiotherapy up to C1.

2.1 Introduction

The treatment of oropharyngeal cancer patients requires in some cases, elective irradiation of at least the cervical level II-IV lymph nodes in order to treat possible microscopic disease (Robbins *et al.*, 2001; Weiss *et al.*, 1994; Bataini, 1993). A prevalent side effect of this treatment is xerostomia as the major salivary glands are fully or partially irradiated. Xerostomia has major impact to the quality of life of the patients as it has been reported elsewhere (Wijers *et al.*, 2002; De Graeff *et al.*, 1999; Huguenin *et al.*, 1999; Henson *et al.*, 2001; Harrison *et al.*, 1997).
The degree of parotid gland hypofunction has been shown to be correlated to the radiation dose delivered and to the volume of the gland included in the irradiation field (Roesink *et al.*, 2000; O'Connell, 2000; Roesink *et al.*, 2001; Eisbruch *et al.*, 1999). Numerous studies have been performed, aiming at a reduction of the dose delivered to the parotid glands, employing 3D conformal radiation therapy and more recently IMRT techniques (Claus *et al.*, 2002; Eisbruch *et al.*, 1996, 1998; van Dieren *et al.*, 2000; Chao *et al.*, 2000, 2001a; Wu *et al.*, 2000; Maes *et al.*, 2002). The volume of the parotid glands in the field depends on the size and position of the primary tumor and the adjacent level II lymph nodes due to which a part of the parotid glands is unavoidably included in the high dose region (Van Asselen *et al.*, 2002).
The cranial border of the Level II lymph nodes, according to Robbins classification, is the base of the skull (Robbins *et al.*, 1991; Robbins, 1999). Following these recommendations, radiation oncologists are using the cervical vertebrae-C1 as an anatomical bony landmark when delineating the Level II lymph nodes on a planning CT (Gregoire *et al.*, 2000; Wijers *et al.*, 1999; Nowak *et al.*, 1999; Chao *et al.*, 2002; Shah *et al.*, 1993). Gregoire *et al.* (2000) proposed the bottom edge of the body of C1 and Nowak *et al.* (1999) the top of it, as the cranial border. At our institute the recommendations of Shah *et al.* (1993) are used and the cranial border of the Level II lymph nodes is delineated up to the transverse process of the atlas C1. These delineation approaches differ a few millimeters in the cranio-caudal direction and affect the volume of the parotid gland included in the irradiation field (Claus *et al.*, 2002).
In our study a further reduction of the cranial border of the Level II lymph nodes to the transverse process of the axis C2 is investigated in case of elective node irradiation. The rationale behind this reduction derives from the empirical fact that quite often the axis C2 is the surgical achievable anatomical Level of the upper neck selective dissection. Our main aim is to investigate whether this volume reduction can lead to a sufficient dose reduction in order to decrease the normal tissue complication probability, NTCP, for xerostomia one year after radiotherapy. The

quantification of the parotid dose reduction when the cranial border of the Level II lymph nodes is lowered, was performed for the three dimensional conformal radiation therapy, 3D-CRT, currently used at our institute and the proposed class solution of the intensity-modulated radiation therapy (IMRT) (Van Asselen *et al.*, 2002). Another parallel study was performed to quantify the risk of metastasis in the volume between C1-C2, in order to justify future decisions of lowering the cranial border to the benefit of maintaining salivary function (Prins-Braam *et al.*, 2004). Furthermore, the treatment planning study will be used to set the minimum dose homogeneity requirements for the IMRT class solution and to quantify the expected reduction in NTCP for xerostomia one year after radiotherapy when applying IMRT compared to the conventional treatment.

2.2 Methods and Materials

2.2.1 Patients and target volume definition

Twelve patients with oropharyngeal tumor stage T1-3N0M0 were studied. For all patients planning computerized tomography (CT) scans were available. The CT acquisition was done in 3mm slice intervals using intravenous contrast bolus and a 5-point immobilization thermoplastic mask. The CT data were transferred to the radiation treatment planning system (PLATO, Nucletron BV, Veenendaal, NL) where the gross tumor volume (GTV), the clinical target volume (CTV) of the lymph nodes and the organs at risk (OAR) - spinal cord, brain and parotid glands - were delineated by a radiation oncologist. The GTV was expanded non-uniformly, in three dimensions following the protocol of our institute (2cm cranial; 1cm caudal, ventral and medial; 0.5cm lateral and dorsal) creating the clinical target volume (CTV) of the primary tumor.
The cranial border of the Level II lymph node regions was delineated up to the transverse process of C1, according to (Shah *et al.*, 1993) guidelines, and up to the transverse process C2, for the purpose of this study, resulting in two elective clinical target volumes CTV-C1 and CTV-C2. All CTVs were expanded 5 mm in all directions to account for set up errors, creating the planning target volumes, PTV of the primary tumor and the lymph nodes PTV-C1 and PTV-C2 (Figure 2.1). When necessary PTVs were adjusted manually to assure a minimal distance of 5mm between the PTV and the skin. The PTVs of the lymph nodes can be partially covered by the PTV of the primary tumor. For the remaining of the paper when referring to PTV-C1 and PTV-C2 the non overlapping volume was considered. The parotid gland volume was also partly covered by the PTVs and this volume will be called overlapping parotid volume. The spinal cord was also expanded three dimensionally with 5-mm margin resulting into the planning organ at risk volume (PRV) of the spinal cord.

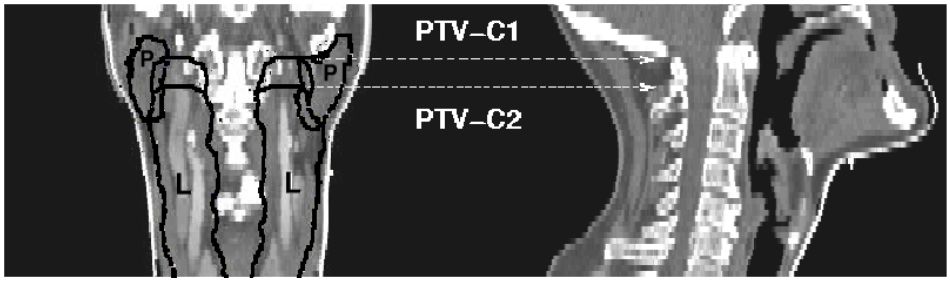

Figure 2.1: Coronal and sagittal view of the cranial border of the planning target volume (PTV) of the Level II lymph nodes delineated up to the transverse process of the atlas C1, (PTV-C1) and axis C2 (PTV-C2).P=parotid gland, L=lymph nodes

2.2.2 Conventional 3D Conformal Treatment Planning

The aim of the conventional 3D conformal radiotherapy technique in oropharyngeal cancers, at our institute, is to deliver 50 Gy to the elective cervical lymph nodes, in 25 fractions, and 70 Gy to the primary tumor PTV in 35 fractions, 5 fractions per week. The maximum dose to the spinal cord and brain should not exceed the 46 Gy.
Typically two lateral opposed or two lateral non-coplanar 6 MV photon beams were employed to deliver 40 Gy and after that the spinal cord was blocked. The rest of the dose to the blocked lymph nodes was given with 8 or 10 MeV electron beams. Effort was made to avoid the contralateral parotid gland and to minimize the dose delivered to the spinal cord while planning the 20 Gy boost. All fields were shaped in order to avoid as much healthy tissue as possible. The above planning technique was applied to all patients twice, once to irradiate the elective nodes up to C1, PTV-C1, and secondly up to C2, PTV-C2. This resulted in two plans per patient, which will be called C1 plan and C2 plan, respectively.
Another two plans were calculated per patient, again up to C1 and C2, but this time without the primary tumor. This means that 50 Gy was delivered to the elective lymph nodes, in order to estimate the pure effect of the cranial border of the Level II lymph nodes to the parotid dose, independently of the size and position of the primary tumor. Dose calculations were performed using a commercial planning system, PLATO-RTS v2.5 (Nucletron BV, Veenendaal, NL).

2.2.3 Intensity Modulation Radiotherapy Planning

IMRT plans were made using the inverse treatment planning module PLATO-ITP v1.0 (Nucletron BV, Veenendaal, NL). The ITP module optimizes the fluency for

fixed beam geometry to obtain a dose distribution that best fits a series of dose constraints. The relative weight of these constraints for the target volumes and the organs at risk is called penalty. The number of beams, dose constraints and penalties which result to the best acceptable dose distribution for head-neck tumors has been reported previously by (Van Asselen *et al.*, 2002).
For the purpose of this study seven equidistant beams were used. One beam had a gantry angle of 0 degrees. The dose constraints for each organ were chosen to deliver simultaneously the biological equivalent dose, BED, of that of the 3D-CRT dose to the lymph nodes and the primary tumor in 30 fractions, thus 54 Gy to the elective irradiated lymph nodes and 66 Gy to the primary tumor. The dose constraint to the spinal cord and brain was 30 Gy with relatively high penalty and to the parotid glands 20 Gy with relatively low penalty. The overlapping parotid volume is treated as target volume by the inverse treatment planning system.
The theoretical fluency with a continuous intensity distribution was converted into fluency with distinct intensity Levels for step-and-shoot IMRT, delivered by a multi-leaf collimator (SL25, Electa Oncology Systems, Crawley, UK). This was done using a sequencer software developed at our institute and incorporated into the commercial inverse treatment planning module PLATO-ITP v1.0. Then the deliverable fluence is transferred to the RTS module for the final dose calculation. Again, as for the 3D CRT, dose calculation was done with and without the primary tumor PTV and for PTV-C1 and PTV-C2. Another plan irradiating the ipsilateral side up to C1 and only the contralateral up to C2 was also calculated for the IMRT technique and this plan will be called C1C2 plan. This plan was not performed for the conventional 3D-CRT planning since for this technique the cranial border of the field is mainly determined by the primary tumor PTV.

2.2.4 Data Analysis, NTCP

The mean dose to the parotid glands was calculated for all plans irradiating the lymph nodes up to C1 and compared with that of the plans irradiating the lymph nodes up to C2. A paired t-test was used for the comparisons and differences were considered to be statistically significant when $p<0.05$. The NTCP for xerostomia one year post-radiotherapy was calculated, using the Lyman model as described by (Roesink *et al.*, 2001). The parameters of the NTCP curve were, TD_{50}=39 Gy, m=0.45 which means that the slope of the curve is not very steep, and n=1 which means that the observed complications correlate best with the mean dose to the parotid glands.
The correlation between the overlapping parotid volume and the mean dose was investigated for the IMRT plans with and without the primary tumor. For the treatment plan evaluation the maximum, minimum and the mean dose to the target volumes and the volume receiving less than 90%, (V_{90}), and 95%, (V_{95}), and more than 105%, (V_{105}), of the prescribed dose were tabulated for both methods.

As dose homogeneity parameter the steepness of the dose volume histogram (DVH) curve in Gy was used. This steepness was derived subtracting the dose received by the 5% of the volume from the dose received by 95% of the volume. The V_{90}, V_{95} and V_{105} were also extracted for the body volume not including the PTV in order to quantify the volume of healthy tissue that receives high dose. The maximum dose to the spinal cord and spinal cord PRV was also evaluated.

2.3 Results

2.3.1 Treatment Plan Evaluation and Comparison

For both methods, 3D-CRT and IMRT, and for all 12 patients, the mean dose to the PTV was similar to the prescribed dose (Table 2.1). The target coverage and dose homogeneity was comparable for both methods, with that of the conformal planning slightly better. The main difference was the volume of the PTV receiving more than 105% of the prescribed dose. This volume was on the average about 6% for the IMRT plans but almost negligible for the conformal plans. The maximum dose in the PTV was approximately 106% of the prescribed dose in case of inverse planning and 103% for the conformal planning.
The volume of the body excluding the PTV (±1 standard deviation, SD) which received more than 90% of the prescribed dose to the PTV was on the average $267 \pm 73 cm^3$ for the conformal plans and $90 \pm 21 cm^3$ for the IMRT plans. The V_{95} was $192 \pm 54 cm^3$ and $45 \pm 13 cm^3$ for the 3D-CRT and IMRT plans respectively. This demonstrates the high dose conformity produced by IMRT (Figure 2.2).
The dose homogeneity and coverage of the contralateral and ipsilateral lymph node regions, was improved significantly with the IMRT technique compared to that of the conformal one (Table 2.1). The minimum dose, however, was about 12% lower than the prescribed dose for both methods. Similar results as that presented in Table 2.1 were obtained for the C2 plans. The maximum dose (± 1 standard deviation, SD) to the spinal cord was 31 ±0.8 Gy and to the spinal cord PRV was 40 ±2 Gy for the IMRT plans. For the 3D-CRT plans the maximum dose to the above mentioned volumes were 45 ±2 Gy and 48 ± 1.5 Gy respectively.

2.3.2 Parotid glands

Plans including the primary tumor

The position and the volume of the parotid glands varied per patient. The average parotid volume was $25 cm^3$ (range 14 - $37 cm^3$). The distance between the cranial border of the PTV-C1 and PTV-C2 varied from 9 to 21 mm; the median value was 15 mm.
The average mean dose (± 1 standard deviation, SD) to the contralateral parotid gland was 33 ±5 Gy for the IMRT C1 plans and reduced to 26 ± 4 Gy for the

Table 2.1: Treatment plan evaluation statistics

	3D-CRT			IMRT		
	PTV	PTV-C1		PTV	PTV-C1	
		contra	ipsi		contra	ipsi
Prescription(Gy)	70	50	50	66	54	54
Delivered Dose						
Mean(SD)(Gy)	69.8(0.4)	53.6(1.8)	58.1(3.0)	66.7(0.4)	55.0(0.8)	56.4(0.9)
Mean(SD)%	99.8(0.6)	107.2(3.6)	116.2(6.0)	101.0(0.6)	101.8(1.4)	104.4(1.6)
Max(SD)(Gy)	72.5(1.1)	66.3(4.4)	71.9(1.2)	70.2(0.7)	59.5(2.6)	64.8(2.3)
Max(SD)%	103.5(1.6)	132.6(8.8)	143.8(2.4)	106.3((1.0)	110.2(4.8)	120.0(4.2)
Min(SD)(Gy)	64.8(2.5)	43.8(3.5)	45.7(4.9)	59.8(2.5)	47.0(2.5)	49.5(3.6)
Min(SD)%	92.6(1.6)	87.6(7.0)	91.4(9.8)	90.6(3.8)	87.0(4.6)	91.6(6.6)
D_{5-95}(SD)(Gy)	4.2(1.1)	16.5(5.8)	22.6(3.3)	5.4(1.1)	6.5(1.7)	10.2(2.6)
V_{90}(SD)%	99.7(0.4)	97.6(2.7)	98.0(2.3)	99.5(0.5)	98.0(1.8)	98.7(2.0)
V_{95}(SD)%	98.3(1.4)	92.4(5.7)	93.2(7.7)	97.4(1.6)	94.6(3.9)	96.6(3.8)
V_{105}(SD)%	0.5(1.3)	42.6(16.4)	62.4(20.5)	6.1(5.0)	17.2(9.5)	32.7(10.3)

3D-CRT=three dimensional-conformal radiation therapy, IMRT=Intensity modulated radiation therapy, PTV=planning target volume of the primary tumor, PTV-C1=the planning target volume of the lymph nodes delineated up to the transverse process of the atlas C1. The overlapping volume of the PTV-C1 with the PTV is not taken into account for the above statistics. contra and ipsi=the contralateral and ipsilateral side of the PTV-C1.

IMRT C2 plans. Almost the same mean dose to the contralateral parotid gland was obtained when only the ipsilateral side was irradiated up to C1 and the contralateral up to C2, C1C2 plan. The mean dose to the contralateral parotid gland was on the average 0.4 Gy higher than that of the C2 plans, demonstrating the high dose conformity of IMRT (Figure 2.2). This reduction in dose when irradiating the PTV-C2 instead of the PTV-C1 was due to a reduction of the overlapping parotid volume with the lymph nodes from 16 ±7% to 4 ±5%. This reduction is statistically significant (p<0.001). The mean dose to the contralateral parotid gland was strongly correlated with the overlapping parotid volume: Parotid mean dose = 0.6 x relative overlapping volume (%) + 24 Gy.
For the 3D-CRT technique the average mean dose to the contralateral parotid gland was 51 ±6 Gy and 49 ±7 Gy for the C1 and C2 plans respectively. The mean dose differences between the C1 and C2 plans were statistically significant, (p=0.027)(Figure 2.3). Statistically significant differences were also obtained for the ipsilateral parotid gland (p<0.05). The mean dose values were higher for this gland as expected, due to the vicinity of the primary tumor PTV. The IMRT C1 plans delivered a mean dose of 40 ±8 Gy to the ipsilateral parotid gland and the IMRT C2 plans a mean dose of 36 ±10 Gy and for the C1C2 plans was 39 ±7 Gy. For the 3D-CRT technique the average mean dose to the ipsilateral parotid gland was 63 ±8 Gy and 61 ±9 Gy for the C1 and C2 plans respectively.

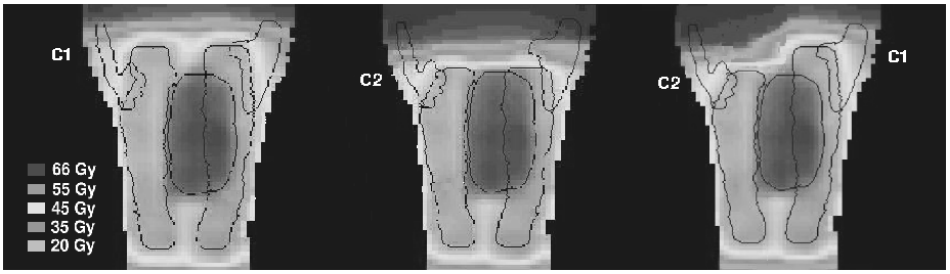

Figure 2.2: Dose distribution of the IMRT C1 plan on the left, C2 plan in the middle and C1C2 plan on the right of the same patient at the same coronal plane. C1 plan=Ipsilateral and contralateral elective volumes were irradiated up to C1, C2 plan=Ipsilateral and contralateral elective volumes were irradiated up to C2, C1C2 plan=Ipsilateral elective volume was irradiated up to C1 and the contralateral up to C2.

The difference in the mean dose between the IMRT C1 and C2 plans for each individual patient varied from 1 to 12 Gy (Figure 2.4).
The above results were used to calculate the NTCP for xerostomia one year after radiotherapy (Table 2.2).

Plans not including the primary tumor

For the conformal planning the mean dose to the parotid gland decreased from 35 Gy (range 46 - 21 Gy) for the C1 plans to 18 Gy (range 4 - 35 Gy) for the C2 plans when the primary tumor site is not included in the planning. For the IMRT planning the average mean parotid dose was 25 Gy (range 14 - 36 Gy) for the C1 IMRT plans and 11 Gy (range 3.5 - 20 Gy) for the C2 IMRT plans. There is a linear correlation between the overlapping parotid volume difference and the mean dose difference (r=0.85 Pearson's correlation). For example a reduction of 6% and 12% overlapping parotid volume resulted in a mean dose reduction of 11 Gy and 16 Gy respectively.

2.4 Discussion

In this study, the reduction in mean parotid dose has been quantified, when the cranial border of the Level II lymph nodes is lowered from the transverse process of the atlas C1 to the transverse process of the axis C2, in case of bilateral elective neck irradiation.

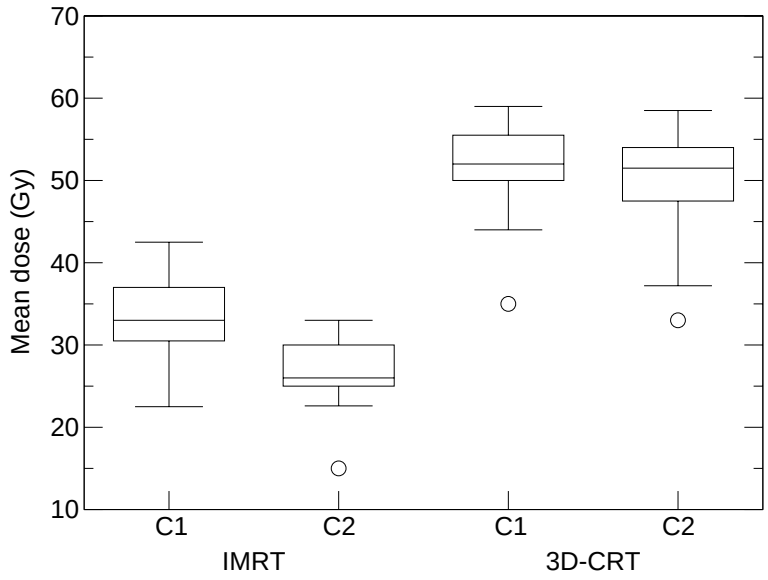

Figure 2.3: Box plot of the mean dose to the contralateral parotid glands of the 12 patients for the IMRT and 3D-CRT plans irradiating the lymph nodes up to the transverse process of the atlas C1 and axis C2.

The reduction in mean dose to the contralateral parotid gland was on average 7 Gy for the IMRT C2 plans compared to the C1 plans. The predicted NTCP for xerostomia one-year after radiotherapy was 24%, a relative reduction of 37% with regard to the C1 plans. This relative reduction was 68% when comparing the predicted NTCP of the currently used conformal irradiation up to C1 with the IMRT irradiation up to C2 (Table 2.2). It has also been demonstrated by the C1C2 plans that the same results were obtained for the contralateral parotid gland, regardless of which cranial border was irradiated on the ipsilateral side.
The NTCP values were derived from the NTCP curve deduced using data from 108 patients at our institute by Roesink *et al.* (2001). Other investigators using different set of patients, other irradiation and / or fractionation and /or different methods of measuring the salivary flow, reported different NTCP curves. The choice of normal tissue endpoints is also very important and complex and interpretations are still evolving. Eisbruch *et al.* (1999) reported for the same end point as Roesink *et al.* (2001) a steeper curve with an m-value of 0.18 and TD_{50} of 28.4 Gy. Maes *et al.* (2002) showed a less steeper curve than Eisbruch and reported that the mean parotid dose should preferably be $\leq$ 20 Gy, to obtain a good chance ($\geq$70%) for preservation of its function as determined using scintigraphy. Chao

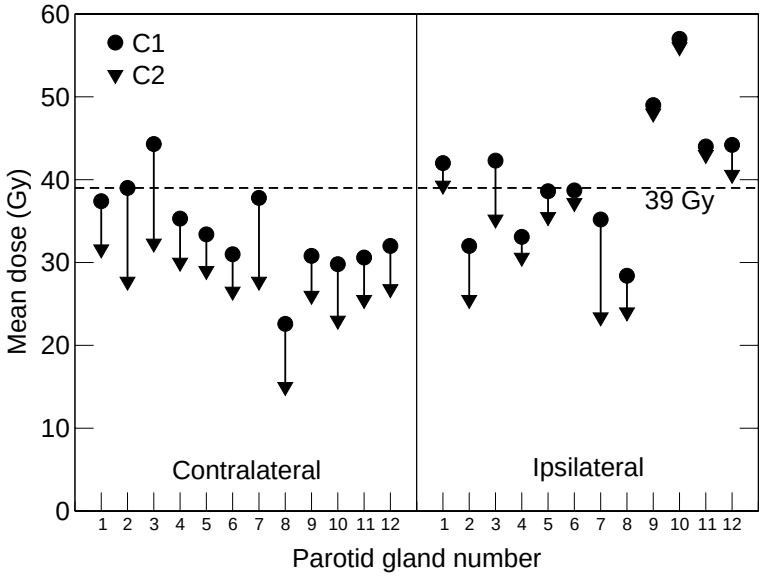

Figure 2.4: Mean dose of the contralateral and ipsilateral parotid gland for both C1 and C2 IMRT plans. The line drawn between the points indicates the mean parotid dose reduction for each individual patient when lowering the cranial border of the Level II lymph nodes from C1 to C2. The horizontal dashed line indicates TD_{50}=39 Gy.

et al. (2001c) reported that the stimulated saliva flow 6 months after radiotherapy was reduced exponentially at a rate of 4% per Gy of mean parotid dose and found a threshold dose of 32 Gy. Therefore the NTCP prediction for xerostomia depends on which model is used. Using another model, other reductions in xerostomia might be predicted. The eventual clinical benefit should be derived from clinical studies. All investigators, however, agree that the mean dose to the whole parotid gland is correlated to the degree of the gland dysfunction and the observed complication. The mean dose to the parotid gland in case of IMRT planning is strongly correlated with the overlapping parotid volume with the target volumes as it has been also demonstrated by Van Asselen *et al.* (2002) and Vineberg *et al.* (2002). In our study for a 10% overlapping contralateral parotid volume, the estimated mean dose will be around 30 Gy. This data could be used by the radiation oncologist as an indication of which patients can benefit from irradiating the Level II lymph nodes up to C2 and not up to C1 using IMRT technique, before the calculation of the actual treatment planning.
In case of the conventional 3D-CRT technique, lowering the cranial border of the

Table 2.2: NTCP for xerostomia of the contralateral and ipsilateral parotid glands and for both irradiation techniques

	NTCP (SD) %			
	contralateral		ipsilateral	
	IMRT	3D-CRT	IMRT	3D-CRT
C1 plans	38(10)	74(12)	53(17)	89(11)
C2 plans	24(6)	71(15)	45(20)	87(12)
C1C2 plans	24(9)	-	52(16)	-

NTCP=Normal tissue complication probability 1 year after radiotherapy where as complication the stimulated salivary flow <25% of the pre-radiotherapy is defined. The parameters used are, TD_{50}=39 Gy, m=0.45 and n=1. SD=1 standard deviation.

Level II lymph nodes did not result in a sufficient reduction of the parotid mean dose. This is due to the cranial location of the primary PTV for the oropharyngeal patients. When the primary tumor is located more caudally than the cranial border of the Level II lymph nodes, then lowering this border could result in large reduction in mean parotid dose, approximately 7 Gy, for the conventional technique as well. This was illustrated by the treatment plans excluding the primary tumor.

Lowering the cranial border of the Level II lymph nodes is obviously only justified when the risk of microscopic disease to the upper part of the Level II lymph nodes is negligible. Prins-Braam *et al.* (2004) have investigated the exact location of the most cranial macroscopic metastatic lymph nodes in a group of patients with oropharyngeal and hypopharyngeal squamous cell carcinoma. This study has shown that in this group of N+ patients metastasis rarely appear high cranially on the contralateral side, indicating that the probability for microscopic metastasis in N0 patients must be small.

The irradiation of the retropharyngeal nodes in case of the oropharyngeal tumors remains unclear. As it derives from the clinical experience at our institute and from Prins-Braam *et al.* (2004) no positive retropharyngeal nodes have been found for this type of tumors. It should be noted though that the ipsilateral side of the retropharyngeal nodes is included most of the time at the high dose area. In case of other tumor sites and types such as nasopharyngeal tumors, where irradiation of the retropharyngeal nodes is necessary other values for the mean parotid dose might be obtained.

Other investigators (Eisbruch *et al.*, 1996; Dawson *et al.*, 2000; Maes *et al.*, 2002) have presented conformal and segmental IMRT irradiation techniques to preserve salivary function. The volume of the contralateral parotid gland in the field was

reduced by not irradiating the upper part of the Level II lymph nodes near the base of the skull at the jugular fossa. The reduction of the mean parotid dose and the NTCP was not quantified in these studies. A careful balance between the advantages and disadvantages of adjusting the target volume should be made and therefore quantifying the advantages appear to be necessary.

Comparing the 3D-CRT technique and the proposed IMRT class solution, the mean dose to the parotid glands, the maximum dose to the spinal cord and spinal cord PRV and the volume of the body receiving high dose were substantially reduced by IMRT. This was demonstrated by other studies as well (Chao *et al.*, 2001c; Wu *et al.*, 2000; Eisbruch *et al.*, 1998; van Dieren *et al.*, 2000; Dogan *et al.*, 2002). The proposed IMRT class solution offers similar coverage to the primary tumor PTV and better coverage to the lymph nodes PTVs suggesting similar tumor control rates which is important to know before implementing the new technique in the clinic.

Further reduction of the dose to the parotid glands could be achieved by reducing the PTV margins, using different optimization strategies (Van Asselen *et al.*, 2002), or beam angle optimization. Manning *et al.* (2001) applied the PRV concept to the contralateral parotid gland. The additional margin increased the sparing of the parotid gland but the parotid PRV was preferentially spared at the expense of the elective target coverage. Systematic errors, may both increase or decrease the volume of the parotid gland receiving a high dose (McKenzie *et al.*, 2002). Consequently the mean dose to a small parallel organ like the parotid gland, for a population of patients will only slightly be affected by positioning inaccuracy. Therefore the PRV concept was not used in our planing study for the parotid gland.

In this study it was shown that step-and-shoot IMRT plans obtained using our software and accelerators, deliver dose homogeneity in the target volumes comparable or even better to what is obtained by the conventional technique. This is achieved using a realistic number of beams and segments. The reduction of the NTCP values for xerostomia, when applying IMRT, was very large especially when the cranial border of the Level II lymph nodes was lowered. These findings have been used to initiate a clinical trial in which we compare the measured salivary output after IMRT irradiation with our previously obtained results for conventional radiotherapy.

2.5 Conclusions

Lowering the cranial border of the Level II lymph nodes from the transverse process C1 to the transverse process of C2, in case of bilateral elective neck irradiation of oropharyngeal cancer could be considered on the contralateral side, when the risk of metastasis on that side is very low. Especially when IMRT irradiation is implemented since the relative reduction of NTCP for xerostomia one-year after radiotherapy could be up to 37% with regard to the C1 plans and up to 68% compared to the conventional conformal radiotherapy up to C1.

Chapter 3

Adequate margins for random set-up uncertainties in head-and-neck IMRT

This chapter has been published as: E. Astreinidou, A. Bel, C.P Raaijmakers, C.H. Terhaard, and J.W Lagendijk. 2005. Adequate margins for random set-up uncertainties in head-and-neck IMRT. *Int J Radiat Oncol Biol Phys*. **61(3)** 938-44.

Abstract

Purpose:The aim of our study was to investigate the effect of random set-up uncertainties on the highly conformal dose distributions produced by IMRT for clinical head-and-neck cases, and to determine adequate margins to account for them.

Methods and Materials: We have implemented in our clinical treatment planning system, the possibility of simulating normally distributed patient set-up displacements, translations and rotations. Planning CT data of 8 patients with oropharyngeal cancer, stage T1-T3N0M0, were used. The clinical target volume of the primary tumor, $CTV_{primary}$, and the lymph nodes, $CTV_{elective}$, were expanded with 0.0, 1.5, 3.0 and 5.0 mm in all directions, creating the planning target volumes, PTVs. We performed the IMRT dose calculation using our class solution for each PTV margin, resulting in the conventional static plans. Then the system recalculated the plan, for each positioning displacement derived from a normal distribution with σ=2 mm and σ= 4 mm (1 SD=standard deviation) for translational deviations and with σ= 1^o for rotational deviations. The dose distributions of the 30 fractions were summed resulting in the actual plan. The CTV dose coverage of the actual plans were compared with those of the static plans.

Results: Random translational deviations of σ=2 mm and rotational deviations of σ= 1^o did not affect the $CTV_{primary}$ volume receiving 95% of the prescribed dose, V_{95}, regardless of the PTV margin used. V_{95} reduction of 3% and 1% for 0.0 mm and 1.5 mm PTV margin respectively, was observed for σ=4 mm. The V_{95} of the $CTV_{elective}$ contralateral was approximately 1% and 5% lower, than the static plan, for σ=2 mm and σ=4 mm respectively, and for up to 3.0 mm PTV margins. A further reduction of 1% was observed when rotational deviations were included. The same effect was observed for the $CTV_{elective}$ ipsilateral but with smaller dose difference than those for the contralateral

side. The effect of the random uncertainties on the mean dose to the parotid glands was not significant. The maximum dose to the spinal cord increased by maximal 3 Gy.
Conclusion: The margins to account for random set-up uncertainties, in our clinical IMRT solution, should be 1.5 mm and 3.0mm in case of σ=2 mm and σ=4 mm respectively, for the $CTV_{primary}$. Larger margins however, 5.0 mm, should be applied to the $CTV_{elective}$, if the goal of the treatment is V_{95} of more than 99%.

3.1 Introduction

Clinical evaluation of treatment plans in radiotherapy is based on dose distributions, calculated on a static representation of the anatomy of the patient, with respect to the radiation beams. The unavoidable geometrical uncertainties are taken into account by adding a margin to the clinical target volume (CTV). The dose to this geometrical volume which is called planning target volume (PTV) is assumed to be representative of the dose to the CTV (ICRU Report No. 62, 1999; ICRU Report No. 50, 1993). Defining the optimal PTV margins is very important in order to treat the tumor adequately and at the same time reduce the damage to healthy tissues (Van Asselen *et al.*, 2002). Therefore the geometrical uncertainties of a particular treatment site and technique, and their influence on the dose distributions should be known (Hunt *et al.*, 1993; Mageras *et al.*, 1999; Stroom and Heijmen, 2002).
The geometrical uncertainties originate from the treatment preparation and machine related errors, the day-to-day patient positioning variations and internal organ motion. An error present throughout the whole treatment, causing a displacement of the dose distribution with regard to the intended one, is called a systematic error. Day-to-day variations, causing dose coverage differences to the CTV between fractions, are random errors (Van Herk *et al.*, 2000; Stroom *et al.*, 1999).
The introduction of electronic megavoltage imaging in combination with fiducial markers and immobilization devices enabled an accurate detection of these errors. By using off-line correction procedures, it became possible to reduce the systematic deviations. On-line correction procedures enabled a further reduction of both systematic and random deviations (Gilbeau *et al.*, 2001; Bel *et al.*, 2000; van Lin *et al.*, 2003; De Boer *et al.*, 2001; Dehnad *et al.*, 2003; Nederveen *et al.*, 2001; Pisani *et al.*, 2000; Stroom *et al.*, 1999; Van Asselen *et al.*, 2003; Bel, 2003).
However, even for well fixated head-and-neck patients (Hurkmans *et al.*, 2001) and the use of fiducial markers (Van Asselen *et al.*, 2003), residual set-up errors remain present. Our effort in this study was not to eliminate those errors further but to investigate their influence on head-and-neck intensity modulated radiation therapy, IMRT, dose distributions, in particular that of the random set-up uncertainties.
The random set-up uncertainties are normally distributed in the 3 directions. Their

influence on the dose distribution has been approximated by most of the investigators using convolution of the dose fluence or dose matrix with a Gaussian distribution (Van Herk *et al.*, 2000; Van Herk, 2004; Stroom *et al.*, 1999; McKenzie *et al.*, 2000; Leong, 1987; Beckham *et al.*, 2002; Lujan *et al.*, 1999). With this approach the effect of random deviations has been quantified and certain margins have been proposed (Bel *et al.*, 1996; Van Herk *et al.*, 2000; Stroom *et al.*, 1999; Van Herk *et al.*, 2003).
The convolution method is blurring the dose distribution assuming that the anatomy of the patient remains invariant. Tissue inhomogeneities and body contour variations with respect to the beams as in case of head-and-neck irradiation can violate this assumption (Craig *et al.*, 2003; Cho and Mijnheer, 2002). A small position variation does not necessarily mean a correspondingly small dose variation and vice versa (Leong, 1987).
Additionally most of the margin studies have been performed on geometrical models or verified on conformal dose distributions mainly for prostate irradiation. Therefore the margins might not properly address the complexity of head-and-neck IMRT dose distributions and should be evaluated. IMRT dose gradients are spread out in the anatomy of the patient and they do not confine only to the field edges. Furthermore, the influence of rotational deviations on the dose coverage is not included in the margin *recipes* nor documented for head-and-neck cases.
Therefore we have implemented in our clinical treatment planning system the possibility of simulating the translational and rotational set-up uncertainties. In this way we were able to compare the conventional dose distribution, calculated on a *static* anatomy of the patient, with that derived by calculating and summing the dose for each positioning displacement of the 30 fractions.
Our aim was to investigate the effect of random set-up uncertainties on the highly conformal distributions produced by our IMRT class solution, for clinical head-and-neck cases. Furthermore, we wanted to evaluate whether the current *recipes* produce sufficient margins to account for them. The dose coverage to the CTV, using different PTV margins and calculating with and without simulating random deviations has been quantified. In addition to that the influence of random errors on the dose received by the organs at risk has also been evaluated.

3.2 Methods and Materials

3.2.1 Patients and PTV margin determination

The planning CT scans of 8 patients with oropharyngeal tumor stage T1-T3N0M0 were used for this study. The CT data were obtained with 3 mm slice thickness and were transferred to the radiation treatment planning system (PLATO, Nucletron BV, Veenendaal, NL). The gross tumor volume (GTV), the clinical target volume of the elective lymph nodes $CTV_{elective}$ and the organs at risk (OAR) -

spinal cord, brain and parotid glands - were delineated by a radiation oncologist. Level II-III-IV lymph nodes were included in the $CTV_{elective}$. The cranial border of the Level II lymph nodes on the ipsilateral side was the transverse process of the cervical vertebra C1 and on the contralateral side the transverse process of the cervical vertebra C2 (Astreinidou *et al.*, 2004; Prins-Braam *et al.*, 2004). The GTV was expanded non-uniformly, in three dimensions following the protocol of our institute (2 cm cranial; 1 cm caudal, ventral and medial; 0.5 cm lateral and dorsal) creating the clinical target volume of the primary tumor $CTV_{primary}$.
As the purpose of this study was to quantify the effect of random errors on the CTVs dose coverage, PTV margins were varied. The CTVs were expanded with 0.0, 1.5, 3.0 and 5.0 mm in all directions, creating the PTV of the primary tumor, $PTV_{primary}$, and the lymph nodes, $PTV_{elective}$. When necessary PTVs were adjusted manually to assure a minimal distance of 5 mm between the PTVs and the skin and 1 cm from the spinal cord.

3.2.2 Dose calculation

IMRT plans were made using the inverse treatment planning module PLATO-ITP v1.1 (Nucletron BV, Veenendaal, NL) which is based on an algorithm developed by Bortfeld et al. (Bortfeld *et al.*, 1997; Preiser *et al.*, 1997). The number of beams, dose constraints and penalties were those used clinically since 2002 in the parotid sparing protocol for oropharyngeal cancer and have been reported previously (Van Asselen *et al.*, 2002). Seven equidistant beams, starting at 0 degrees were used and the dose constraints were chosen to deliver simultaneously in 30 fractions 54 Gy to the $PTV_{elective}$ and 66 Gy to the $PTV_{primary}$.
An extra volume around the $PTV_{primary}$ which was named build-up volume, was used in the optimization process. The dose to the build-up volume was the same as that of the $PTV_{primary}$, 66 Gy, but with very low penalty for under-dosage. That means that the dose gradient from the 66 Gy of the $PTV_{primary}$ to the 54 Gy of the adjacent ipsilateral $PTV_{elective}$ and to the 40Gy of the body, is shifted within that volume. In this way under-dosage of the $PTV_{primary}$ was avoided and the 95% isodose highly encompasses the $PTV_{primary}$.
The theoretical fluence, with a continuous intensity distribution was converted into discrete intensity levels for step-and-shoot IMRT, delivered by a multi-leaf collimator (SL25, Electa Oncology Systems, Crawley, UK). Then the deliverable fluence was transferred to the PLATO-RTS v2.6 module for the final dose calculation with 1x1x3 mm^3 resolution. The calculation algorithm is a pencil beam model with an inhomogeneity correction method based on the equivalent tissue-air ratio (ETAR) method (Bortfeld *et al.*, 1993; Yu and Wong, 1993).
The dose calculation was performed for each PTV margin resulting in 4 *static* dose distributions per patient. The *static* dose distribution, σ= 0 mm, or *static* plan represented the intended plan which is used for evaluation in the every day clinical routine. Next to the conventional dose calculation we performed a calculation

simulating the daily random set-up deviations. A random generator produced patient displacements in all three directions derived from a normal distribution with standard deviation (1 SD) of σ=2 mm and σ=4 mm. The system recalculated the dose for each set-up deviation and summed the dose distributions of the 30 fractions resulting in the *actual* dose distribution or *actual* plan. The simulated calculation time was about 6-8 minutes per beam (Fuel 600 system, Silicon graphics).
The σ-value of 2 mm is in the order of what has been reported in the literature (1.3 - 2.1 mm) and measured at our institute (1.4 - 1.6 mm) for head-and-neck-treatment using immobilization masks (Hurkmans *et al.*, 2001). The σ-value of 4 mm has been used to check the linearity of the *recipes* and examine the influence of larger random errors than those reported. On those plans that the PTV margin was considered to be sufficient to account for translational random errors (99% or more of the CTV received 95% of the prescribed dose) we applied rotational deviations (1 SD) of σ=1^o as well in all 3 directions. In this way we investigated the additional effect of rotational uncertainties. The center of rotations was the isocenter which was located in the center of gravity of the primary oropharyngeal tumors for this group of patients.

3.2.3 Plan evaluation

The dose distribution of the *actual* plan was compared and subtracted from that of a *static* plan in order to visualize where and whether differences occur between the intended and the *actual* dose. To evaluate the CTV dose coverage, the CTV volume receiving 95% of the prescribed dose, V_{95}, and the mean dose were compared for each margin and set-up deviation with that of the *static* plan. The V_{95} has been used in the literature as the dose level criterion to produce the margin recipe of 0.7 x σ (Bel *et al.*, 1996; Van Herk *et al.*, 2000; Stroom *et al.*, 1999) and was consequently used in this study as evaluation parameter for choosing adequate margins.
Additionally the effect of the random set-up translational and rotational deviations on the dose volume histograms of each plan was evaluated. Furthermore the effect to the OARs was determined. As the spinal cord is considered to be functionally organized as serial organ the maximum dose to it for each *actual* plan was extracted and compared to that of the *static* plan. For the parotid gland the mean dose was reported as it is considered to be a parallel organ.

3.3 Results

Dose differences between the *static* and *actual* plan were mainly observed near the cranial and caudal field boundaries because of the steep dose gradients in those directions (Figure 3.3). These differences varied per patient and σ-values and

ranged from ±8 Gy to ±12 Gy. Near the edges of the dose gradient between the $CTV_{elective}$ and the spinal cord the dose was 2 to 4 Gy higher than the *static* one. Differences of approximately ±2 to ±5 Gy where observed at other parts of the non-delineated tissue such as skin and at the back of the neck.

3.3.1 Plan evaluation

The coverage of the CTVs obviously increased as the PTV margins increased (Figure 3.1). Random translational deviations of σ=2 mm in all directions did not affect the V_{95} value of the $CTV_{primary}$ regardless of the PTV margin used indicating that the PTV margins were sufficient. A reduction of 0.3% for a PTV margin of 0.0 mm was observed. Deviations from the V_{95} of the *static* plan, were seen for σ=4 mm in combination with a PTV margin of 0.0 mm and 1.5 mm (Figure 3.1).

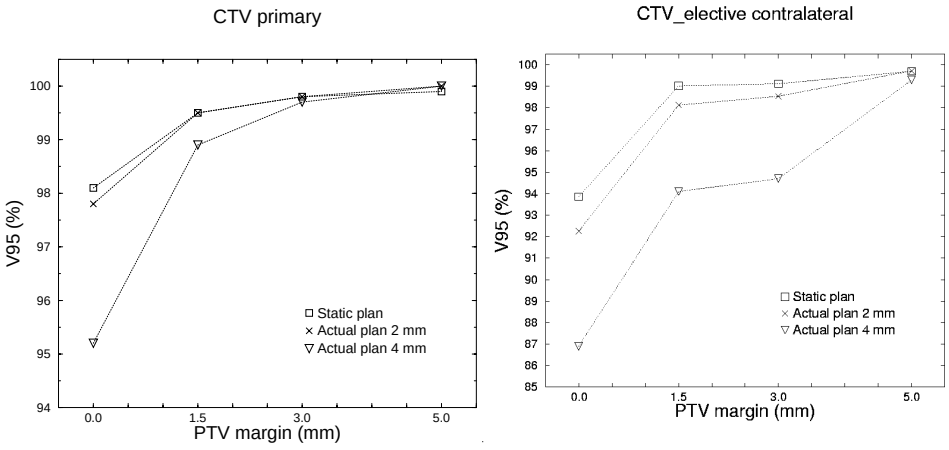

(a) (b)

Figure 3.1: The percentage (%) of the CTV volume receiving 95% of the prescribed dose (V_{95}) as a function of the PTV margin, averaged for the 8 patients. The V_{95} was calculated for the *static* plan and for random translational set-up deviations of σ=2 mm and σ=4 mm, the *actual* plans. a) $CTV_{primary}$ b)$CTV_{elective}$ contralateral. (The standard deviation of the average values is given in Table 3.1, and not plotted here for the clarity of the graph.

The mean dose to the CTVs of the *static* plans was similar to that of the *actual* plans with σ=2 mm and reduced approximately by 1-1.5 Gy for the *actual* plans

Table 3.1: CTV coverage

PTV margin	V_{95}(SD)%			Mean Dose		(SD)Gy
	σ=0 mm	σ=2 mm	σ=4 mm	σ=0 mm	σ=2 mm	σ=4 mm
$CTV_{primary}$						
0.0 mm	98.1(1.5)	97.8(1.4)	95.2(1.9)	66.7(1.1)	66.4(1.2)	65.8(1.2)
1.5 mm	99.5(0.8)	99.5(0.6)	98.9(1.0)	67.4(0.5)	67.3(0.6)	66.9(0.7)
3.0 mm	99.8(0.5)	99.8(0.4)	99.7(0.3)	67.6(0.4)	67.4(0.4)	67.0(0.5)
5.0 mm	99.9(0.2)	100.0(0.0)	99.9(0.1)	67.6(0.3)	67.6(0.3)	67.2(0.3)
$CTV_{elective}$ ipsilateral						
0.0 mm	96.3(1.4)	95.1(1.5)	91.2(2.2)	57.0(1.6)	56.6(1.6)	55.7(1.7)
1.5 mm	99.7(0.2)	99.3(0.5)	96.9(1.9)	57.9(1.6)	57.7(1.5)	57.1(1.8)
3.0 mm	99.8(0.1)	99.4(0.4)	97.2(1.7)	58.4(1.7)	58.2(1.7)	57.6(1.9)
5.0 mm	100(0.0)	99.9(0.1)	99.4(0.5)	58.9(1.8)	58.5(1.9)	58.1(2.0)
$CTV_{elective}$ contralateral						
0.0 mm	93.8(1.0)	92.2(1.2)	86.9(1.6)	54.8(0.5)	54.3(0.5)	53.2(0.5)
1.5 mm	99.0(0.8)	98.1(1.2)	94.2(3.1)	55.6(0.5)	55.2(0.5)	54.5(0.5)
3.0 mm	99.2(0.6)	98.3(1.1)	94.3(3.0)	55.4(0.5)	55.1(0.5)	54.4(0.6)
5.0 mm	99.7(0.5)	99.7(0.4)	99.3(0.5)	55.7(0.7)	55.6(0.8)	55.2(0.7)

The percentage (%) of the CTV volume receiving 95% of the prescribed dose, (V_{95}) and the mean dose for each margin, 0.0, 1.5, 3.0 and 5.0 mm and set-up deviation σ=2 mm, σ=4 mm. SD=1 standard deviation.

with σ=4 mm (Table 3.1).
The coverage of the $CTV_{elective}$ ipsilateral was higher than that of the contralateral but random deviations influenced it in a similar way. It should be noted that the V_{95} coverage was similar, with and without the random set-up deviations, for plans with PTV margin of 1.5 mm and 3.0 mm.
Rotational errors had no effect on the coverage of $CTV_{primary}$ but influenced slightly that of the $CTV_{elective}$ (Figure3.2). A maximum reduction of the V_{95} by 1% was observed for the contralateral $CTV_{elective}$.

3.3.2 Organs at Risk

The average maximum dose to the spinal cord (± 1 SD) for this group of patients, was 33 ±1.6 Gy for all margins and *static* plans. An increase of 0.6 ±0.4 Gy was obtained for the *actual* plans with σ=2 mm. For the *actual* plans with σ=4 mm the increase was 1.3 ±0.8 Gy, 1.6 ±1.0 Gy, 2.0 ±1.0 Gy and 3.0 ±0.8 Gy as the PTV margin increased respectively.
The average mean dose to the parotid glands (±1 SD) for this group of patients, was 29 ±7 Gy, 31 ±6 Gy, 33 ±6 Gy and 36 ±6 Gy, for 0.0 mm, 1.5 mm, 3.0 mm and 5.0 mm PTV margin respectively. Taking into account the random set-up errors

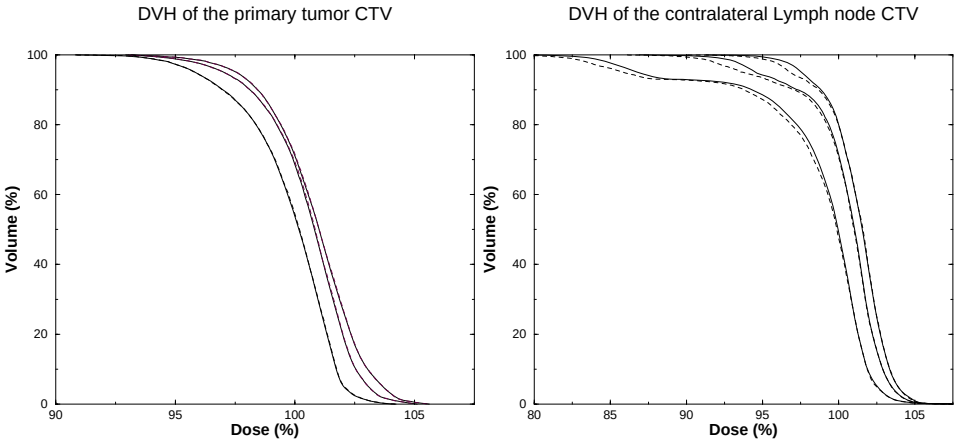

(a) (b)

Figure 3.2: A typical example of the DVH a) $CTV_{primary}$ and b) $CTV_{elective}$ contralateral, for one of the patients, calculated with a PTV margin of 1.5mm . Solid lines from right to the left represent the calculations performed with translational deviations of σ=0 mm, σ=2 mm and σ=4 mm respectively. Dashed lines represent the same calculations with additional rotational deviation of σ=1^o.

in the dose calculation resulted only in very small variations, increase or decrease, in the mean dose of the parotid glands. Variations of approximately $\pm$0.4 Gy and $\pm$0.7 Gy for σ=2 mm and σ=4 mm respectively were observed.

3.4 Discussion

We have implemented a tool in our clinical treatment planning system which can simulate translational and rotational set-up errors. Using that tool we evaluated the influence of random set-up errors on clinical head-and-neck IMRT dose distributions produced by our class solution (Van Asselen *et al.*, 2002). The *actual* dose delivered to the $CTV_{primary}$ and $CTV_{elective}$ when random errors were taken into account was less than the intended dose, calculated by the *static* plan (Figure 3.2). The impact of random errors on the V_{95} of the $CTV_{primary}$ was almost negligible for small, clinically relevant, random errors σ=2 mm, regardless of the PTV margin used. On the other hand the V_{95} of the $CTV_{elective}$ was more sensitive to translational and rotational random errors, especially on the contralateral side.

As proposed by several groups a margin of 0.7 x σ should be applied to assure that 99% of the CTV receives 95% of the prescribed dose (Stroom *et al.*, 1999; Van Herk *et al.*, 2000). Applying that to our clinical IMRT cases implies that 1.5 mm and 3.0 mm margins should be adequate for σ=2 mm and σ=4 mm respectively. Our results (Figure 3.1) indicate that for the $CTV_{primary}$ these margins were indeed sufficient. Even for a PTV margin of 0.0 mm the reduction of the V_{95} was very small, about 0.3%. But when the σ increased from 2 mm to 4 mm the effect on the V_{95} did not increase analogously. A reduction of almost 3% was observed demonstrating that the influence of the random errors was not linear.
For $CTV_{elective}$, however, larger margins were required. That could be explained by the fact that the shape of the $CTV_{elective}$ deviates strongly from the spherical model for which the above formula was derived (Fontenla *et al.*, 1996). Furthermore, IMRT produces sharp dose gradients in all directions around the $CTV_{elective}$ due to their location with respect to the body surface and spinal cord. Dose conformality was more difficult for those volumes. Moreover, the dose differences occurring near the cranial and caudal field boundaries were up to 12 Gy. Since the cranio-caudal field limits were defined mostly by the $CTV_{elective}$, the coverage of the $CTV_{elective}$ was more influenced by those differences. This result suggests that a larger margin should be applied in the cranio-caudal direction and that is in agreement with the asymmetrical margins proposed by McKenzie *et al.* (2000). That applies mainly to the $CTV_{elective}$ contralateral. On the ipsilateral side, part of the $PTV_{elective}$ is overlapping with the $PTV_{primary}$ where a dose of 66 Gy was prescribed. That means that when set-up deviations occurred from the cranial to the caudal direction, higher dose area was entering to the $CTV_{elective}$ ipsilateral volume while the opposite happened to the $CTV_{elective}$ contralateral volume.
When applying margins in clinical plans the limitations of the calculation resolution should be taken into consideration as well. As it was shown in Table 3.1 the $CTV_{elective}$ coverage for 1.5 mm and 3.0 mm margins were similar. In both cases the margin in the cranio-caudal direction was 3.0 mm due to the slice thickness in that direction resulting in almost the same volume for the optimization. Moreover, the linearity of the margins produced by the *recipes* might not be valid in all clinical cases and target volumes as it was shown by our results. The tool implemented in our planning system could be used to evaluate individual clinical dose distributions in the presence of set-up uncertainties.
The PTV margin required to provide an adequate CTV coverage for IMRT planning accounts not only for the set-up errors. It depends also on whether the inverse optimization solution provides an acceptable solution. As shown in Table 3.1 the dose coverage values for 0.0 mm PTV margin which practically means that CTV equals the PTV, were in accordance with those reported for the PTV by an earlier study evaluating our IMRT class solution (Astreinidou *et al.*, 2004). In practice though 0.0mm PTV margin would not be used even if the effect of the random error was negligible. Expanding the CTV volume with at least 1 voxel possible

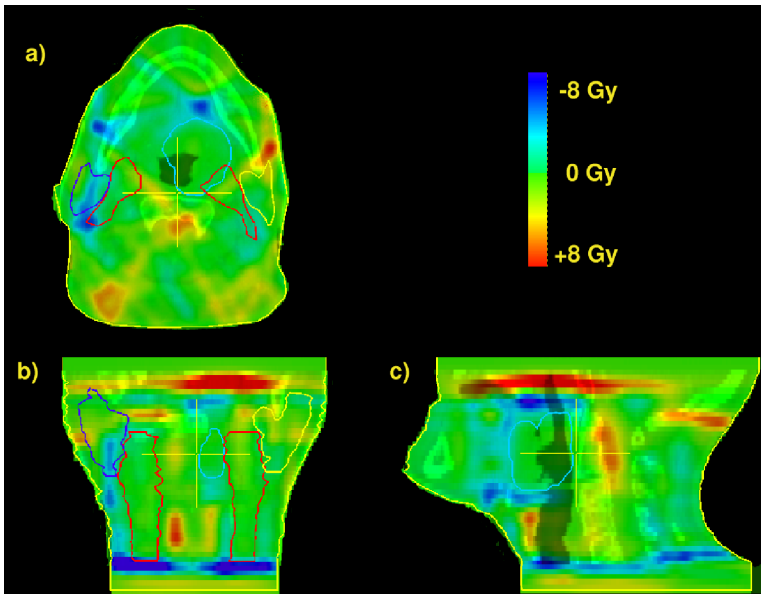

Figure 3.3: a) Transverse, b) coronal and c) sagittal plane of the dose difference map between an *actual* plan, with random translational set-up deviation of σ=4 mm and a *static* plan, σ=0 mm, calculated for 3.0 mm PTV margin, for one of the patients. The dose difference map is projected on the CT and the solid lines are the delineated volumes, red=$CTV_{elective}$, light blue=$CTV_{primary}$, dark blue=right parotid gland, yellow=left parotid gland. The dose prescription was 66 Gy to the $CTV_{primary}$ and 54 Gy to the $CTV_{elective}$in 30 fractions. The colors indicate where in the patient's anatomy more dose, red, or less dose, blue, was actually received.

discretization problems diminish and the IMRT delivers adequate coverage.
Rotational set-up deviations seem to have a negligible effect on the dose distributions derived by our class solution. It should be noted however that as was observed for the translational deviations the effect of rotational deviations was different for the $CTV_{primary}$ and $CTV_{elective}$. The origin of rotations was the isocenter but in clinical practice the rotation would probably be around the axis through the spine. That might affect the dose coverage of the $CTV_{elective}$ less and that of the $CTV_{primary}$ more than that observed in Figure 3.2.
The mean dose to the parotid glands increased as the PTV margin of the $CTV_{elective}$ increased and that is in agreement with van Van Asselen *et al.* (2002). The random positioning deviations had almost no effect on the mean parotid dose. The

maximum dose to the spinal cord, however, could increase by 3 Gy for σ=4 mm, but still it was much lower than the acceptable upper limit of the 45 Gy. In case that the maximum dose to the spinal cord is already close to the upper acceptable limit already at the *static* plan the use of the planning organ at risk volume, PRV, should be considered (ICRU Report No. 62, 1999).

The systematic component which is not known a priori for each individual case, was not included in our simulated calculations but eventually it should. Samuelsson *et al.* (2003) have investigated the influence of systematic errors on IMRT head-and-neck dose distributions. The worst case scenario of 5 mm displacements in all directions and for the whole course of the treatment was examined. The ICRU approach of adding margins was considered sufficient for the IMRT cases but the case of elective target volumes was not investigated. Various correction protocols have been proposed in order to early detect and correct for the systematic errors up to a certain limit of course (Wyman *et al.*, 2002; Xing *et al.*, 2000; Bortfeld *et al.*, 2002; De Boer and Heijmen, 2001). Van Asselen *et al.* (2003) have shown that it is feasible to use fiducial markers in head-and-neck cases. That approach could contribute in minimizing set-up errors. Another approach would be the off line daily correction protocol proposed by Bel (2003). With this approach systematic deviations could be virtually eliminated at the price of increasing the random deviations. In all cases though a residual systematic error still remains. Our simulated calculations should be extended to include a number of these systematic deviations as well.

Our approach, based on the brute force method, is recalculating the dose for each fraction and set-up deviation. That is possible in an acceptable time for immediate clinical use and evaluation of all plans, whether they are IMRT or conventional. Eventually the tool should be used not only to evaluate whether the margins used were adequate for an individual patient case but also to modify them if necessary. However, ideally all the known uncertainties should be taken into account already in the optimization process. Lof *et al.* (1998) have presented a sophisticated algorithm for IMRT, by dynamically refining the beam configuration from fraction to fraction, accounting for the set-up uncertainties.

However, systematic errors due to the delineation uncertainties of the target volumes are not eliminated by the above mentioned correction procedures. These systematic errors could only be reduced by advances in imaging modalities and image registration (Nishioka *et al.*, 2002).

Calculations have been repeated for different set of displacements of the same σ, by choosing different number of seeds at our random generator. That resulted in almost the same dose distributions and evaluation parameters. Therefore we believe that the average dose parameters reported in this study for this group of patients were representative of the effect of the random errors on the IMRT dose distributions. Due to the finite number of fractions used by our calculation a systematic error of about 0.36 mm SD and 0.73 mm SD for σ=2 mm and σ=4 mm

was introduced respectively. Such residual errors which are ignored by the convolution methods will be present in fractionated radiotherapy (Van Herk *et al.*, 2003; Van Herk, 2004).
The decision of which margins should be applied to account for random errors should include some biological considerations as well (Van Herk, 2004). The results of this study indicate that the $CTV_{primary}$ dose coverage was almost unaffected by the clinically observed random errors, σ=2 mm, for all margins above 0.0mm, suggesting similar tumor control probability (TCP) values. However, the $CTV_{elective}$ dose coverage was reduced significantly especially for larger random errors, σ=4 mm. Since the probability of microscopic disease is relatively low, approximately 30% in our clinical experience, V_{95} values lower than 99% for the $CTV_{elective}$ are accepted in practice. Therefore, the dose reduction to the $CTV_{elective}$, due to the random set-up uncertainties, observed in this study, does not reflect necessarily similar reduction of TCP values. These effects have to be investigated further by using appropriate TCP models and the clinical output from IMRT studies.

3.5 Conclusion

The margins to account for random set-up uncertainties in our clinical IMRT solution, should be 1.5 mm and 3.0mm for σ=2 mm and σ=4 mm respectively, for the $CTV_{primary}$. Larger margins however, 5.0 mm, should be applied to the $CTV_{elective}$, if the goal of the treatment is V_{95} of more than 99%. These findings confirm that the recipe 0.7 x σ produce sufficient margins for the $CTV_{primary}$ but not for the $CTV_{elective}$.

Chapter 4

Parotid volume reduction after head-and-neck radiotherapy

This chapter is part of the manuscript submitted as: E. Astreinidou, J. Roesink, C.P Raaijmakers, T. Witkamp, H. Dehnad, W. Bartels, and C.H. Terhaard. 2006. Parotid volume reduction after head-and-neck radiotherapy. *Int J Radiat Oncol Biol Phys.*

Abstract

Purpose: To quantify the parotid gland volume reduction at specified time intervals after head-and-neck radiotherapy using MR imaging and evaluate a methodology to investigate the spatial distribution of the parotid gland volume changes with regard to the dose distribution.

Materials and Methods: Nine patients, treated with primary or post-operative irradiation for T1-4N0-2M0 nasopharyngeal or oropharyngeal cancer, were included in the study. Seven of these patients were treated with IMRT and two with 3D-conformal RT. T_1-weighted and T_2-weighted MR scans were performed on a 1.5-T MR scanner before RT, 6 weeks and 6 months after RT. A record of the patient's weight was kept and stimulated salivary flow measurements were carried out at the same time intervals, as well. Patients were scanned in the same immobilization mask used for RT treatment. Image registration of the MR scans and the planning CT was performed. The parotid gland volumes before and after RT were compared with a paired t-test and the pearson's correlation, r, was used to correlate any volume changes with various dose parameters such as the mean dose and the salivary flow measurements.

Results: Parotid gland volume reduction of 24 % (SD 11 %) and 21 % (SD 13%) was observed at 6 weeks and 6 months after RT, respectively. The average mean dose to the parotid gland for this group of patients was 35 Gy. No correlation was found between the volume reduction and the mean dose and with the salivary flow. A correlation between the weight loss and the volume reduction was observed ($r = 0.58$). Image registration was inspected visually and it was considered to be satisfactory in all cases. The shrinkage of the parotid gland was in some cases more pronounced in the medial part.

Conclusion: In this study the parotid glands volumes after RT were not only compared to those before treatment quantitatively by their size but also qualitatively by successful

image registration. An average parotid gland volume reduction of 24% at 6 weeks after RT persisted at 6 months after RT. The reduction appeared in all directions and sometimes more in the medial part and it correlated with the weight loss of the patients rather than the dose or the salivary output.

4.1 Introduction

Radiation-induced xerostomia is a common side effect suffered by patients receiving radiation therapy for nasopharyngeal and oropharyngeal cancer (Roesink *et al.*, 2004). With the introduction of intensity modulated radiation therapy (IMRT) it became possible to deliver highly conformal doses to the targets, primary tumour and cervical lymph nodes resulting in reduction of the mean dose the parotid glands more than the conventional and 3 dimensional conformal radiotherapy (3D-CRT) techniques (Butler *et al.*, 1999; Chao *et al.*, 2002; Van Asselen *et al.*, 2002). This is because of the high dose gradients produced by IMRT within the glands in contrast to the more homogeneous dose distribution produced by the conventional techniques. Depending on the position of the primary tumour and the involvement of the cervical lymph nodes the caudal-medial part of the parotid glands could receive a dose as high as 54 to 66 Gy but the lateral-cranial part could receive dose as low as 5 Gy with IMRT (Astreinidou *et al.*, 2004).
It is assumed that the parotid gland reacts as a parallel organ to the radiation damage; therefore the mean dose to the whole organ is used as dose constraint for the IMRT planning. However, regional differences in gland radiosensitivity were observed in an animal model. Experiments irradiating partially and fully the parotid glands of rats have shown different degree of late radiation damage depending on which part of the gland, upper or lower, was irradiated (Konings *et al.*, 2005b,c). Thus, it is quite important to know whether there is a similar dependency on the human parotid gland, in order to steer the dose with IMRT properly.
Similar studies in humans are not applicable, but based on human studies the mean dose leading to a complication probability of 50% for xerostomia 1 year after the end of the treatment was found to be 26 Gy for a group of patients treated with intensity modulated techniques and 39 Gy for a group of patients treated with lateral opposed fields (Roesink *et al.*, 2004; Eisbruch *et al.*, 1999). The question that arises from those data is whether the dose-response difference could be explained by the difference in the dose distribution within the glands.
An option would be to use imaging to record radiation-induced changes to the parotid glands and investigate whether there is spatial dose dependence to these changes. It has already been reported that one of the radiation-induced changes to the parotid glands is volume reduction. A parotid volume reduction of up to 50% was observed at 4-6 months after the end of the treatment that persisted even 1 year after radiotherapy. These observations were based on magnetic resonance, MR, imaging that was performed before and after RT (Nomayr *et al.*, 2001).

Figure 4.1: Patient positioning at the MR scanner. The immobilization mask is the same as used during radiotherapy. On the masker the two circular surface coils, FLEX L, are placed.

Another recent study based on repetitive computerised tomography (CT) imaging during the treatment reports a volume reduction of 0.6 % per day for 35-day treatment duration (Barker *et al.*, 2004). Nevertheless no inter- or intra-observer variability was given. In both studies, however, conventional radiation techniques were used, no information on the location of the volume changes was given and the influence of those changes on the salivary function was not investigated.
A pilot study was conducted that included patients treated with IMRT in order to study the radiation-induced volume changes to the parotid glands on specified time intervals, 6 weeks and 6 months, after radiotherapy using MRI. It was further investigated whether image registration of the MRI scan before RT with those after RT and with the planning CT can be used to evaluate the location of the volume reduction with regard to the dose distribution. Moreover, salivary flow measurements were performed at the same time intervals as the MRI scans.

4.2 Materials and Methods

Nine patients, treated with primary or post-operative irradiation for T1-4N0-2M0 nasopharyngeal or oropharyngeal cancer, were included in the study. Seven of these patients were treated with IMRT and two with 3D-conformal RT.
MR imaging was performed on a 1.5-T system (Intera, Philips Medical Systems,

Best, NL) using a 2 element circular coil (FLEX L) with opening diameter 170 mm. The patients were positioned in the MR scanner with the RT immobilization mask, as in the treatment position (Figure 4.1). The MRI protocol was performed before RT, at the same day as the planning CT and repeated 6 weeks and 6 months after RT. Before each follow up MR scan, it was checked whether the RT immobilization mask was still fitting and the patient was still feeling comfortable in it. The MRI protocol included T_1- and T_2-weighted spin echo imaging of the head-and-neck. The T_1- weighted scan parameters were: slice thickness 3.0 mm, number of slices 30, slice gap 1.0 mm, field of view (FOV) $256x256$ mm^2, acquisition matrix and reconstruction matrix $256x256$, resulting in a total scan duration time of 2.5 minutes. The T_2- weighted scan parameters were: slice thickness 4.0 mm, number of slices 20, slice gap 1.5 mm, field of view (FOV) $256x256$ mm^2, acquisition matrix $200x200$ and reconstruction matrix $256x256$, resulting in a total scan duration time of 3.5 minutes.
Salivary flow measurements were performed at the same time intervals and often at the same day, directly after the MRI scan. Stimulated parotid saliva was collected from both parotid glands, simultaneously, with Lashley cups. Stimulation was achieved by applying 50 μl of a 5% acid solution to the mobile part of the tongue every 1 minute, and saliva collection was carried out for 10 minutes (Roesink *et al.*, 2004). On the day of the salivary flow measurements the weight of the patients was recorded as well.

4.2.1 Parotid gland delineation

The analysis of the scans was performed using in-house developed software that allowed us to visualize the transversal, coronal and sagittal view of the dataset together. Additionally, both T_1 and T_2-weighted datasets were simultaneously analysed using the *"linked cursor"* approach. Both datasets had the same coordinate system, therefore when the location of a point in one dataset was selected, a visible mark was positioned automatically at the corresponding location in the *"linked"* dataset (Bol *et al.*, 2003). Thus any selected point of the datasets was viewed not only in all three dimensions but also on both scan sequences simultaneously. This property was used during the delineation process.
Delineation of the parotid glands was performed on the T_1-weighted datasets but practically information from both sequences was eventually used as the delineated contour was projected on both of them Figure 4.2. Two observers delineated the parotid gland volumes and consensus was reached. Then an experienced radiologist was involved to approve the definite parotid volumes.
A paired t test was used to compare the parotid volumes before RT with those after RT and with the parotid gland volumes as delineated on the planning CT. The differences were considered to be statistically significant when $p < 0.05$. In order to have an estimate of the intra-observer variability 6 parotid glands were

delineated 3 times for all MR scans, before RT and after RT. The coefficient of variation, CV, was calculated according to the equation:
(standard deviation (SD)÷ mean volume) x 100 %.

4.2.2 Image registration

Image registration of the CT and the T_1-weighted spin echo imaging before RT was performed using a mutual information algorithm (Ceylan *et al.*, 2005). In this way the 3D-dose distribution could be registered on the MRI scan. The MRI scans 6 weeks and 6 months after RT were also registered to the MRI scan after RT. The image registration was inspected visually using the *"linked cursor"* approach described above. The registration was considered to be good when there was a successful match of the body contour, base of the skull, brain tissue and other recognizable structures such as blood vessels and bony structures. When the image registration was considered to be successful the parotid volumes after RT were superimposed on the MRI scan before RT and the other way around, in order to examine the location of the volume differences. The same was applied to the CT and MRI parotid volume comparisons.
Furthermore, we investigated whether there was a correlation between the parotid gland volume reduction with dose parameters such as mean dose, maximum and minimum dose, dose to 90%, 50% and 10% of the parotid volume as delineated on the MRI before RT. The correlation between the parotid volume and the parotid volume reduction after RT with the weight of the patient and the salivary flow measurements was also investigated using the pearson's correlation coefficient r.

4.3 Results

MR imaging was performed successfully and it was well accepted by all 9 patients. One patient was lost from the 6 months after RT follow up. The repositioning of the RT immobilization masks at 6 weeks and 6 months after RT was still good and there was no need of remaking the masks. The image registration was inspected visually and it was considered to be satisfactory in all cases. The body contours were in good agreement and no differences larger than 2 to 3 voxels (2-3 mm) were observed when checking on specific anatomical landmarks, such as bony structures.

4.3.1 CT-MRI comparison

The average parotid gland volume for this group of patients, as delineated on the MRI scan before RT, was 23 cc (standard deviation=SD 10 cc) and it was not significantly different (p=0.19) from the parotid volume as delineated on the planning CT, 22 cc (SD 8 cc). The range of the volume differences between CT

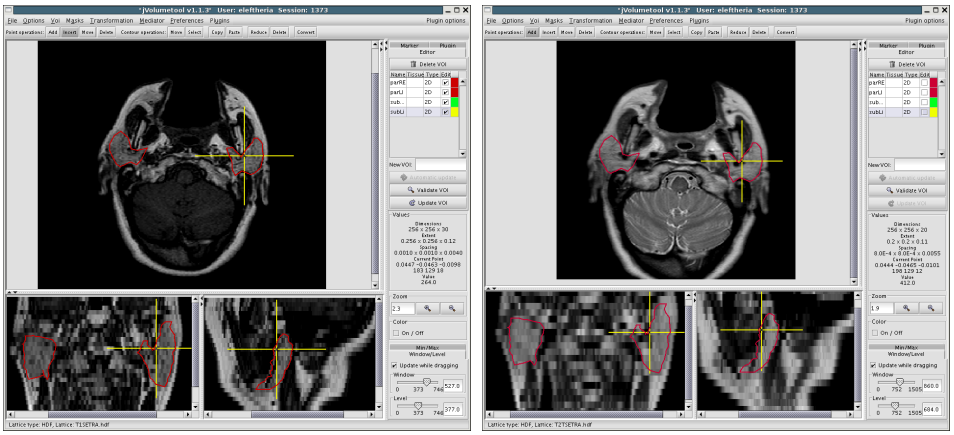

(a) (b)

Figure 4.2: Screen shot of the volumetool, in-house developed software used for the delineation of the parotid glands (a) T_1-weighted MR scan and (b) T_2-weighted MR scan. The transversal plane, and the reconstructed coronal and sagittal planes are displayed at the same window for each scan. The red contours are the delineated parotid glands and the yellow cursor represents the same location in the patient because (a) and (b) are *"linked"*.

and MR was ±5 cc and occurred mostly in the cranial and caudal-medial part of the parotid glands. In one case the difference in volumes was 12 cc, but in that case the auxiliary parotid gland was not delineated on the CT Figure 4.3.
The dose calculation was performed using the parotid gland volumes delineated on the CT. The average mean dose to the parotid glands was 34 Gy (SD 12 Gy). After the image registration of the MR scans with the planning CT, the dose distribution could be superimposed on the MRI. The average mean dose to the MRI parotid gland volumes was 35 Gy (SD 13 Gy) and not significantly different (p=0.43) from that calculated for the CT parotid volumes. For individual parotid glands, however, the dose differences ranged up to ±9 Gy. For the rest of the analysis the mean dose to the MRI parotid gland volumes was used.

4.3.2 MRI-MRI comparison

An average parotid gland volume reduction of 24% (SD 11%) and 21% (SD 13%) was observed at 6 weeks and 6 months after RT, respectively compared to the parotid volume before RT. The volume reduction after RT was statistically signif-

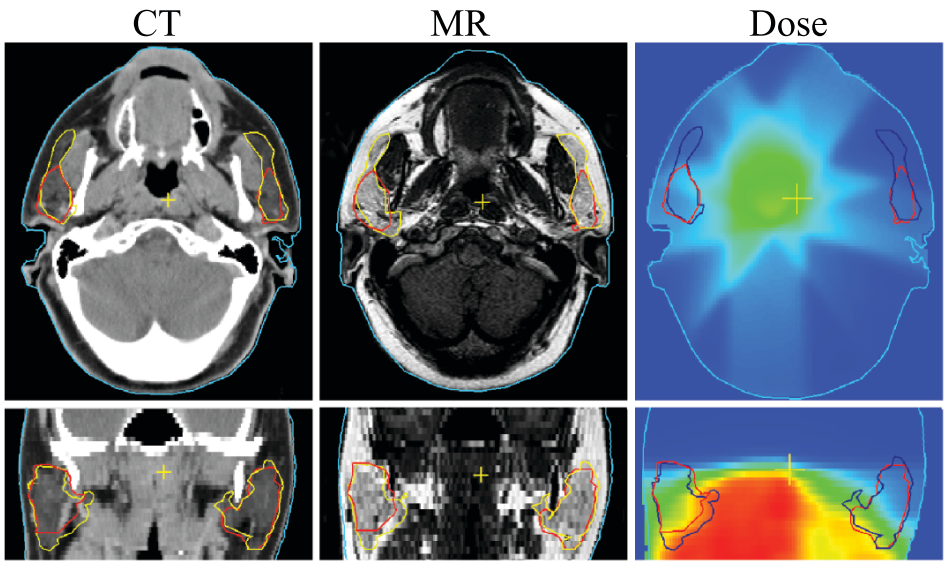

Figure 4.3: Registered transversal (top row) and coronal (bottom row) planes of the CT and MR scans of one patient pre-RT, and the dose distribution at the same planes. The red contours are the parotid glands, as delineated on the CT, and the yellow contours are the parotid glands as delineated on the MR. For clarity, the latter are given in dark blue on the dose distribution planes.

icant (p <0.05). The parotid gland volumes at 6 months after RT, however, were not found to be statistically significant different from those at 6 weeks after RT, (p=0.44) (Figure4.4). The CV for repeated delineation was 8% (SD 2%). No correlation or trend was found between the volume reduction and dose parameters such as the mean dose (Figure 4.5), maximum and minimum dose and dose to 90%, 50% and 10% of the volume. The weight loss for this group of patients was on the average 10% (SD 5%) at 6 weeks post RT and remained so at 6 months after RT. The pearson's correlation coefficient between the parotid volume and the patient's weight before RT and 6 weeks after RT was r=0.89 and r=0.83, respectively. The correlation between the weight loss and the volume reduction was less stronger, r=0.58.

The overall impression was that the shape of the parotid glands was similar to that before RT but smaller. However, in some patients it appeared that the shrinkage of the parotid volume was mostly in the medial part of the glands. The patient example in Figure 4.6 represents the average situation for this group of patients.

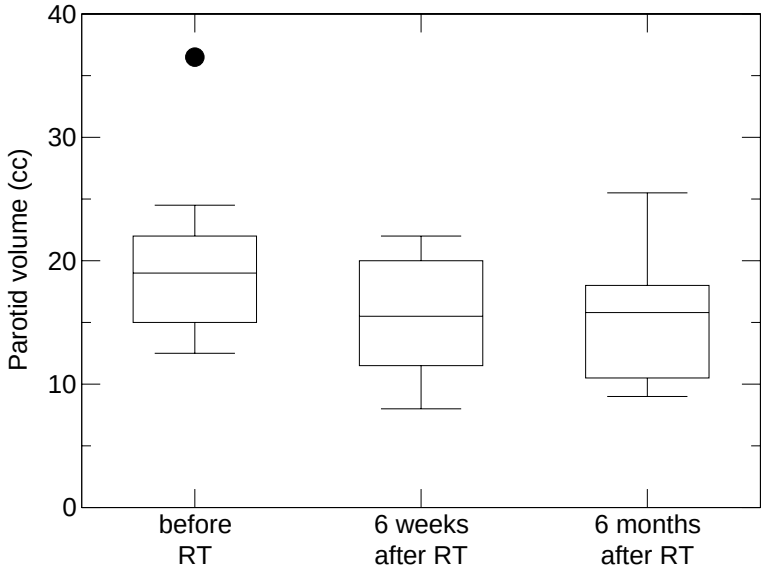

Figure 4.4: Mean dose to the parotid glands before RT and at 6 weeks and 6 months after RT.

Salivary flow measurements were successful in all 9 patients before RT and in 8 after RT. That patient, who was excluded from the analysis, experienced pain at the floor of the mouth during stimulation with the citric acid after RT and the measurement had to be stopped.

The average amount of saliva collected from the parotid glands in 10 minutes, was 1.72 ml before RT, 0.32 ml and 0.28 ml 6 weeks and 6 months after RT, respectively. The parotid glands that produced some saliva was after RT were those, n=4, that received a dose <20 Gy and two glands that had an auxiliary parotid gland. From the rest of the parotid glands no saliva was collected. There was neither a correlation between the parotid volume and salivary flow before RT nor between parotid volume reduction and salivary flow reduction after RT.

4.4 Discussion

In this study, the parotid gland volume was investigated before and at specified time intervals after head-and-neck irradiation using MR imaging. An average volume reduction of 24% (SD 11%) was observed at 6 weeks after the end of the treatment, with no significant signs of improvement at 6 months after the end of

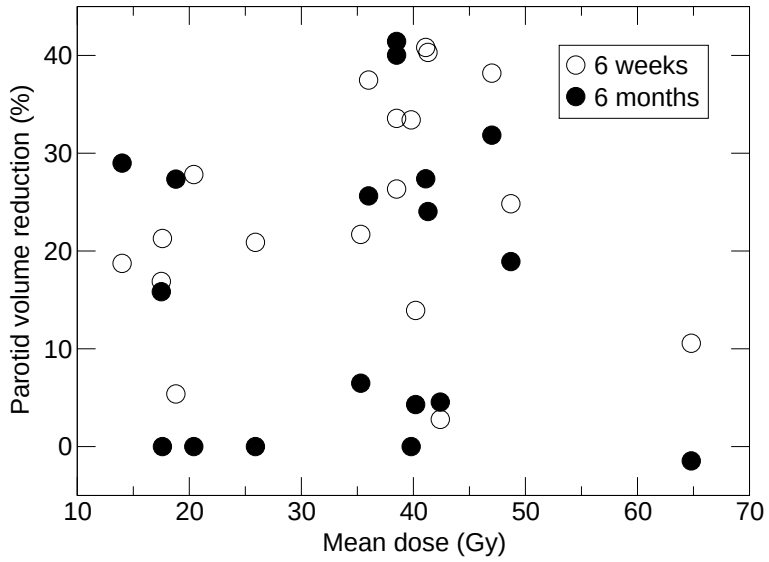

Figure 4.5: Parotid volume reduction expressed in % at 6 weeks and 6 months post-RT versus the mean dose to the parotid gland

treatment (Figure 4.4). Similar results were reported by Nomayr *et al.* (2001) who also used MRI for the delineation of the parotid glands. Nevertheless, the spatial distribution of those changes with regard to the dose distribution, especially after the implementation of IMRT techniques has been neither investigated nor reported.

The use of the same RT immobilization mask every time the patient was scanned resulted in successful image registration that allowed us to compare the parotid volumes before and after radiotherapy with each other and with the dose distribution. Based on qualitative evaluation of the registered images it appeared that there was shrinkage of the whole parotid gland, which in some cases was more pronounced in the medial part (Figure 4.6).

The majority of the patients in this study received IMRT treatment and the mean dose to the parotid glands was between 30 and 45 Gy. A large inter-patient variability in volume reduction in that dose range was observed (Figure 4.5). For those parotid glands the caudal-medial part was receiving at least 54 Gy and the cranial part about 10 to 15 Gy. More data would be necessary with equal number of glands at the various dose intervals and especially data from patients receiving unilateral irradiation or at least one of their parotid glands is much more spared than the other one in order to obtain any significant correlation between dose distribution and spatial volume reduction.

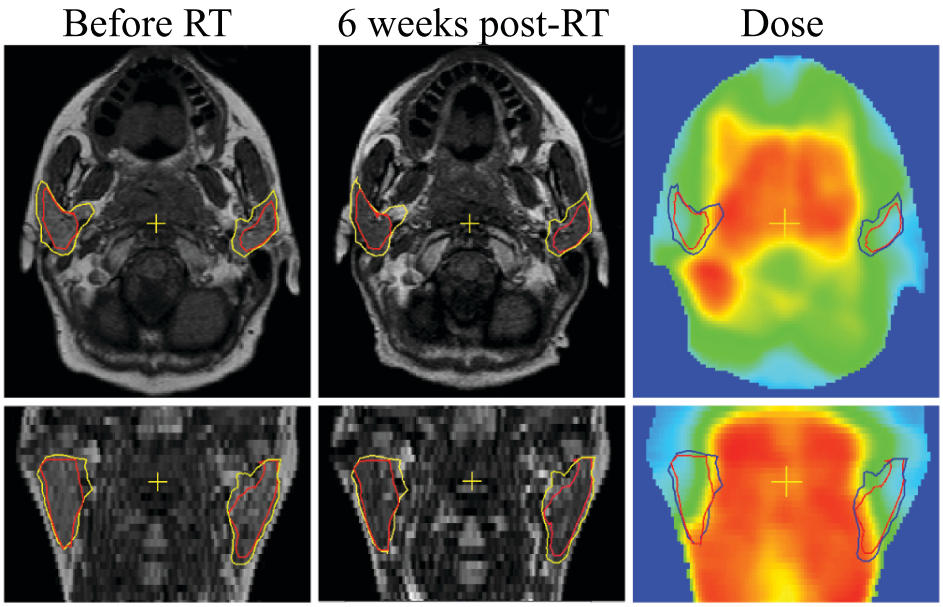

Figure 4.6: Registered transversal (top row) and coronal (bottom row) planes of the T_1-weighted MR scan before RT and MR scan at 6 weeks post-RT of one patient and the dose distribution at the same plane. The yellow contours are the parotid glands as delineated on the MR scan before RT and the red contours are the parotid glands as delineated on the MR scan at 6 weeks post-RT. For clarity, the latter are given in dark blue on the dose distribution planes.

Volume reduction and weight loss of the parotid glands after irradiation was observed in animal studies as well. Loss of serous cells, increase in fibrotic tissue and gland atrophy were some of the histopathological findings. Furthermore, the weight loss of the animals due to bad nutrition after irradiation or due to liquid diet instead of solid diet seemed to correlate with the loss of weight and atrophy of rat parotid glands (Leal *et al.*, 2003).
Similarly for our study group the volume reduction seemed to correlate with the weight loss of the patients and the patients had indeed a liquid diet during treatment and for a couple of months after the end of the treatment. In that case, the development of special water selective or fat selective MRI sequences might help to investigate the possible changes in the acinar/fat cells ratio after treatment and

to correlate them with the dose distribution using the image registration methods described in this study.
At the same time intervals and often just after the MRI scans, salivary flow measurements were performed in order to investigate whether the parotid volume reduction correlated with the salivary output. There was no correlation found before or after RT between the parotid volume and the amount of saliva produced. Salivary flow measurements provide information on the secretory capacities of the whole parotid gland. The different degree of late radiation damage that was shown in the parotid glands of rats was supported not only by the salivary flow measurements but also with histology. Late radiation damage was dependent on which part of the gland was irradiated and the location of blood vessels, ducts and neurons with regard to the irradiated part. Therefore other methods that could provide 3D information of structures such as blood vessels and salivary ducts should be employed to investigate further whether there is difference in regional radiosensitivity of the human parotid glands as well.
Methods like MR sialography for example could provide insight on the salivary duct system. Bussels *et al.* (2004) have registered salivary single photon emission computerized tomography (SPECT) images to the planning CT . They found regional differences in saliva excretion fraction, which were dose-dependent. Nevertheless, because of the lower spatial resolution of SPECT with regard to CT and the lack of anatomical information, the matching of regional dose distribution and salivary function is sensitive to registration errors, which could be even larger after radiotherapy due to parotid volume reduction.
In any case, minimizing the mean dose to the parotid gland is at the moment the treatment-planning goal by IMRT. The delineation of the parotid glands requires more attention now than in the conventional irradiation techniques. Despite the fact that a systematic comparison of CT and MRI delineation was not the primary aim of this study, a mean dose difference up to $\pm$ 9 Gy was observed between the CT and MR delineated parotid glands. The influence of those delineation differences to the outcome of the NTCP modelling should be further considered in future studies. The inclusion of the auxiliary parotid glands in the planning process is another issue that involves about 20% of the patients. This part is nearly always spared by IMRT (Figure 4.3). However, the contribution or not of this part to the salivary function after RT has not been evaluated.

4.5 Conclusion

In this pilot study it was shown that successful image registration of the MRI before RT with that after RT and with the planning CT can provide quantitative and qualitative information of the radiation-induced changes to the parotid glands. The parotid gland volume reduction at 6 weeks after RT persisted at 6 months

after RT as well. The reduction appeared in all directions and sometimes more in the medial part but it did not correlate to the dose or to the salivary output.

Chapter 5

3D MR sialography protocol for post-radiotherapy follow up of the salivary duct system

This chapter has been accepted as: E. Astreinidou, W. Bartels, C.P Raaijmakers, J. Roesink, C.H. Terhaard, and J.W Lagendijk. 2006. 3D MR sialography protocol for post-radiotherapy follow up of the salivary duct system. *Journal of Magnetic Resonance Imaging. In press.*

Abstract

Purpose: To develop and evaluate an MR sialography protocol that reproducibly images the parotid and submandibular ducts over time, in 3D. Such a protocol is needed in order to investigate the possible radiation-induced changes to the salivary ducts in patients receiving radiotherapy to the head-and-neck.
Materials and Methods: MR sialography was performed on a 1.5-T MR scanner. Sequence parameters were optimised on 11 healthy volunteers. A 3D water selective Turbo Spin Echo pulse sequence (TR/TE 6000 ms / 190 ms), using a 2 element circular surface coil was applied twice in one MR session. In order to assess the reproducibility the same procedure was repeated 4 to 6 months later. The quality of the MR sialograms was measured subjectively by developing a visibility scoring system and objectively by the means of contrast-to-noise ratio of the ducts versus fat ($CNR_{duct-fat}$).
Results: High quality, 3D MR sialographic images were obtained. The quality of the MR sialograms and the subjective visibility score of the salivary ducts were constant over time. The $CNR_{duct-fat}$ varied between volunteers (standard deviation, SD 26 %) but it was relatively constant per volunteer (SD 5%).
Conclusion: 3D MR sialography and the visibility scoring is a useful tool comparing the salivary ducts of an individual over time and can be used to detect potential ductal changes as a consequence of radiotherapy.

5.1 Introduction

Xerostomia is a very common side effect in patients having received radiation therapy for head and neck cancers (Vissink *et al.*, 1988; Braam *et al.*, 2005). Salivary flow can be measured using Lashley cups or ^{99m}Tc scintigraphy, and these methods indeed show a considerable reduction of saliva production in such patients (Roesink *et al.*, 2001, 2004; Blanco *et al.*, 2005; Eisbruch *et al.*, 2001a). Although these methods provide a way to quantify salivary flow, they do not provide spatial information on the salivary dysfunction. To gain such information we set out to investigate whether MR sialography could be a suitable technique to provide insight into the salivary duct architecture, and the possible damage inflicted to that system as a consequence of radiotherapy (Dreizen *et al.*, 1976; De Rossi, 1987).
Stationary fluids, such as saliva, appear hyper intense on heavily T_2-weighted MR images (Lomas *et al.*, 1996; Becker *et al.*, 2000). The technique of MR sialography exploits this property, using saliva itself as the MR contrast medium for the imaging of the salivary ducts. The great advantage of MR sialography over conventional X-ray sialography is that it does not bring about the risks resulting from the cannulation of the ducts, administration of contrast agent and the use of ionizing radiation (Becker *et al.*, 2000; Kalinowski *et al.*, 2002).
MR sialography has already been proven to be a sufficiently accurate, non-invasive technique for the detection of salivary duct and gland disorders such as Sjögrens's syndrome, sialolithiasis, duct stenosis and sialadenitis (Becker *et al.*, 2000; Kalinowski *et al.*, 2002; Jager *et al.*, 2000; Niemela *et al.*, 2004; Takagi *et al.*, 2005). The aim of the present study was to develop and evaluate an MR sialography protocol that could depict potential differences between the healthy salivary ducts before radiotherapy and the salivary ducts after radiotherapy. Such a comparison has not been, to our knowledge, reported yet.
Such a protocol should meet certain specific requirements. First of all, it should produce three dimensional (3D) data, to facilitate registration with the 3D-dose distribution. In that way direct spatial information of the possible radiation-induced changes in relation to the received dose could be provided. So far the evaluation of the diagnostic value of MR sialography for the detection of salivary duct and gland disorders has generally been restricted to a comparison of projection techniques, and reconstructed maximum intensity projections (MIPs), with standard 2D X-ray sialography. Sartoretti-Schefer *et al.* (1999), however, have shown that 3D pulse sequences provide an equally reliable diagnosis compared to that of 2D, with the supplementary advantage of increased post-processing possibilities (Becker *et al.*, 2000).
Secondly, the protocol should provide good quality images of the Wharton's ducts (submandibular ducts), as well as Stensen's ducts (parotid ducts) and high-order intraparotid duct branches, all in one single scan as these could all be situated in the irradiation field. In most of the studies employing MR sialography only the side and the gland suspected for disease are included in the scan volume (Takagi

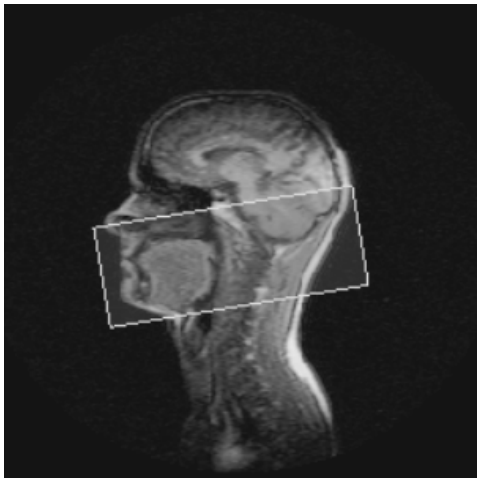

Figure 5.1: Sagittal view of a localizer image showing the imaging slab for the MR sialography.

et al., 2005).
Finally, but most importantly, the protocol should be able to reproducibly image the salivary duct architecture over time. In contrast to other investigators, rather than comparing MR sialograms with other imaging modalities (Kalinowski *et al.*, 2002; Jager *et al.*, 2000) we intend to compare MR sialograms of the same individual, recorded at different moments in time. Only when the quality of the MR sialography and the visibility of healthy salivary ducts are reproducible over time, it will be possible to reliably conclude whether the duct differences from pre- and post-treatment images result from radiotherapy. In this study we present an MR sialography protocol, conforming to the above-mentioned criteria, as applied to healthy volunteers for optimization.

5.2 Materials and Methods

5.2.1 MR sialography protocol

A total of eleven healthy volunteers with no previously reported disorders of the salivary glands or complains of salivary gland function were scanned for the purpose of this study. All of the volunteers gave their written consent for this study. MR sialography was performed on a 1.5-T system (Intera, Philips Medical Systems, Best, NL). Either the quadrature head coil or a 2 element circular coil (FLEX L), opening diameter 170 mm, was used. The reason for using the FLEX L coil

was that the immobilization mask in patients excludes the use of the head coil. Additionally, the FLEX L coil might offer better quality images as it is placed closer to the area of interest (salivary glands and ducts).
A 3D turbo spin echo (TSE) both with and without proset water selective excitation pulse was applied with the following imaging parameters: TSE factor 88, slice thickness 1.5 mm, number of slices between 47 and 55 depending on the anatomy, acquisition matrix $256x256$ half scan factor 0.6, reconstruction matrix $512x512$, field of view (FOV) $200x200$ mm^2, resulting in a total scan duration time between 8 to 9 minutes depending on the number of slices. The slight angulation of the scan volume around the right left (RL)-axis (Figure 5.1) was applied in an effort to get a large segment of the Stensen's duct trajectory in a single stack.
The visibility of the duct systems was assessed from the source images. We used in house developed software that allows us to visualize the transversal, coronal and sagittal views of the dataset together. Thus any selected point of the data sets was viewed in three dimensions. Transverse, coronal and sagittal maximum intensity projections (MIPs) of the whole volume were obtained as well.
We developed a scoring system to evaluate the visibility of the ducts for which the parotid ducts were divided into four parts (two intraglandular and two extraglandular parts) and the submandibular ducts into two parts (Figure 5.2). The score was 1 if the subpart was visible and 0 if it was not, resulting in total maximum score of 4 for the parotid ducts and 2 for the submandibular ducts. The scoring system will serve as a tool to compare the visibility of the duct systems in patients before and after radiotherapy. In our effort to understand the salivary dysfunction, it is important to know not only whether changes in the visibility of the ducts occur after radiation therapy, but also where they occur (in the intraglandular and /or extraglandular parts).
The quality of the images was determined not only subjectively but also objectively by comparing the contrast-to-noise-ratio of the signal intensity in the ducts to that in (fat) tissue adjacent to the ducts ($\mathrm{CNR}_{duct-fat}$). We compared the $\mathrm{CNR}_{duct-fat}$ of the MR sialograms obtained (i) with fat suppression (water selective) versus no fat suppression and (ii) the head coil versus the FLEX L coil.
The $\mathrm{CNR}_{duct-fat}$ was calculated according to the formula

$$\mathrm{CNR}_{duct-fat} = \mid \mathrm{SI}_{duct} - \mathrm{SI}_{fat} \mid / \mathrm{SD}_{noise}$$

Where SI_{duct} was the mean signal intensity of a volume of interest (VOI), which included partially *part 1* and *3* of the parotid duct and *part 1* of the submandibular duct. SI_{fat} was the signal intensity of a VOI of subcutaneous fat tissue superficially to the masseter muscle adjacent to *part 1* and *3* of the parotid duct and in case of the submandibular gland was a VOI including the submandibular tissue itself. SD_{noise} was the standard deviation of the background noise signal intensity as measured in a VOI in air outside the head in the read out direction.
Image registration between the MR sialograms due to comparison was performed,

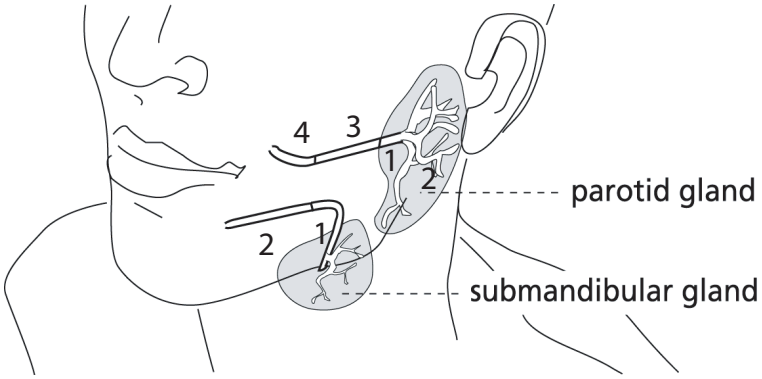

Figure 5.2: Schematic overview of the parotid duct and submandibular duct visibility scoring system. Numbers indicate the parts in which the ducts were divided. **Parotid duct**: *part 1*: Intraglandular main duct, *part 2*: Intraglandular higher order duct branches, *part 3*: Extraglandular segment of Stensen's duct that runs superficially to the masseter muscle, *part 4*: Extraglandular last segment of the duct that turns nearly 90 degrees to pierce the buccinator muscle before opening to the oral cavity. **Submandibular duct**: *part 1*: Intraglandular duct and the posterior bend of Wharton's duct around the posterior edge of the mylohyoid muscle *part 2*:Extraglandular segment that runs through the sublingual space and opens to the anterior floor of the mouth near the lingual frenula.

using a mutual information algorithm; therefore the delineated VOIs were exactly the same on both data sets.

5.2.2 MR sialography reproducibility

Six of the healthy volunteers were involved in the reproducibility study of the protocol. In one scanning session MR sialography was performed twice. Between the two scans the volunteer was removed from the scanner, such that the volunteer, the table and the FLEX L coil had to be re-positioned for the second scan. This complete procedure was repeated in a second session 4-6 months later. In this way we could assess the reproducibility of the measurement method, and the long-term reproducibility of the visibility of the duct systems in a single volunteer, not undergoing radiation therapy.
The volunteers received no gustatory stimulation for at least an hour before the scanning, and they were lying on the radiation therapy (RT) positioning cushion. The MRI set up resembles that used for head-and-neck patients during RT and

Figure 5.3: Screenshot of our in-house software window used to score the visibility of the parotid ducts. 3D water selective heavily T2-weighted TSE (TR/TE 6000 ms / 190 ms) image of the parotid ducts in a) transverse, b) coronal and c) sagittal planes. White arrows indicate the same point of the intraglandular main parotid duct, *part 1*, in all planes.

planning CT and it is the same set up that will be used when scanning patients in the MR. The influence of the customized immobilization mask on the quality of the images was evaluated in one healthy volunteer.
Scoring according to the system described above, $\mathrm{CNR}_{duct-fat}$, as well as the length from the point of entry up to the last visible part and diameters of the Stensen's and Wharton's ducts upon entry to the glands were recorded for both sessions of the reproducibility study. The diameter of the duct was defined as the full width of half maximum (FWHM) of a gaussian fit of a profile drawn perpendicular to the ducts, at the beginning of *part 3* for the parotid ducts and the beginning of *part 2* for the submandibular ducts, on a transverse plane of the source data.

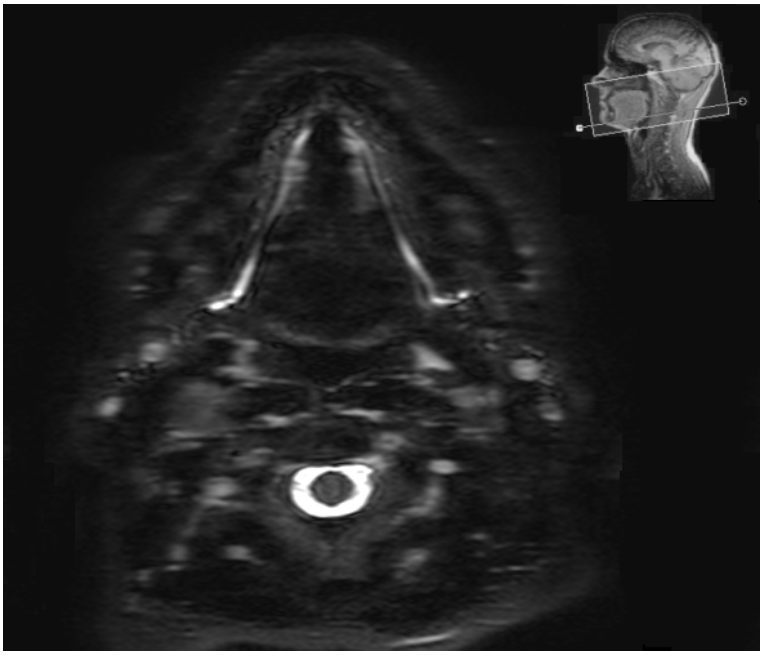

Figure 5.4: 3D water selective heavily T2-weighted TSE (TR/TE 6000 ms / 190 ms) image of the submandibular ducts on a transverse plane at the floor of the mouth (indicated on the localizer image) of the source data as used for scoring the visibility of the submandibular ducts.

5.3 Results

The main intraglandular parotid duct and the first order small duct branches were visible in all volunteers. The trajectory of the small branches could be traced in the sagittal plane and in some cases in the coronal plane while detecting them as white dots on the transverse plane (Figure 5.3). Higher order small branches were visible in 9 of the 11 volunteers. *Part 3* and *4* of the parotid duct and *part 1* and *2* of the submandibular duct were clearly visible in the transverse plane (Figure 5.4) and partly on the sagittal plane. Using a signal intensity thresholding it was possible to get a 3D representation of the salivary duct architecture (Figure 5.5). Using only the MIPs for evaluation could result in loss of information particularly in the intraglandular space and last part of both Stensen's and Wharton's ducts. The use of fat suppression appeared to be important especially in the visibility of the higher order branches. The average $\mathrm{CNR}_{duct-fat}$ and the standard deviation (SD) for the group of volunteers scanned with the head coil and without fat sup-

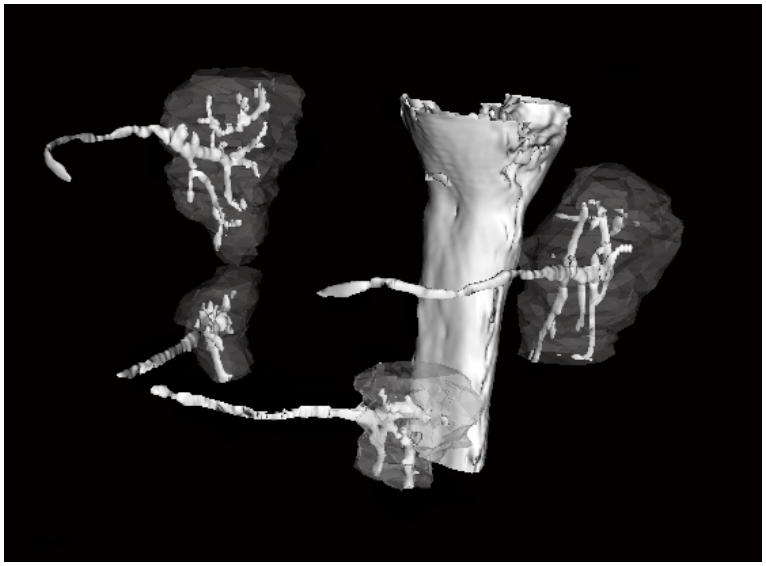

Figure 5.5: Parotid ducts and submanibular ducts in 3D of a healthy volunteer as derived by thresholding the source data of the MR sialography (3D water selective heavily T2-weighted TSE ,TR/TE 6000 ms / 190 ms). Different thresholds were used for the intraglandular parts of the ducts, than that of the extraglandular parts and the cervical vertebrae. The location of the parotid and submandibular glands is given by the grey transparent volumes, as they were delineated on the MR sialography data set.

pression were 5 (SD 2). That value increased to 31 (SD 5) when fat suppression was applied and it was 48 (SD 11) when the FLEX L coil was used. It should be noted that the visibility score was exactly the same with both coils. Furthermore the immobilization mask neither altered the quality nor the visibility score of the sialogram.
Although the applied pulse sequence used was not optimized for imaging of the parotid and submandibular tissue, those glands could be distinguished from the surrounding muscle and fat tissue, the signal of which was suppressed. The retromandibular vein at the medial part of the parotid gland had high signal intensity in some cases, comparable to that of the ducts. Repositioning the volunteer and the FLEX L coil during the same MR session and at the repeated MR session 4 to 6 months later resulted in a reproducible measurement (Figure 5.6). Five of the six volunteers involved in the reproducibility study had total visibility score of 4 for the parotid ducts and one had 2 and 3 for the right and left parotid ducts

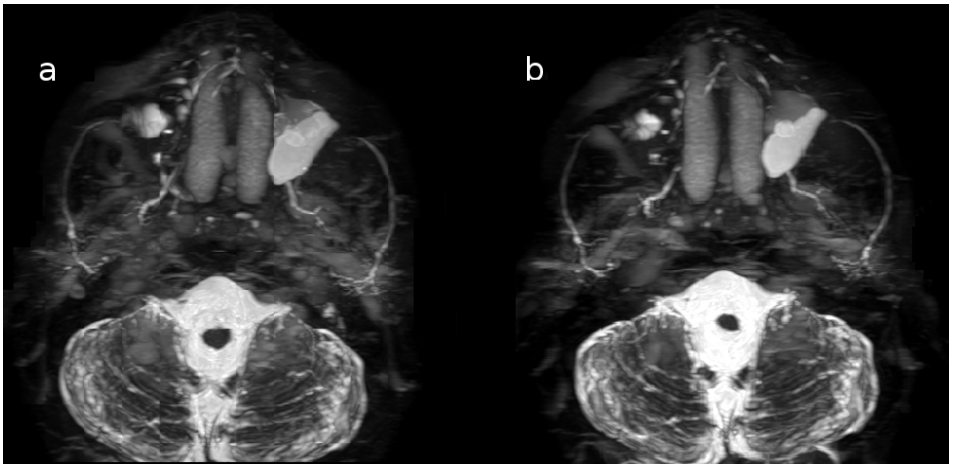

Figure 5.6: Transverse maximum intensity projection (MIP) images of the MR sialogram (3D heavily T2-weighted TSE) of a healthy volunteer a) base line measurement b) 6 months later demonstrating the reproducibility of the MR sialography in time.

respectively. In the later case the extraglandular segments, *part 3* and *4* were not visible. All of the volunteers had total visibility score of 2 for the submandibular ducts. The $\mathrm{CNR}_{duct-fat}$ of all 24 sialograms of the reproducibility study is given in Table 1. The $\mathrm{CNR}_{duct-fat}$ varied between volunteers (SD 26%) but it was relatively constant per volunteer (SD 5%). The average length was approximately 3.5 cm (SD 0.4 cm) for the Wharton's ducts and 4.8 cm (SD 0.6 cm) for the Stensen's duct. The average diameters of the parotid ducts and submandibular ducts upon entry to the glands were 2.1 mm (SD 0.2 mm) and 2.2 mm (SD 0.4 mm) respectively.

5.4 Discussion

The MR sialography protocol presented in this study has shown to provide good quality 3D images of the submandibular and parotid duct architecture Figure 5.5. The images are reproducible, both technically at one moment in time, as in a single volunteer at different moments in time (Figure 5.6). The quality of the source images was comparable or even superior to that of images have reported in literature, using other 3D pulse sequences (Sartoretti-Schefer *et al.*, 1999). Particularly in the intraglandular space the high image quality was notable, as the full trajec-

Table 5.1: CNR$_{duct-fat}$

					Parotid duct CNR$_{duct-fat}$
	Sialo1a	Sialo1b	Sialo2a	Sialo2b	CV(%)
1	90	96	88	92	4
2	34	40	42	49	15
3	29	30	33	35	9
4	69	65	72	70	4
5	24	28	21	21	14
6	78	81	57	64	16
					Submandibular duct CNR$_{duct-fat}$
1	90	96	88	92	4
2	34	40	42	49	15
3	29	30	33	35	9
4	69	65	72	70	4
5	24	28	21	21	14
6	78	81	57	64	16

Contrast-to-noise-ratio of the parotid and submandibular duct to fat,CNR$_{duct-fat}$,for the MR sialograms of the reproducibility study. Sialo1a and Sialo1b are the two MR sialograms of the first MR session and Sialo2a and Sialo2b are those of the second one 4-6 months later. CV (%) is the coefficient of variation expressing the variability of the standard deviation (sd) of the CNR$_{duct-fat}$ for each subject as a proportion of the mean CNR$_{duct-fat}$ for the same subject.CV = (sd/mean)x100%.

tory of the higher order small duct branches could be traced. That is important to us, as our effort is to use MR sialography as a tool to investigate whether the intaglandular parts *part 1-2* of the ducts are damaged causing salivary dysfunction in patients receiving radiation therapy of the head and neck or whether obstruction or damage of the other parts does not permit flow (De Rossi, 1987).
MR sialography was initially developed to replace the conventional 2D x-ray sialography. Therefore most investigators employed a projection technique or used the MIPs to evaluate the visibility and the abnormalities of the ducts. While the main advantage of the projection technique is the short acquisition time, artifacts of slow-flowing blood in veins could be superimposed on the MR sialographic images (Tonami *et al.*, 2001). Recently, (Takagi *et al.*, 2005) have presented high resolution, excellent quality sialographic images, of the higher order small branches of the parotid duct (*part 2*). Those images were produced with the projection technique by using a microscopic coil improving the quality of the images obtained with larger coils. However, 3D spatial information of submandibular and parotid glands in one scan is not provided with that technique. For our purpose, 3D MR

sialography is vital in order to be able to register the sialogram and eventually the potential radiation induced changes of the ductal architecture to the 3D dose distribution. Lately with the implementation of intensity modulated radiation therapy (IMRT) clinically, the 3D dose is not anymore homogeneously distributed over a large head-and-neck volume including the salivary glands as in conventional irradiation techniques (Astreinidou *et al.*, 2004; Chao *et al.*, 2001b). High dose gradients are created and therefore not all parts of the salivary ducts receive necessarily the same dose.
In the case of the healthy volunteers used in this study, potential motion artifacts due to the long acquisition time did not seem to affect the visibility of the ducts. First order small branches were visible in all volunteers and the second order branches approximately in 80 % of them. Visualizing higher order small branches is more likely to be restricted by the resolution than the motion artifacts.
We have shown that the visibility score was reproducible in time for all of the healthy volunteers. In all cases but one the maximum visibility score was recorded. In that case that not all parts of the parotid duct were visible, we performed salivary stimulation with citric acid (single shot) before scanning but neither improve the visibility scoring nor the quality of the sialogram, in contrast with what (Kalinowski *et al.*, 2002) has reported using projection MR technique. This can be explained by the longer acquisition time required for our MR sialogram.
While the visibility score of the salivary ducts did not vary in time a variation of the $\mathrm{CNR}_{duct-fat}$ ranging from 2 % up to 16% was found (Table 1). That can be partly due to measurement variation and partly due to the amount of saliva present in the ducts at the moment of the MR scan. As mentioned before MR sialography is based on imaging the saliva in the ducts. This property could be exploited further as it might give us rather than only anatomical information of the salivary duct system, also functional information, or offer an alternative method in measuring saliva production.

5.5 Conclusion

We have proposed an MR sialography protocol for the visualization of the salivary duct architecture in 3D. The quality of the MR sialogram and the visibility scoring of the ducts proved to be reproducible in time. From these promising results we conclude that this MR sialography protocol can be used as a follow up tool to detect the location of potential radiation-induced changes to the salivary ducts, in patients having received radiotherapy to the head and neck.

Chapter 6

3D MR sialography as a tool to investigate radiation-induced xerostomia: Feasibility study

This chapter is part of the manuscript submitted as: E. Astreinidou, J. Roesink, W. Bartels, C.P Raaijmakers, T.Witkamp, H Dehnad, J.W Lagendijk, and C.H. Terhaard. 2006. 3D MR sialography as a tool to investigate radiation-induced xerostomia: Feasibility study. *Int J Radiat Oncol Biol Phys.*

Abstract

Purpose: To evaluate whether MR sialography could be used as a new tool to investigate radiation-induced xerostomia, by imaging and comparing the saliva content of the major salivary ducts, parotid and submandibular, post-radiotherapy (RT) with that pre-RT.
Materials and Methods: MR sialography was performed pre-RT, 6 weeks and 6 months post-RT on 9 patients with T1-4N0-2M0 naso- or oropharyngeal tumors, on a 1.5-T MR scanner. Patients were positioned in the same immobilization mask used for the RT treatment. Image registration of MR sialography pre-RT with that post-RT and the planning CT was performed. A subjective scoring system was used to compare the visibility of the ducts pre- and post-RT. Stimulated salivary flow measurements were carried out at the same time intervals.
Results: Good quality MR sialographic images were obtained and the image registration was successful in all cases. The pre-RT visibility score of the major salivary ducts was reproducible 6 weeks and 6 months post-RT for those glands receiving mean dose < 20 Gy, but reduced when the mean dose was > 20Gy. At 6 months post-RT the visibility score started to improve for the parotid ducts but not for the submandibular glands. Similar trends were observed for the salivary measurements.
Conclusion: 3D MR sialography is a promising approach for investigating xerostomia because radiation-induced changes to the salivary glands and the saliva content of the ducts can be visualized and registered to the 3D dose distribution.

6.1 Introduction

Salivary dysfunction is a prevalent side effect suffered by patients receiving head-and-neck radiotherapy (RT). Lack of saliva production results in impaired quality of life and can be permanent (Dreizen *et al.*, 1977; Braam *et al.*, 2005; Chambers *et al.*, 2004; Duncan *et al.*, 2005). The elucidation of the exact mechanism of radiation damage to the salivary glands has been subject of many studies (Konings *et al.*, 2005a). It has been suggested that damage to the acinar and ductal systems are the main cause of salivary gland dysfunction in humans after RT (Dreizen *et al.*, 1976). The acinar cells of the salivary glands are responsible for the production of saliva, which is then excreted into the oral cavity by the salivary ducts. It has also been suggested that edematous stenosis of the major salivary ducts takes place progressively during irradiation, leading to symptoms of acute sialadenitis with an excretory obstacle (De Rossi, 1987). In these studies either the changes in saliva and serum electrolyte levels were investigated or salivary gland scintigraphy with ^{99m}Tc-pertechnetate was performed. Yet, neither of these nor other studies systematically investigated the salivary ducts directly.

Recent experiments in animals, have indicated regional differences in the radiosensitivity of the parotid glands (Konings *et al.*, 2005a,c, 2006). It is concluded that the observed region-dependent volume effect for late function loss in the rat parotid gland after partial irradiation is mainly caused by secondary events in the shielded lateral lobe. By injuring major excretory ducts and supply routes for blood and nerves in this area, the facility system necessary for proper functioning of the non-exposed lateral lobe is seriously affected (Konings *et al.*, 2006). This hypothesis should be investigated in humans as it might influence the intensity-modulated radiation therapy (IMRT) planning strategies.

The conventional method of visualizing the ductal system is the X-ray sialography. This 2-dimensional (2D) technique requires injection of contrast medium and special manual skills for the cannulation of the ducts, with a risk of failure in case that the opening of the ducts cannot be clearly seen (Kalinowski *et al.*, 2002). That might very well be the case after RT. Moreover, it can be performed only to one salivary duct at the time and the salivary gland tissue itself is not visible. One study applying X-ray sialography post-RT has been published to our knowledge (Kashima *et al.*, 1965). Reduced parotid duct filling and a less detailed pattern of the small parotid ducts was observed compared to that of the pre-RT X-ray sialography.

Recently, several investigators have proposed that MR sialography has the potential to replace the conventional method in detecting various salivary gland disorders such as Sjörgen's syndrome and sialolithiasis (Sartoretti-Schefer *et al.*, 1999; Becker *et al.*, 2000; Kalinowski *et al.*, 2002; Takagi *et al.*, 2005; Niemela *et al.*, 2004). With this technique stationary fluids, such as saliva, appear hyperintense in contrast to the hypointense signal from other surrounding tissues such as muscle. The great advantage of MR Sialography versus the conventional X-ray sialography is that

it uses saliva itself as contrast medium. That practically means, that the salivary ducts are actually imaged due to the containing saliva. This property alone makes MR sialography an attractive method to use when studying hyposalivation. Another advantage of using MR is that it is a 3-dimensional (3D) imaging modality and consequently has the potential to provide spatial information on the salivary (dys)function.
That could prove to be beneficial if a correlation is established between the 3D dose distribution and the salivary (dys)function, as it could result in a more efficient IMRT treatment planning (Chao *et al.*, 2002; Eisbruch *et al.*, 1998; Wu *et al.*, 2003; Astreinidou *et al.*, 2004). Using conventional radiotherapy techniques the salivary glands are mostly included fully in the irradiation fields and receive homogeneous doses. With IMRT, however, dose painting is possible and therefore is more important now than ever to investigate whether there is regional radiosensitivity in the human parotid glands with regard to function and dose.
We have developed and evaluated a 3D MR sialography protocol on healthy volunteers that provides good quality 3D images of the submandibular and parotid duct systems in a single scan. Moreover, we have shown that MR sialograms of the same individual, recorded at different moments in time, are reproducible.
In this feasibility study we performed this 3D MR sialography protocol to a group of patients receiving RT for head-and-neck tumors pre-RT, 6weeks and 6 months post-RT. Salivary flow measurements were performed at the same time interval as MR sialography. The primary goal of the study is to evaluate whether MR sialography could be used as a new tool investigating radiation-induced xerostomia by imaging and comparing the saliva content of the salivary ducts pre-RT and post-RT. Furthermore the image registration of the MR sialograms pre- and post-RT with each other and the 3D dose distribution was evaluated.

6.2 Materials and Methods

Nine patients, treated with primary or post-operative irradiation for T1-4N0-2M0 nasopharyngeal or oropharyngeal cancer, were included in the study. Seven of these patients were treated with IMRT and two with 3D-conformal RT (Astreinidou *et al.*, 2004).
MR sialography was performed on a 1.5-T system (Intera, Philips Medical Systems, Best, NL). The patients were positioned in the MR scanner with the RT immobilization mask, as in the treatment position. A 3D water-selective turbo spin echo pulse sequence, with TR/TE 6000 ms/190 ms, using a 2 element circular surface coil (FLEX L), opening diameter 170 mm, was applied as described in detail by our previous study (Astreinidou *et al.*, 2006). The acquired image resolution was $0.8x1.4x1.5$ mm^3 and the reconstructed image resolution was $0.4x0.4x1.5$ mm^3. MR sialography was performed pre-RT, at the same day as the planning CT and repeated 6 weeks and 6 months post-RT. Before each MR follow up scan, it was

checked in the mould room whether the RT immobilization mask was still fitting the patient.
The scan volume included the parotid glands and the submandibular glands bilaterally, and was slightly tilted (5 -8 degrees) around the right-left axis. It has also included a small tube filled with 25ml $MnCl_2.4H_2O$ solution, 19.2 ml/l, which was taped on the immobilization mask at the level of the parotid gland. The signal intensity of that solution was used for normalization purposes when comparing MR sialograms.
The analysis of the 3D data sets was carried out using in-house developed software that allows visualization of the transversal, coronal and sagittal views of the dataset together. Thus any selected point of the data sets was viewed in three dimensions. The trajectory of submandibular (Wharton's) ducts and parotid (Stensen's) ducts were mainly visible on the transversal planes and the higher order small parotid duct branches were better visible on the sagittal planes (chapter 5).
A subjective scoring system was used to evaluate the visibility of the salivary ducts (Figure 5.2). In short, the parotid ducts were divided into four parts, two intraglandular (*part 1*=main duct, *part 2*=higher order small duct branches) and two extra glandular (*part 3*= segment of Stensen's duct superficially to the masseter muscle, *part 4*= last segment of Stensen's duct that turns 90 degrees to pierce the buccinator muscle before opening to the oral cavity). The submandibular ducts were divided into two parts (*part 1:* intra-glandular duct and the posterior bend of Wharton's duct around the posterior edge of the mylohyoid muscle, *part 2:* extra-glandular segment that runs through the sublingual space and opens to the anterior floor of the mouth near the lingual frenula). The score was 1 if the part was visible and 0 if it was not. If the whole trajectory of the Stensen's duct including the small intra-glandular duct branches were visible the total score was 4 for the parotid ducts.
For the submandibular duct the total score was 2 if the whole trajectory of the Wharton's duct and the intra-glandular part of the duct were visible. The visibility score was given for each MR sialogram by two observes and consensus was reached. It was used to compare the visibility of the ducts post-RT to that pre-RT and indirectly quantify whether the whole or only part of the duct trajectory was detectable.
The MR sialograms 6 weeks and 6 months post-RT and the planning CT were registered to the MR sialogram pre-RT, using a mutual information algorithm. The registration was inspected visually using a *"linked cursor"* approach. Two windows with the registered datasets were simultaneously opened. When the location of a point in one dataset was selected, a visible mark was positioned automatically at the corresponding location in the registered dataset (Ceylan *et al.*, 2005; Bol *et al.*, 2003). The registration was considered to be good when there was a successful match of the body contour, base of the skull, brain tissue and other rec-

ognizable structures such as blood vessels. Afterwards the matching of the location of the salivary ducts on the registered MR sialograms was checked and the 3D-dose distribution was superimposed on the sialogram pre-RT. The dose calculation was performed using commercial software, PLATO IMRT and PLATO RTS, Nucletron BV, Veenendaal, the Netherlands. Mean dose to the salivary glands and to the dose to the salivary duct parts was obtained as well.
The diameters of the Stensen's and Wharton's ducts upon entry to the glands were recorded. The diameter of the duct was defined as the full width of half maximum (FWHM) of a Gaussian fit of a profile drawn perpendicular to the salivary ducts (at end of the intra-glandular ductal part) on a transversal plane of the datasets. A paired t-test was used to compare the diameters before and after RT. Differences were considered to be statistically significant when $p < 0.05$.
Salivary flow measurements were performed at the same time intervals and often the same day, right after the MR sialography. Stimulated parotid saliva was collected from both parotid glands, simultaneously, with Lashley cups, and mixed submandibular and sublingual saliva was collected from the floor of the mouth using a pipette. Stimulation was achieved by applying 50 μl of a 5% acid solution to the mobile part of the tongue every 1 minute, and saliva collection was carried out for 10 minutes (Roesink *et al.*, 2001).

6.3 Results

MR sialography was performed successfully and was well accepted by all 9 patients. The repositioning of the RT immobilization mask at 6 weeks and 6 months post-RT was still good and there was no need of making a new mask. The 3D image registration of the pre-RT MR sialograms with the post-RT MR sialograms and the CT data and consequently the 3D dose distribution was inspected visually and it was considered to be satisfactory in all cases. The body contours were in good agreement and no differences larger than 2 to 3 voxels were observed when checking on specific points. The average diameter of the parotid ducts for this group of patients was 2.1 mm (standard deviation (SD) 0.5 mm) pre-RT, 2.2 mm (SD 0.8 mm) at 6 weeks post-RT, and 2.3 mm (SD 0.5 mm) at 6 months post-RT. For the submandibular ducts the average diameters were 2.2 mm (SD 0.5 mm), 2.0 mm (SD 0.3 mm) and 2.1 mm (SD 0.4 mm), respectively. The diameters as measured 6 weeks and 6 months post-RT were not considered to be statistically different from the diameters measured before RT ($p > 0.05$ in all cases).

6.3.1 Visibility of the salivary ducts

We assessed the visibility of the salivary ducts of 18 parotid glands and 16 submandibular glands. Two submandibular glands were excluded because they were in the vicinity of the operated area. One patient was lost from the 6 months post-RT

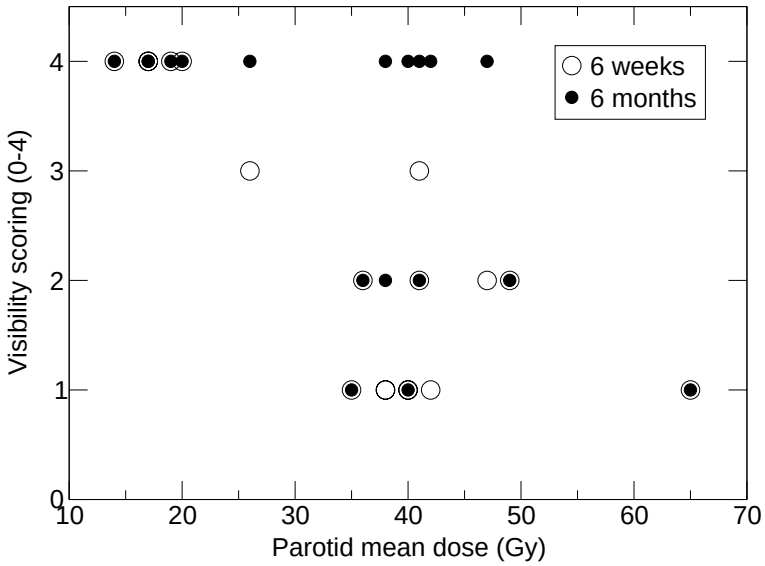

Figure 6.1: Duct visibility score versus the parotid mean dose. The visbility score 6 weeks after RT is given by the large open circle and 6 months after RT is given by the smaller solid circle.

follow up. In general, the trajectory of the extra-glandular parotid duct, Stensen's duct, was well to follow scrolling through the transverse planes of the sialograms. The small parotid duct branches were detectable as small hyperintense dots in the hypointense surrounding of the parotid tissue on the transverse planes. Scrolling trough the sagittal planes at the level of the parotid glands, the full trajectory of the small ducts as they converge from the second order branches to the first order branches and eventually to the main intra-glandular parotid duct could be nicely followed (Figures 6.2 and 6.4). The visibility score of the parotid ducts was the maximum 4 for all parotid glands and was constant during the follow-up scans for those parotid glands receiving mean dose <20 Gy. The visibility score reduced for all glands receiving a mean dose >20 Gy at 6 weeks post-RT and started to improve for some patients at 6 months post-RT (Figures 6.1, 6.3 and 6.4). An interesting observation was that the intra-glandular main parotid duct, *part 1,* was always visible, pre- and post-RT. The average dose to that part was 33 Gy (SD 13) similar to the average mean dose to the whole parotid gland, 35 Gy (SD 13). The changes in the visibility score post-RT were due to the reduced visibility of the other ductal parts, the extra-glandular and the intra-glandular small parotid ducts. The continuity of the smaller duct branches to the larger ones was lost. There was no indication of regional damage to the small ducts within the gland.

The dose to *part 3* and *part 4* of the parotid duct was 25 Gy (SD 17) and 33 Gy (SD 22), respectively.

The lower dose to *part 3* was because it is situated superficially to the masseter muscle and that part is mostly spared by IMRT, while *part 4* is situated more medially and it is closer to the high dose area.
The full trajectory of the submandibular ducts was visible, maximum score 2, for all submandibular glands pre-RT. The visibility score remained unchanged in one patient at the post-RT measurements. In that patient the mean dose to the left and right submandibular glands was 15 Gy and 2 Gy, respectively. For all the other patients only the intra-glandular *part 1* was visible at 6 weeks post-RT. The visibility score did not improve at 6 months post-RT (Figure 6.5) as it did for the parotid ducts.
The average mean dose to the submandibular glands and ducts was higher than that of the parotid glands, 62 Gy (SD 8 Gy). They were included in the high dose area as no treatment planning effort was made to spare them.
The signal intensity of the whole salivary gland tissue was higher post-RT compared to that pre-RT, for all submandibular glands and the parotid glands receiving a mean dose higher than 20 Gy (Figures 6.5 and 6.3).

6.3.2 Saliva measurements

Salivary flow measurements were successful in all 9 patients pre-RT and in 8 post-RT. That patient, who was excluded from the analysis, experienced pain at the floor of the mouth during stimulation with the citric acid at the post-RT follow up and the measurement had to be stopped. The MR sialography, however, was performed in that case.
The average amount of saliva collected from the parotid glands in 10 minutes, was 1.7 ml (median 1.2 ml) pre-RT, 0.3 ml (median 0.0 ml) and 0.3 ml (median 0.0 ml) 6 weeks and 6 months post-RT, respectively. Despite the fact that the visibility score of some parotid ducts improved back to the pre-RT maximum 4, at 6 months post-RT, still no saliva was collected from them.
Saliva from the submandibular glands could not be measured separately like in the parotid glands. The saliva collected from the floor of the mouth was assigned to both of the submandibular glands. The average amount of saliva was 3.4 ml (median 3.6 ml) and reduced to 0.2 ml (median 0.0 ml) and 0.1 ml (median 0.0 ml) 6 weeks and 6 months post-RT, respectively. The same 4 patients produced the collected saliva from the floor of the mouth at the post-RT measurements.

6.4 Discussion

In the present study a 3D MR sialography protocol was applied, for the first time, in patients receiving radiotherapy for head-and-neck tumors. MR sialography was

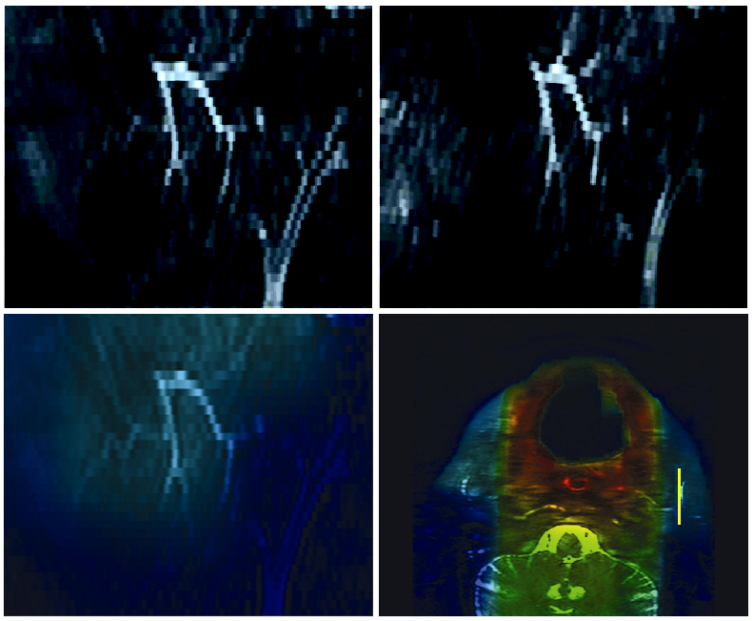

Figure 6.2: A sagittal plane of the 3D MR Sialogram (TR/TE 6000 ms / 190 ms) through the left parotid gland of a patient where the main intra-glandular parotid main duct *(part 1)* and a part of the small duct branches were clearly visible a) before and b) 6 weeks post-RT. The dose distribution is superimposed on the c) same sagittal plane and d) on a transverse plane. The yellow line on the transverse plane indicates the position of the sagittal planes. The dose received by the gland and duct at that part was 16 Gy.

performed using a heavily T_2-weighted sequence that allows the imaging of the salivary ducts because the containing saliva appears hyperintense and the surrounding tissue hypointense (Becker *et al.*, 2000). The use of the same RT immobilization mask, every time the patient was scanned, resulted in successful image registration of the MR sialograms pre-RT with that post-RT and of the MR sialograms with the planning CT and consequently the dose distribution.
The comparison of MR sialographic images of patients pre- and post-RT has revealed radiation-induced changes in the visibility of the salivary ducts and in the signal intensity of the salivary gland tissue itself. The visibility of the whole trajectory of the salivary ducts as described by a subjective scoring system was reduced post-RT in comparison to that pre-RT. In healthy volunteers, however, the visibil-

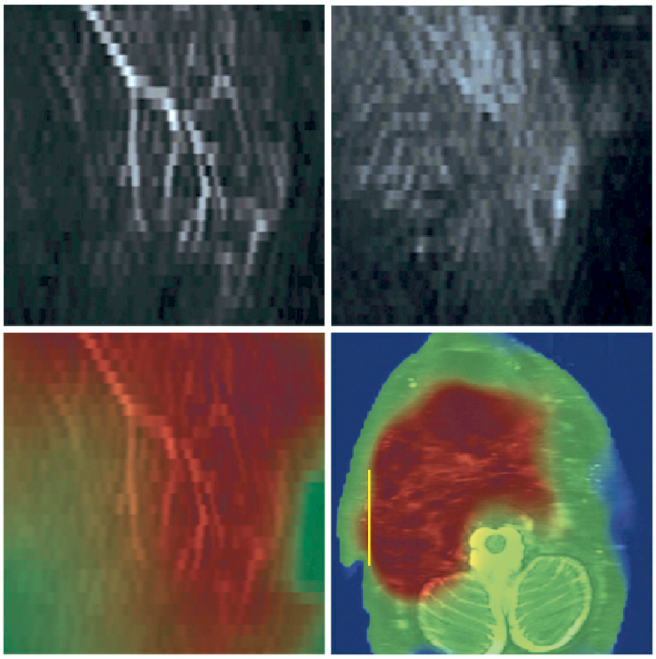

Figure 6.3: A sagittal plane of the 3D MR Sialogram (TR/TE 6000 ms / 190 ms) through the right parotid gland of a patient where the main intra-glandular parotid main duct *(part 1)* and the small duct branches were clearly visible a) before but not b) 6 weeks post-RT. The dose distribution is superimposed c) on the same sagittal plane and d) on a transverse plane. The yellow line on the transverse plane indicates the position of the sagittal planes. The dose received by the gland and duct at that part was 62 Gy.

ity score was reproducible in long-term time intervals. Thus it can be concluded that the reduced visibility score in patients indicated lack of saliva, hyposalivation. Mainly the extra-glandular parts of both parotid and submandibular ducts were not visible post-RT, while the intra-glandular main duct was always visible, pre- and post-RT (Figure 6.2 and 6.4). The diameters of the ducts, as measured at the end of the intra-glandular main duct, *part 1*, were similar to that observed in healthy volunteers. Furthermore, the diameters of the ducts post-RT were not significantly different from that pre-RT, for this group of patients.

This finding suggests that there was no dilatation of the ducts due to obstruction that could possibly explain the lack of saliva at the extra-glandular parts post-RT (Becker *et al.*, 2000; De Rossi, 1987). It is in accordance, however, with what has

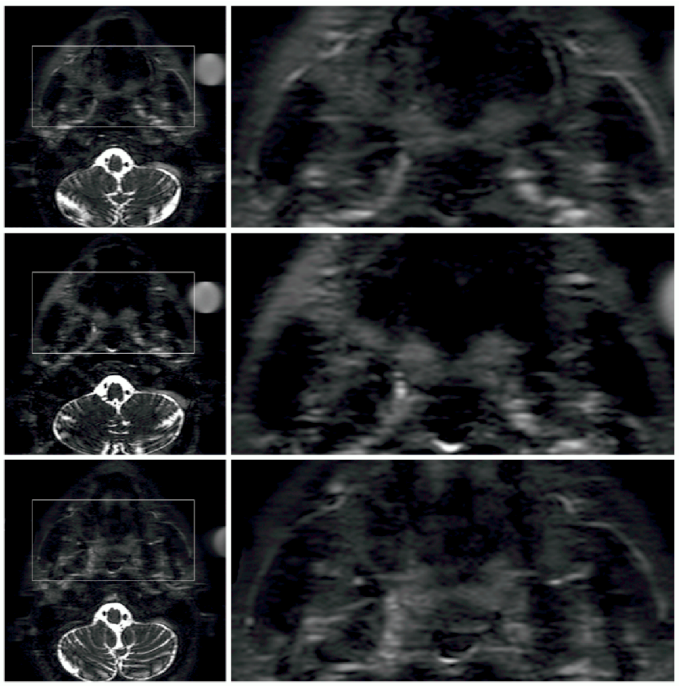

Figure 6.4: An (oblique) transverse plane of the 3D MR Sialogram (TR/TE 6000 ms / 190 ms) of a patient, at a level through the base of maxilla that includes a segment of part 3 and part 4 of the parotid ducts a) before RT. Scrolling through the other transverse planes the rest of the trajectory of the Stensen's duct was visible before RT but not b) 6 weeks post-RT and it became visible again c) 6 months post-RT.The hyperintense circular form area on the left side is a part of the tube containing the $MnCl_2.4H_2O$ solution that was used for signal normalization.

been observed by Kashima *et al.* (1965). In the same study, a less detailed pattern of the parotid duct, without small duct filling, was observed using X-ray sialography 20 weeks post-RT.
Similar findings were observed with MR sialography. The small duct branches could not be visualized for some of the parotid glands post-RT (Figure 6.3). Whether that was because of the higher signal intensity of the parotid tissue itself post-RT or because the small ducts were damaged (Konings *et al.*, 2005b) cannot be concluded with certainty. It seemed that the signal intensity was homogeneously increased in the whole salivary gland tissue even if the dose was not homogeneously

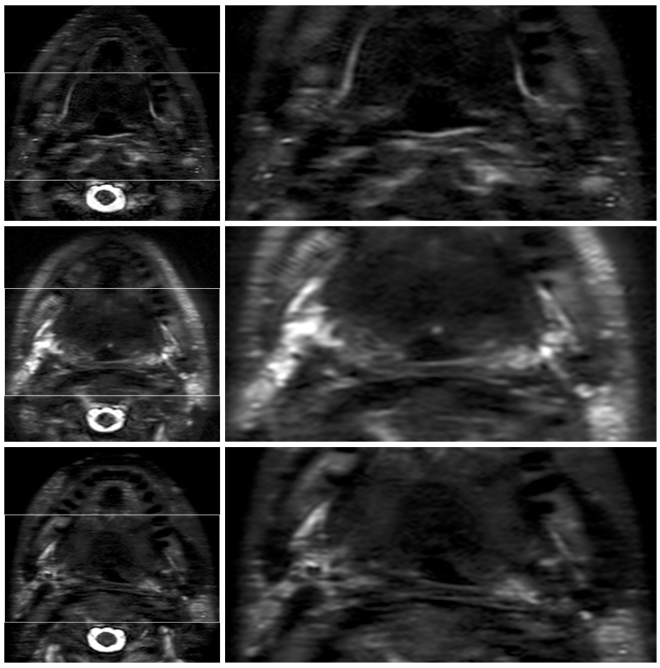

Figure 6.5: An (oblique) transverse plane of the 3D MR Sialogram (TR/TE 6000 ms/190 ms) of a patient, at a level through the transverse process of the atlas C1 and the mandible that includes a part of the submandibular ducts indicated with the arrows, cranial part of submandibular glands indicated with the S and a caudal part of the parotid gland indicated with P a) before RT. Scrolling through the other transverse planes the rest of the trajectory of the Wharton's duct was visible before RT but not b) 6 weeks post-RT and c) 6 months post-RT. The signal intensity in the glands is higher compared to that before RT.

distributed.
The higher signal intensity of the salivary glands and in general of the rest of the tissues, post-RT was likely due to edema. Edema is a known radiation-induced tissue reaction and appears hyperintense on T_2-weighted MR imaging (Nomayr *et al.*, 2001). The visibility score is a subjective method but nevertheless, it reflects the radiation-induced changes to the salivary system and quantifies somehow qualitative information. The increased score at 6 months post-RT compared to that at 6 weeks post-RT for the parotid ducts suggests that a repair mechanism took place. The same, however, cannot be concluded for the submandibular glands and ducts.

Although more data will be needed to support any correlation between the dose and the visibility score, a certain trend was observed in our data. For mean dose to the salivary glands below 20 Gy no changes post-RT were observed. Above 50 Gy the decreased score at 6 weeks post-RT was irreversible at 6 months post- RT. In the dose interval from 20 to 50 Gy that involves mainly the parotid glands an inter-patient variability in radiation response was observed.

Therefore MR sialography in combination with the existing image registration techniques could be seen as an imaging method to investigate, for each individual patient, at which dose level detectable radiation-induced reactions to the entire salivary gland and duct system, including the oral cavity, occur.

Furthermore, it is possible to follow how, when and for which tissues these effects decrease in time, by repetitive imaging. That increases the value of the information and gives to MR sialography a 4D character. The following step would be to investigate the possibility of quantifying this information in order to assess a direct correlation between the subjective observations and the objective feeling of xerostomia. The use of a tissue like object or water solution, with invariable in time T_1 and T_2 properties might be an option.

The standard method of quantifying xerostomia is salivary flow measurements using Lasley cups (Roesink *et al.*, 2004) and it has been performed in this study as well. Saliva was, indeed, collected post-RT from those parotid glands that received a mean dose <20 Gy and the full salivary duct trajectory was still detectable in the MR sialograms. There were parotid glands, however, from which no saliva was collected at 6 months post-RT despite the fact that the whole duct trajectory could be visualized again. That might be because the saliva composition is not normal and cannot flow as pre-RT, or that the lag phase of those glands at that stage was longer than the 10 minutes measurement time.

It should also be taken into account that there is a variation in the salivary measurement itself of about 27 % in healthy volunteers (Blanco *et al.*, 2005). Nevertheless, by taking the salivary measurement as the golden standard for the salivary function, the fact that the duct trajectory was visible again at 6 months post-RT before even any saliva drop was coming into the mouth, might have a predictive value for the improvement of the salivary function of those patients in the future. Subsequently, for those patients for whom there was not any *"visible"* improvement, the prognosis might be assumed worse. Longer follow-up will be needed for that reason.

Based on the salivary flow measurement and the visibility of the submandibular ducts the salivary function of the submandibular glands decreased even more at 6 months post-RT. The amount of saliva collected from the floor of the mouth was so little and that could explain why the full trajectory of the submandibular ducts was not visible. There is a certain detection and resolution limit in all imaging modalities. We should be aware of that when evaluating our data and the salivary ducts are not visible.

In addition to that, we should also bear in mind that the amount of saliva collected from the floor of the mouth is produced not only by the submandibular glands but also by the rest of the minor salivary ducts distributed allover the oral cavity and the sublingual glands. Therefore the qualitative information on the radiation-induced changes to the whole salivary gland and duct system, obtained by MR sialography, should be included in our evaluation.
In order to establish a correlation between salivary flow measurements and MR sialography, more patient data are required and most importantly the acquisition of MR sialographic images during and after salivary stimulation would be necessary.

6.5 Conclusions

MR sialography is a non-invasive 3D imaging technique that saliva itself is imaged along the full trajectory of the major salivary ducts, from the intra-glandular space to the oral cavity. It has been demonstrated by this study that MR sialography can depict radiation-induced changes to the salivary glands and ducts post-RT. Those radiation-induced effects cannot only be registered to the 3D dose distribution but also to the salivary flow measurements and they can be followed in time post-RT. This combination makes MR sialography a novel and promising tool in investigating radiation-induced xerostomia.

Chapter 7

General conclusions and suggestions for future work

Radiation therapy (RT) is one of the principle treatment modalities for the management of cancer. In recent decades, advances in the radiation delivery technology and parallel advances in anatomical and biological imaging and computer science have changed the clinical routine of radiotherapy. It has evolved from a therapy based on 2 dimensional (2D) X-ray images to 3D-image based conformal RT. An advanced form of conformal RT is intensity-modulated radiotherapy (IMRT), which allows position-dependent attenuation of the beam intensity over each treatment field. IMRT yields dose distributions that conform more accurately to the 3D configuration of the target volumes. As a result of that, the sparing of the adjacent normal tissues is improved considerably using IMRT as compared to conventional RT techniques. One could say that to radiation oncologists IMRT is like a brush that helps them perform dose painting.
The obvious advantages for an anatomically complex area such as the head-and-neck, have pushed IMRT in the standard treatment of this site faster than other cancer sites. The IMRT has a double role to play in that anatomical region. The first role would be to increase the dose to the tumor in order to achieve higher tumor control probability (TCP). That is not possible with the conventional techniques, because of the tolerance dose to the adjacent normal tissues, more specifically that to the spinal cord. The second role would be to reduce the dose to the normal tissues and improve the normal tissue complication probability (NTCP). The side effects of head-and-neck irradiation are some of the worse in radiotherapy. One of the prevalent side effects is xerostomia. Irradiating the healthy salivary glands results in salivary hypofunction and xerostomia. Xerostomia predisposes a person to oral disease and discomfort and consequently to deteriorated quality of life (QoL). An effort should be made to avoid long-term xerostomia or reverse it as soon as possible after the end of the treatment. Therefore IMRT is the way to choose for head-and-neck irradiation.

It should be noted, however, that IMRT by itself would not solve all problems in RT. In order for IMRT to be effective the accuracy in volume delineation and in dose delivery are essential. Erroneous volume delineation or dose delivery could result in either an under- or an overestimation of the target volume. The former would result in an under-dosage of the tumor whereas the latter would cause over-dosage of the adjacent normal tissues. In either case the benefits of IMRT would be lost. Imaging is of vital importance to meet the requirements that IMRT poses upon the treatment planning. Moreover, imaging can be used as a tool to evaluate the treatment in terms of tumor regression and response, and eventually to assess the radiation damage to normal tissues.

In this **thesis** various issues related to radiation-induced xerostomia are addressed. Volume delineation, treatment planning, and dose delivery are the subject of chapters 2, 3 and part of chapter 4. In chapters 4-6 the use of imaging as a tool for measuring radiation-induced damage to the salivary gland and duct system is investigated.

Volume delineation

In **chapter 2** it was demonstrated that a reduction of the mean dose to the parotid glands could not only be achieved by replacing conventional 3D-CRT planning by IMRT treatment but also by a change of target delineation strategy. Our calculations showed that by lowering the cranial border of the Level II lymph nodes from the transverse process of the cervical vertebra C1 to that of the C2, a reduction of the NTCP for xerostomia 1 year post-RT up to 37 % relative to IMRT planning up to C1 (from 33 Gy to 26 Gy) and 68% with regard to the conventional 3D-CRT (from 51 Gy to 26 Gy) can be achieved.
Of course such an alteration of the delineation strategy should not have adverse effects on the outcome of the treatment. In a separate study, conducted at our institute, Prins-Braam *et al.* (2004) have demonstrated that the probability of microscopic disease extending to the Level II lymph nodes between the C1 and C2 bony landmarks on the contralateral side of the neck is indeed very low. Therefore a lowering of the cranial border of the level II lymph nodes should be considered, as it could spare more of the parotid gland.
Delineation of both the targets and organs at risk is important for IMRT dose planning in any region, not only for head and neck. Accurate dose planning may require the combination of different imaging modalities. Therefore imaging modalities such as PET and MRI are being employed in addition to CT, in order increase the knowledge of tumor location, and consequently to improve the accuracy of the delineation (Mutic *et al.*, 2001; Nishioka *et al.*, 2002). CT provides anatomical imaging, which is necessary, not only for the delineation of the target volumes, but also for the dose calculation. MRI is another anatomical imaging technique but provides much better soft tissue contrast as compared to CT. PET on the other

hand provides functional imaging. Currently efforts are being made to also obtain functional information using MR and CT (Harvey *et al.*, 2001; Mizowaki *et al.*, 2002). In order to combine the information provided by different imaging modalities, images from the different modalities need to be registered (aligned) (Ceylan *et al.*, 2005; Daisne *et al.*, 2003). In the head-and-neck region organ motion is not such an important issue as it is, for instance, for lung or prostate tumors. Therefore the use of an immobilization mask each time the patient is scanned will guarantee successful image registration. To further reduce registration problems, combined CT / PET scanners, which do not require the patient to be moved between the different scans are commercially available and in clinical use. After registration, the information of the different imaging modalities can be combined, improving the staging of the disease and consequently the treatment strategy.

Setup errors and margins

The first important step in the IMRT treatment planning process is the delineation of the clinical target volumes. The second step is to set the margins around the target volumes to account for the geometric uncertainties that are unavoidable in fractionated radiotherapy. The smaller these margins, the lower the mean dose to the parotid glands. Especially the reduction of the margins around the lymph nodes will lead to a significant reduction of the dose to the parotid glands. Every mm of margin that is saved counts (Van Asselen *et al.*, 2002).
Margins can be reduced only if the daily set-up accuracy is increased. This can be achieved by daily position verification using, for example, electronic portal imaging (EPID)(Nederveen *et al.*, 2000; Vieira *et al.*, 2002; Wendling *et al.*, 2006). In the head-and-neck region commonly the bony anatomy is used for position verification but alternatives, such the use of fiducial markers, has been suggested (Van Asselen *et al.*, 2003).
Another approach to improve patient positioning accuracy is the use of a combined linear accelerator/cone beam CT device is, which has recently be introduced clinically (Smitsmans *et al.*, 2005).
In clinical practice most correction protocols are off-line. The ideal situation, however, would be if position verification and correction could be performed on-line. Recently the possibility of combining an MRI scanner with a linear accelerator has been coined, and this idea is currently under investigation (Raaijmakers *et al.*, 2005a,b). The MR imaging would provide on-line position verification, which would serve to update the treatment planning during treatment. This should lead to an improvement of both the tumor coverage, and the sparing of healthy tissues. The MRI imaging would not only provide for on-line position verification but also for daily treatment evaluation and follow up of the tumor regression.
Even with the perfect position verification, system residual errors will always remain. In **chapter 3** we have evaluated to what extent translational and rotational setup errors in our commercial planning system cause the delivered dose to deviate

from the planned dose. To do so, we simulated the delivered dose, not simply by convolving the planned dose distribution, but by actually calculating the delivered dose from the planned dose and the translated patient anatomy for all 30 fractions. It was shown that the margins used by our clinical IMRT class solution to account for random set-up uncertainties as derived by the margin *recipes* 0.7 x σ, is more than sufficient for the primary tumor CTV, however not for the lymph nodes CTV. This is also the case if rotational errors are taken into account as well, which is not done in current margin *recipes*. It appeared that random set up errors did not have a significant effect on the mean dose to the parotid glands.
However, the margins *recipes* currently used to account for the random errors for the lymph nodes could result in under-dosage of the lymph nodes. Therefore an increase of the positioning margins around the lymph nodes could be considered, which would certainly affect the dose to the parotid glands.
Also areas were observed where the dose deviated up to ±12 Gy from the planned dose. We note that in our study only random errors were taken into account. Systematic errors were not included, since their values are not known a priori. However, since they account for the larger part of the margins, the effect of systematic errors should be further investigated.
This study shows that it is important that dose distributions, especially the complex dose distributions such as employed in IMRT, are evaluated, and that these dose distributions need to be simulated on a *dynamic* patient geometry rather than on a *static* patient geometry. It makes one realize once more that not everything goes exactly as planned... We should also bear in mind that although the *static* dose distribution is used for the modelling of TCP and NTCP modelling, the *actual* dose distribution is what eventually defines it.

Imaging of the parotid glands post-RT

NTCP modelling for xerostomia is based on the mean dose that the parotid gland is exposed to. In **chapter 4**, it appeared that the mean dose to the parotid glands could differ as much as ±9 Gy from the dose calculated on the CT treatment planning, if the MRI parotid volume delineation was considered. Since the planned dose turned out to be higher in some cases and lower in other cases as compared to the dose computed using the MRI volumes, it is to be expected that averaged over a large population both ways of calculating the dose will not result in large differences. Therefore an NTCP parameter such as the dose corresponding to a 50% probability for xerostomia, TD_{50}, which is computed from the average planned dose for a large population of patients, would probably not change much if, instead of the dose calculated on the CT planning, the dose computed by means of the MRI volumes would be used, presupposing that the parotid glands can be considered as parallel organs.
If, however, the radiosensitivity would vary over the volume of the glands, such as observed in the parotid glands of rats, not only the average dose delivered to

the parotid glands would matter, but also the dose distribution. This would call for the inclusion of the dose distribution in the computation of TD_{50}, which could result in a dependence of the value of TD_{50} on the modality that the dose computation was based on. $TD_{50}$was found to be 26 Gy for a group of patients treated with IMRT and 39 Gy for a group of patients treated with laterally opposed fields (Eisbruch *et al.*, 1999; Roesink *et al.*, 2001). This remarkable finding raises the question if this difference is caused by the difference in the delivered dose distribution between these two methods of treatment. If that were the case it would be important to know which part of the gland receives a higher dose than expected. It appears that delineation differences between CT and MR occur predominantly in the caudal-medial part of the parotid glands, which is actually the part that receives the highest dose in the case of IMRT treatment.

In **chapter 4** it appeared that within the group of patients included in the study, upon comparison of the MRI images taken before RT and 6 weeks after RT the parotid gland volume showed an average reduction of 24% with no clear signs of improvement at 6 months after the end of treatment. Only histology can answer the question whether this volume reduction was caused by loss of acinar cells due to radiation damage, loss of fatty cells due to weight loss, or atrophy of the gland (Leal *et al.*, 2003; Konings *et al.*, 2006).

However, by registering the MR scans taken before and after radiotherapy the volume changes could be located, visually investigated and presented for the first time in the literature. In some patients it seemed that indeed the caudal-medial part of the gland was shrinking more than the rest of the gland but by and large the general shape of the gland appeared similar to that before radiotherapy but just smaller. These results call for a more quantitative study, such that the dose to the *missing* parotid tissue can be extracted from the data. Such results could change the IMRT planning strategy with regard to parotid gland sparing.

For sure, more data will be needed to support any statistically significant correlations between volume reduction and any dose parameters or the saliva output. Furthermore, patients treated with unilateral irradiation, for whom the dose received by the two glands differs significantly should be included in future studies investigating the radiosensitivity within the parotid glands.

The use of higher-resolution MRI imaging of the parotid gland or other MRI sequences that provide more functional information should be considered (Saito *et al.*, 2002; Habermann *et al.*, 2004). Furthermore, the observations obtained by MRI should be correlated with the dose distribution. This combined information could both provide insight into the salivary function as well as lead to a more efficient IMRT treatment planning.

In the conventional radiotherapy most often the salivary glands are irradiated fully and homogeneously. IMRT treatment planning allows for dose painting, and therefore can account for variations in radio-sensitivity over the parotid gland volume. Therefore it is important to know whether regional enhancements in radio-

sensitivity as observed in the parotid glands of the rats, also occur within the salivary glands of humans, in order to select the proper dose constraints and plan strategy.

3D MR sialography

Our efforts to obtain spatial information on the radiation-induced damage to the salivary glands continued in **chapter 5** and **chapter 6** but this time the major salivary ducts of both parotid glands and submandibular glands were included in the investigation as this information is lacking from the literature. Also, these studies featured a novel imaging technique, MR sialography. On images recorded using this technique, stationary fluids, such as saliva, appear hyperintense whereas surrounding tissues such as the salivary gland tissue itself and muscle appear hypointense. Thus it is saliva itself, which is imaged along the full trajectory of the major salivary ducts, all the way from the intraglandular space to the oral cavity. This unique property renders MR sialography a valuable tool in the study of hyposalivation, with the additional advantage of MR being a 3D imaging modality.
Chapter 5 describes the development of an MR sialography protocol providing good quality, single scan, 3D images of the submandibular duct and parotid duct systems. By recording MR sialograms of a healthy volunteer at different moments in time, it was demonstrated that the results of this MR sialography protocol are reproducible. In **chapter 6** we reported a feasibility study using this protocol. This study demonstrated that MR sialography could be used to reveal radiation-induced changes to the salivary glands and ducts resulting from radiotherapy. Those radiation-induced effects can be correlated to the 3D dose distribution as well as to salivary flow measurements. Furthermore, one could follow how, when, and for which tissues these effects decrease in time by imaging at multiple points in time after RT. This could provide valuable additional information on the response of the parotid glands to RT, and provides MR sialography with a 4D character.
The following step, which is even more challenging, would be to quantify this information. An effort in that direction was made in **chapter 6** by using a (subjective) duct visibility scoring system, but more objective methods should be developed. The ultimate goal would be to combine all this information for the best assessment of xerostomia with regard to the pattern of patient's complaints.
Eisbruch *et al.* (2001a) have shown that in addition to the dose to the parotid glands, also the dose to the oral cavity plays an important role in the subjective feeling of xerostomia in patients. Furthermore, Coppes *et al.* (2002) have reported an animal study that revealed that the radiosensitivity for late effects after fractionated irradiation of the was higher in the submandibular glands, as compared to the parotid glands. Using 3D MR sialography it is possible to determine the radiation damage anywhere in the salivary gland- and duct system, including the oral cavity. Eventually MR sialography could result in the development of an NTCP model bridging the objective and subjective perception of xerostomia.

Can we get more from 3D MR sialography?

Currently the golden standard for quantification of xerostomia is provided by salivary flow measurements from the parotid glands using Lashley cups (Roesink *et al.*, 2004) which exhibit a measurement variability of about 30 % (Blanco *et al.*, 2005). An alternative method of xerostomia quantification is salivary scintigraphy using ^{99m}Tc-pretechnetate. However, it has been shown by Roesink et.al that such scintigraphy measurements do not yield a better correlation with the mean dose to the parotid glands than the parotid flow measurements using the Lashley cups. The large individual variations as seen in the cup measurements were also seen in the scintigraphy. What's more, neither of these two methods provides any spatial information on salivary (dys)function. Bussels et.al have attempted to spatially resolve the salivary function within the parotid glands using salivary SPECT. They also observed a large inter-patient variability in dose response. However, due to the lower spatial resolution of SPECT with respect to CT, the matching of the dose and salivary function was more sensitive to registration errors. Furthermore, anatomical information is not available in SPECT scans.

In **chapters 5 and 6** it has been demonstrated that MR sialography image resolution is even higher than that of CT and that the image registration can be performed successfully. However, in order to establish a proper correlation between salivary function and MR sialography, more patient data are required and, most importantly, imaging both during and after salivary stimulation is required. Figure 7.1 shows an example for which 3 consecutive MR sialography scans were made. The first scan was performed without stimulation, the second one during stimulation , and the third directly after stimulation (not shown in Figure 7.1). The stimulation during the second scan consisted of administering a 5% acid solution on the mobile part of the tongue at a rate of 1ml per minute by means of an automated syringe. This stimulation is similar to that applied for salivary flow measurements using Lashley cups.

The salivary glands and ducts were delineated and the signal intensity of the 3D volumes was quantified after normalization to the signal intensity of reference tissues. The spine, the brain and subcutaneous fat served as reference tissues. In those tissues the signal intensity did not vary between the scans but that of the ducts and parotid glands did.

For the three healthy volunteers included in this study, the average signal increased by 40% during stimulation and by 20 % post- stimulation, relative to the signal before stimulation was applied.

One could also consider collecting the saliva during stimulation in order to obtain a correlation between signal intensity increase and the amount of saliva produced. This way MR sialography could become a tool for measuring and imaging salivary gland function in 3D.

Improvement of the image resolution in the intraglandular space could be achieved by using a small surface coil rather than a full head coil. Figure 7.2 shows that

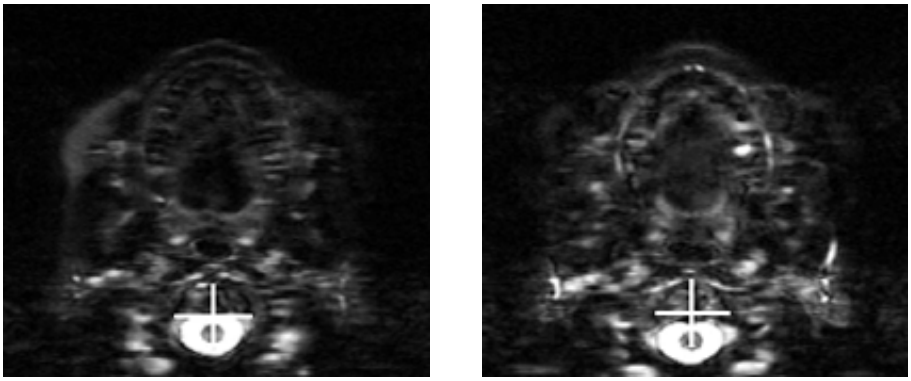

(a) (b)

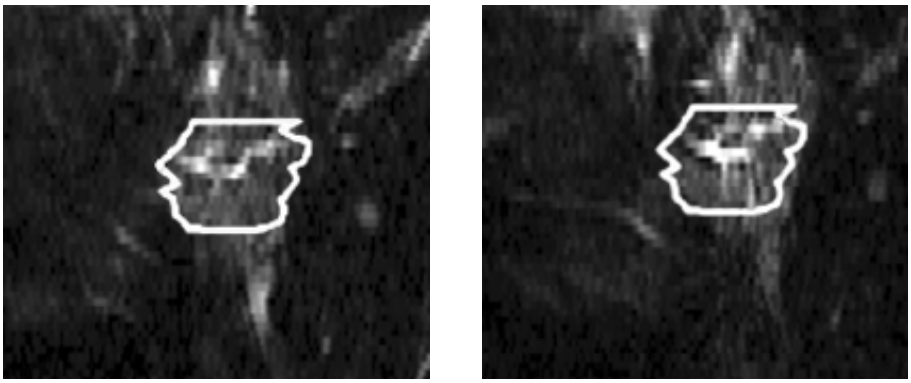

(c) (d)

Figure 7.1: The same transverse and sagittal and planes of 3D MR sialographic images performed on a healthy volunteer. The first scan ((a) and (c))was performed without gustatoty stimulation and the following scan ((b) and (c) were performed during gustatory stimulation with citric acid. The white lines on the sagittal planes indicate the contour of the parotid glands.

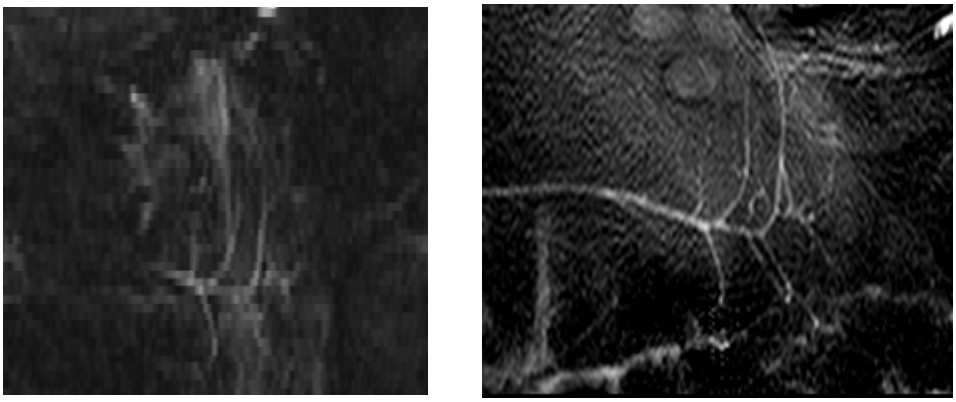

(a) (b)

Figure 7.2: (a) An intra-parotid sagittal plane of a 3D MR sialographic scan performed on a healthy volunteer using the quadrature head coil. (b) 2D MR sialography of the parotid gland of the same healthy volunteer, performed using the a small (diameter 47 mm) surface coil and the single slice technique, thickness 4 cm.

the use of such a small surface coil certainly leads to an improvement in the visualization of the small ducts within the glands. Also, the acquisition time for the small surface coil is very sort, 45 s, and by performing consecutive imaging without and with salivary stimulation it is possible to simulate the salivary scintigraphy measurement. The downsides are that the imaging is 2D instead of 3D and that simultaneous imaging of the whole salivary duct system is not possible.
The general conclusion of this thesis is that MR sialography is a new and powerful technique which provides new insights in the radiation-induced salivary (dys)function and which has the potential to grow to a standard technique for evaluation of RT in the head-and-neck region, simply by allowing saliva to speak for itself!

Hoofdstuk 8

Samenvatting

Radiotherapie (RT) is een van de meest toegepaste behandelmethoden voor kanker. Ontwikkelingen die gedurende de recente decennia hebben plaatsgevonden op het gebied van de techniek van de toediening van straling en tegelijkertijd op het gebied van anatomische en biologische imaging-technieken, hebben veranderingen teweeg gebracht in de wijze waarop radiotherapie in de kliniek bedreven wordt. RT heeft zich ontwikkeld van een techniek gebaseerd op tweedimensionale Röntgen beelden tot de hedendaagse conformele RT. Een geavanceerde vorm van conformele RT is intensiteits-gemoduleerde radiotherapie (IMRT), die voorziet in een positie-afhankelijke variatie van de bundelintensiteit over het bestralingsveld. De toepassing van IMRT resulteert in dosisverdelingen die nauwkeurig op de vorm en afmetingen van de doelvolumes zijn toegesneden. Als een gevolg daarvan kunnen met IMRT aangrenzende, gezonde weefsels aanzienlijk beter gespaard worden dan met conventionele RT technieken mogelijk is. Men zou IMRT kunnen beschouwen als het potlood dat in de handen van de radiotherapeuten gebruikt kan worden om de dosis-verdeling nauwkeurig in te tekenen.
De bijwerkingen van bestraling in het hoofd-hals gebied behoren tot de ergste in de gehele radiotherapie. Dientengevolge vormt de stralingstolerantie van de aan de tumor grenzende gezonde weefsels de dosis-limiterende factor in dit gebied. Het gaat hierbij met name om het ruggemerg, maar zeker ook om de speekselklieren. Stralingsschade aan de speekselklieren is de oorzaak van xerostomie, droge mond, één van de meer voorkomende bijwerkingen van radiotherapie in het hoofd-halsgebied. Xerostomie is buitengewoon onaangenaam voor de patient en heeft derhalve een negatief effect op de kwaliteit van leven. Het mag duidelijk zijn dat IMRT duidelijke voordelen biedt in het hoofd-hals gebied, daar het een grote verbetering teweeg brengt in de balans tussen de dosis geleverd aan het doel, en de schade aangebracht aan het omringende weefsel. IMRT is dan ook dé te kiezen methode voor hoofd-hals bestraling en is hard op weg de standaard behandelingsmethode te worden voor dit gebied.
Hierbij moet worden aangetekend dat er meer nodig is dan IMRT alleen om alle

problemen in RT de baas te kunnen. Om ervoor te zorgen dat IMRT effectief kan worden toegepast zijn een nauwkeurige volume-delineatie en dosislevering essentieel. Onjuiste volume-delineatie leidt tot of een onder- dan wel een overschatting van het doelvolume. Het eerste geval zou een onder-dosering van de tumor tot gevolg hebben, terwijl het tweede geval een over-dosering van de naburige gezonde weefsels zou betekenen. In beide gevallen zouden de voordelen van IMRT grotendeels teniet gedaan worden. Imaging van het doelgebied is van essentieel belang om te kunnen voldoen aan de eisen die IMRT stelt aan de kwaliteit van het behandelingsplan. Imaging kan bovendien een belangrijke rol spelen bij de evaluatie van de behandeling in termen van tumor regressie, en uiteindelijk bij het vaststellen van de schade toegebracht aan gezonde weefsels.

In dit **proefschrift** komen verschillende aspecten van stralings-geïnduceerde xerostomie aan de orde. Volume-delineatie, behandelingsplan en dosislevering worden behandeld in de hoofdstukken 2, 3 en een gedeelte van hoofdstuk 4. In de hoofdstukken 4 tot en met 6 wordt onderzocht hoe (MR) imaging gebruikt kan worden als middel om stralings-genduceerde schade aan de speekselklieren te meten.

In **hoofdstuk 2** wordt aangetoond dat een verlaging van de gemiddelde dosis toegediend aan de parotiden niet alleen bewerkstelligd kan worden door de conventionele 3D-CRT planning te vervangen door een IMRT behandeling, maar ook door het gebruik van een aangepaste delineatie-strategie. Onze berekeningen lieten zien dat een verlaging van de craniële grens van de Level II lymfklier van de ruggewervel C1 naar dat van de C2, de NTCP voor xerostomie één jaar ná RT met maximaal 37% kan verlagen in vergelijking met IMRT planning tot C1 (van 33 Gy naar 26 Gy) en 68% in vergelijking tot conventionele 3D-CRT (van 51 Gy naar 26 Gy).

Zelfs wanneer de positie-verificatie perfect is zullen residuele systeemfouten altijd blijven bestaan. In **hoofdstuk 3** wordt geëvalueerd in welke mate translationele en rotationele setup fouten in ons commerciële planningssysteem de geleverde dosis doen afwijken van de geplande dosis. Daarvoor werd de toegediende dosis gesimuleerd, niet simpelweg door de geplande dosis distributie te convolueren, maar door toegediende dosis daadwerkelijk uit te rekenen aan de hand van de geplande dosis en de getransleerde anatomie van de patient, voor elk van de 30 fracties. Het bleek dat de marges die bij onze clinische IMRT class solution worden aangehouden voor willekeurige setup-afwijkingen, gegeven door *recipes* 0,7 x σ meer dan ruim genoeg zijn voor de primaire tumor CTV, echter niet voor de CTV van de lymfklieren. Dit is tevens het geval als rotationele fouten ook meegenomen worden in de simulatie, hetgeen niet gebeurt in de huidige marge *recipes*. Het bleek tevens dat willekeurige setup-afwijkingen geen significant effect hebben op de gemiddelde dosis toegediend aan de parotiden. Echter, daar de huidige marges *recipes* voor willekeurige afwijkingen kunnen leiden tot een te lage dosering in de lymfklieren. Daarom zou een vergroting van de marges rond de lymfklieren overwogen kunnen worden, hetgeen zeker een nadelig effect zou hebben op de dosis aan de parotiden.

Ook werden er gebieden waargenomen waar de geleverde dosis tot ± 12 Gy afweek van de geplande dosis. We benadrukken dat in deze studie enkel willekeurige fouten werden beschouwd. Systematische fouten bleven buiten beschouwing daar hun omvang niet bij voorbaat bekend is. Echter, daar systematische fouten verantwoordelijk zijn voor belangrijkste deel van de in acht genomen marges, dienen de gevolgen van deze fouten nader bestudeerd te worden.
Deze studie benadrukt nogmaals hoe belangrijk het is dat dosisverdelingen, en zeker de complexe dosisverdelingen zoals toegepast in IMRT, geëvalueerd worden en dat deze niet op de *statische*, maar op de *dynamische* patient-geometrie gesimuleerd dienen te worden. Dit wijst ons weer eens op het feit dat niet alles gaat zoals gepland.... Men dient tevens niet te vergeten dat, alhoewel het de *statische* dosisverdeling is die gebruikt wordt voor de bepaling van TCP en NTCP, het de *werkelijke* dosis is die de waarden van deze grootheden bepaalt.
NTCP modellering van xerostomie gaat uit van de gemiddelde dosis waaraan de parotiden zijn blootgesteld. In **hoofdstuk 4** wordt aangetoond dat de gemiddelde dosis aan de parotiden tot 9 Gy kan afwijken van het behandelingsplan opgesteld aan de hand van CT beelden, indien de op MRI beelden gedelinieerde parotidevolumes aangehouden werden. Daar de geplande dosis in het ene geval hoger, en in het andere geval lager uitviel dan de dosis bepaald aan de hand van de MRI volumes, valt te verwachten dat gemiddeld over een groot aantal gevallen er geen groot verschil zal optreden tussen beide dosisbepalingen. Dus een NTCP modelparameter zoals de dosis die correspondeert met een kans van 50% op xerostomie, TD_{50}, die bepaald wordt aan de hand van de gemiddelde geplande dosis voor een grote populatie patienten, zal vermoedelijk weinig veranderen indien in plaats van de op CT geplande dosis, de dosis wordt gebruikt die aan de hand van MRI volumes bepaald is, vooropgesteld dat de parotiden als parallelle organen kunnen worden beschouwd.
Indien er echter sprake is van verschillen in stralingsgevoeligheid binnen de klieren, zoals waargenomen in de parotiden van ratten, is niet alleen de gemiddelde dosis die de parotiden ontvangen van belang, maar ook de dosisverdeling. Dan zou het wenselijk zijn de dosisverdeling te betrekken in de bepaling van TD_{50}, hetgeen ertoe zou kunnen leiden dat de waarde van TD_{50} afhankelijk zou kunnen worden van de modaliteit aan de hand waarvan de dosisberekening was uitgevoerd.
In **hoofdstuk 4** bleek binnen de onderzochte groep patienten bij vergelijking van MRI beelden opgenomen vóór en 6 weken ná behandeling dat het parotidevolume gemiddeld met 24% was afgenomen, en dat dit 6 maanden na de behandeling nog niet duidelijk verbeterd was. Het antwoord op de vraag of deze volume-afname het gevolg was van een verlies van acinare cellen als gevolg van stralingsschade, een verlies van vetcellen ten gevolge van gewichtsverlies, of atrofie van de klier, kan uitsluitend door histologie gegeven worden.
Echter, door de MR beelden opgenomen vóór en ná RT naar elkaar te registreren kon de precieze locatie van de volumeveranderingen worden vastgesteld, en

onderzocht, hetgeen een primeur opleverde voor de literatuur. In enkele patienten leek het inderdaad alsof het caudaal-mediale gedeelte van de klier meer gekrompen was dan de rest van de klier, maar over het algemeen was de vorm van de klier vergelijkbaar met die voor RT, maar dan kleiner.
Onze pogingen om ruimtelijke informatie te verkrijgen met betrekking tot de stralings-geïnduceerde schade aan de speekselklieren worden voorgezet in **hoofdstuk 5** en **hoofdstuk 6**, waarbij het afbeelden van de hoofdspeekselkanalen van zowel de parotiden als de submandibulaire klieren tot doel werd gesteld. Voor deze studie werd een nieuwe imaging techniek gebruikt, MR sialografie. Met deze techniek worden stilstaande vloeistoffen, zoals speeksel, hyperintens afgebeeld, terwijl omliggende weefsels zoals dat van de speekselklier zelf, en spierweefsel hypointens worden afgebeeld. Het is dus het speeksel zelf dat met deze techniek wordt afgebeeld over de gehele lengte van de hoofdspeekselkanalen, beginnend by de intraglandulaire ruimte en eindigend in de mondholte. Deze unieke eigenschap maakt MR sialografie tot een waardevol hulpmiddel voor de studie van speekseltekort, met als toegevoegde waarde het feit dat MR een 3-dimensionale imaging modaliteit is. In hoofdstuk 5 wordt de ontwikkeling beschreven van een MR sialografie protocol waarmee met één enkele scan, een goede kwaliteit 3D opname van het submandibulaire kanaal en het parotide kanaal systeem verkregen wordt.Door op verschillende momenten MR sialogrammen op te nemen van een gezonde vrijwilliger werd aangetoond dat de beelden verkregen met dit protocol reproduceerbaar zijn. In **hoofdstuk 6** wordt een feasibility studie beschreven op basis van dit protocol. Deze studie toonde aan dat MR sialografie gebruikt kan worden om stralings-geïnduceerde veranderingen aan de speekselklieren aan het licht te brengen. Deze stralings-geïnduceerde veranderingen kunnen gecorreleerd worden met zowel de 3-D dosisdistributie als ook met speeksel-productie metingen. Men zou zelfs kunnen volgen hoe, wanneer, en voor welke weefsels deze veranderingen afnemen in de tijd door opnamen te maken op verschillende tijdstippen na RT. Dit zou waardevolle aanvullende informatie kunnen verstrekken met betrekking tot de reactie van de parotiden op radiotherapie, en zou MR sialografie maken tot een (quasi) 4-D modaliteit. De volgende, nog meer uitdagende stap zou zijn om deze informatie te kwantificeren. Een poging in deze richting werd gedaan in **hoofdstuk 6**, aan de hand van een (subjectief) kanaal-zichtbaarheids scoringssysteem, maar meer objectieve methoden dienen ontwikkeld te worden.
De uiteindelijke conclusie van dit proefschrift is dat we met MR sialografie beschikken over een nieuwe, krachtige techniek die ons een beter inzicht geeft in de problemen die optreden in speekselvoorziening als gevolg van radiotherapie. Deze techniek zou een standaardtechniek kunnen worden voor de evaluatie van radiotherapie in het hoofd-hals gebied, simpelweg door speeksel voor zichzelf te laten spreken!

References

Astreinidou E, Dehnad H, Terhaard C H J and Raaijmakers C P J 2004 Level II lymph nodes and radiation-induced xerostomia *International Journal of Radiation Oncology, Biology and Physics* **58** 124–131

Astreinidou E, Lagendijk J W, Raaijmakers C P J, Roesink J, Terhaard C H J and Bartels W L 2006 3d mr sialography protocol for post-radiotherapy follow up of the salivary duct system *J. Magn. Reson. Imaging* **Accepted**

Barker JL Jr, Garden AS, Ang KK, O'Daniel JC, Wang H, Morrison WH, Rosenthal DI, Chao KS, Tucker SL, Mohan R and Dong L. 2004 Quantification of volumetric and geometric changes occurring during fractionated radiotherapy for head-and-neck cancer using an integrated ct/linear accelerator system. *International Journal of Radiation Oncology, Biology and Physics* **59** 960–70

Bataini J P 1993 Radiotherapy of N0 head and neck cancer patients *Eur Arch Otorinolaryngol* **250** 442–445

Becker M, Marchal F, Becker CD, Dulguerov P, Georgakopoulos G, Lehmann W and Terrier F 2000 Sialolithiasis and salivary ductal stenosis: diagnostic accuracy of mr sialography with a three-dimensional extended-phase conjugate-symmetry rapid spin-echo sequence *Radiology* **217** 347–358

Beckham W A, Keall P J and Siebers J V 2002 A fluence convolution method to calculate radiation therapy dose distributions that incorporate random set up error *Physics in Medicine and Biology* **47** 3465–3473

Bel A 2003 A new approach to reduce systematic geometrical deviations with off line set up verification *Radiotherapy and Oncology* **68** S18

Bel A, Petrascu O, Van de Vondel I, Coppens L, Linthout N, Verellen D and G Storme 2000 A computerized remote table control for fast on-line patient repositioning: Implementation and clinical feasibility *Medical Physics* **27** 354–358

Bel A, Van Herk M and Lebesque J V 1996 Target margins for random geometrical treatment uncertainties in conformal radiotherapy *Medical Physics* **23** 1537–1545

Bergdahl M 2000 Low unstimulated salivary flow and subjective oral dryness: association with medication, anxiety, depression, and stress. *J Dent Res.* **79** 1652–8

Bergonie J and Speder E. 1911 Sur quelques formes de reactions prococes apres des irradiations rontgen. *Arch.elect.med.* **19** 241–5

Blanco AI, Chao KS, El Naqa I, Franklin GE, Zakarian K, Vicic M and Deasy JO. 2005 Dose-volume modeling of salivary function in patients with head-and-neck cancer receiving radiotherapy. *International Journal of Radiation Oncology, Biology and Physics* **62** 1055–69

Bol G H, Kotte A N T J and Lagendijk J J W 2003 jvolumetool: an image evaluation, registration, and delineation system for radiotherapy *PM* **XIX** 80

Bortfeld T, Schlegel W and Rhein B 1993 Decomposition of pencil beam kernels for fast dose calculations in three-dimensional treatment planning *Medical Physics* **20** 311–318

Bortfeld T, Stein J and Preiser K 1997 Clinical relevant intensity modulation optimization using physical criteria in *Proc. of XIIth ICCR*

Bortfeld T, vanHerk M and Jiang SB 2002 When should systematic patient positioning errors in radiotherapy be corrected? *Physics in Medicine and Biology* **47** N297–302

Braam P M, Roesink J M, Moerland M A, Raaijmakers C P J, Schipper M and Terhaard C H 2005 Long-term parotid gland function after radiotherapy *International Journal of Radiation Oncology, Biology and Physics* **62** 659–64

Bucci MK, Bevan A and Roach M 3rd. 2005 Advances in radiation therapy: conventional to 3d, to imrt, to 4d, and beyond.review. *CA Cancer J Clin.* **55** 117–34

Bussels B, Maes A, Flamen P, Lambin P, Erven K, Hermans R, Nuyts S, Weltens C, Cecere S, Lesaffre E and Van den Bogaert W. 2004 Dose-response relationships within the parotid gland after radiotherapy for head and neck cancer. *Radiother Oncol.* **73** 297–306

Butler E B, Teh B S, Grant W H, Uhl B M, Kuppersmith R B, Chiu J K, Donovan D T and Woo S Y 1999 Smart (simultaneous modulated accelerated radiation therapy) boost: a new accelerated fraction schedule for the treatment of head and neck cancer with intensity modulated radiotherapy *International Journal of Radiation Oncology, Biology and Physics* **45** 21–32

Buus S, Grau C, Munk OL, Bender D, Jensen K and Keiding S. 2004 11c-methionine pet, a novel method for measuring regional salivary gland function after radiotherapy of head and neck cancer. *Radiother Oncol.* **73** 289–96

Ceylan C, van der Heide U A, Bol G H, Lagendijk J J W and Kotte A N T J 2005 Assessment of rigid multi-modality image registration consistency using the multiple sub-volume registration (msr) method *Physics in Medicine and Biology* **50**

Chambers MS, Garde AS, Kies MS and Martin JW 2004 Radiation-induced xerostomia in patients with head and neck cancer: pathogenesis, impact on quality of life, and management.review *Head Neck* **26** 796–807

Chao K S, Majhail N, Huang C J, Simpson J R, Perez C A, Haughey B and Spector G 2001a Intensity-modulated radiation therapy reduces late salivary toxicity without compromising tumor control in patients with oropharyngeal carcinoma: a comparison with conventional techniques. *Radiotherapy and Oncology* **61** 275–280

Chao K S C, Bosch W R, Mutic S, Lewis J S, Dehdashti F, Mintun M A, Dempsey J F, Perez C A, Purdy J A and Welch M J 2001b A novel approach to overcome hypoxic tumor resistance: Cu-atsm-guided intensity-modulated radiation therapy *International Journal of Radiation Oncology, Biology and Physics* **49** 1171–1182

Chao K S C, Deasy J O, Markman J, Haynie J, Perez C A, Purdy J A and Low D A 2001c A prospective study of salivary function sparing in patients with head-and-neck cancers receiving intensity-modulated or three-dimensional radiation therapy:initial results *International Journal of Radiation Oncology, Biology and Physics* **49** 907–916

Chao K S C, Low D A, Perez C A and Purdy J A 2000 Intensity-modulated radiation therapy in head and neck cancers: The mallinckrodt experience *International Journal of Cancer* **90** 92–103

Chao K S C, Wippold F J, Ozyigit G, Tran B N and F Dempsey J 2002 Determination and delineation of nodal target volumes for head-and-neck cancer based on patterns and failure in patients receiving definitive and postoperative imrt *International Journal of Radiation Oncology, Biology and Physics* **53** 1174–1184

Cho B C J and Mijnheer B J 2002 The effect of set-up uncertainties, contour changes, and tissue inhomogeneities on target dose-volume histograms *Medical Physics* **29** 2305–2318

Claus F, Duthoy W, Boterberg T, De Gersem W, Hyus J, Vermeersch H and De Neve W 2002 Intensity modulated radiation therapy for oropharyngeal and oral cavity tumors: clinical use and experience *Oral Oncology* **38** 597–604

Cooper J S, Fu K, Marks J and Silverman S 1995 Late effects of radiation therapy in the head and neck region. *International Journal of Radiation Oncology, Biology and Physics* **31** 1141–1164

Coppes RP, Vissink A and Konings AW. 2002 Comparison of radiosensitivity of rat parotid and submandibular glands after different radiation schedules. *Radiother Oncol* **63** 321–8

Coppes RP, Zeilstra LJ, Kampinga HH and Konings AW. 2001 Early to late sparing of radiation damage to the parotid gland by adrenergic and muscarinic receptor agonists. *Br J Cancer.* **85** 1055–63

Cox JD, Stetz J and Pajak TF. 1995 Toxicity criteria of the radiation therapy oncology group (rtog) and the european organization for research and treatment of cancer (eortc) *International Journal of Radiation Oncology, Biology and Physics* **31** 1341–6

Craig T, Battista J and Van Dyk J 2003 Limitations of a convolution method for modeling geometric uncertainties in radiation therapy. I. the effect of shift invariance *Medical Physics* **30** 2001–2011

Daisne JF, Sibomana M, Bol A, Cosnard G, Lonneux M and Gregoire V. 2003 Evaluation of a multimodality image (ct, mri and pet) coregistration procedure on phantom and head and neck cancer patients: accuracy, reproducibility and consistency. *Radiotherapy and Oncology* **69** 237–45

Dawson L A, Anzai Y, Marsh L, Martel M K, Paulino A, Ship J A and Eisbruch A 2000 Patterns of local-regional recurrence following parotid sparing conformal and segmental intensity-modulated radiotherapy for head and neck cancer *International Journal of Radiation Oncology, Biology and Physics* **46** 1117–1126

De Boer H C J and Heijmen B J M 2001 A protocol for the reduction of systematic patient setup errors with minimal portal imaging workload *International Journal of Radiation Oncology, Biology and Physics* **50** 1350–1365

De Boer H C J, van Sörnsen de Koste J R, Creutzberg C L, Visser A G, Levendag P C and Heijmen B J M 2001 Electronic portal image assisted reduction of systematic set-up errors in head and neck irradiation *Radiotherapy and Oncology* **61** 299–308

De Graeff A, De Leeuw J R J, Ros W J G, Hordijk G J, Blijham G H and Winnubst J A M 1999 A prospective study on the quality of life of patients with cancer of the oral cavity or oropharynx treated with surgery with or without radiotherapy *Oral Oncology* **35** 27–32

De Rossi G 1987 *Radioisotopic studies under pathologic conditions* (Boca Raton, FL: CRC Press)

Dehnad H, Nederveen A J, Van der Heide U A, Van Moorselaar R J A, Hofman P and Lagendijk J J W 2003 Clinical feasibility study for the use of implanted gold seeds in the prostate as reliable positioning markers during megavoltage irradiation *Radiotherapy and Oncology* **67** 295–302

Dogan N, Leybovich L B, King S, Sethi A and B Emami 2002 Improvement of treatment plans developed with intensity-modulated radiation therapy for concave-shaped head and neck tumors *Radiology* **223** 57–64

Dreizen S, Brown LR, Handler S and Levy BM 1976 Radiation-induced xerostomia in cancer patients. effect on salivary and serum electrolytes. *Cancer* **38** 273–278

Dreizen S, Daly TE, Drane JB and Brown LR 1977 Oral complications of cancer radiotherapy. *Postgrad Med.* **61** 85–92

Duncan GG, Epstein JB, Tu D, El Sayed S, Bezjak A, Ottaway J and Pater J;National Cancer Institute of Canada Clinical Trials Group. 2005 Quality of life, mucositis, and xerostomia from radiotherapy for head and neck cancers: a report from the ncic ctg hn2 randomized trial of an antimicrobial lozenge to prevent mucositis. *Head Neck.* **27** 421–8

Eisbruch A, K, Kim H M, Terrell JE, Marsh L H, Dawson LA and Ship J A 2001a Xerostomia and its predictors following parotid-sparing irradiation of head-and-neck cancer. *International Journal of Radiation Oncology, Biology and Physics* **50** 695–704

Eisbruch A, Marsh L H, Martel M K, Ship J A, Ten Haken R K, Pu A T and Fraass B Aand Lichter A S 1998 Comprehensive irradiation of head and neck cancer using conformal multisegmental fields: assessment of target coverage and noninvolved tissue sparing *International Journal of Radiation Oncology, Biology and Physics* **41** 559–568

Eisbruch A, Ship J A, Kim H M and Ten Haken RK. 2001b Partial irradiation of the parotid gland.review *Semin Radiat Oncol.* **11** 234–9

Eisbruch A, Ship J A, Martel M K, Ten Haken R K, Marsh L H, Wolf G T, Esclamado R M, Bradford C R, Terrell J E, Gebrarski S S and Lichter A S 1996 Parotid gland sparing in patients

undergoing bilateral head and neck irradiation: techniques and early results *International Journal of Radiation Oncology, Biology and Physics* **36** 469–480

Eisbruch A, Ten Haken R K, Kim H M, Marsh L H and Ship J A 1999 Dose, volume, and function relationships in parotid salivary glands following conformal and intensity-modulated radiation of head and neck cancer *International Journal of Radiation Oncology, Biology and Physics* **45** 577–587

Fontenla E, Pelizzari C A and Chen G T 1996 Implications of 3-dimensional target shape and motion in aperture design *Medical Physics* **23** 1431–1441

Fox PC, van der Ven PF, Sonies BC and Weiffenbach JMand Baum BJ. 1985 Xerostomia: evaluation of a symptom with increasing significance. *J Am Dent Assoc.* **110** 519–25

Gilbeau L, Octave-Prignot M, Loncol T, Renard L, Scalliet P and Grégoire V 2001 Comparison of set-up accuracy of three different thermoplastic masks for the treatment of brain and head and neck tumors *Radiotherapy and Oncology* **58** 155–162

Gregoire V, Coche E, Cosnard G, Hamoir M and Reychler H 2000 Selection and delineation of lymph node target volumes in head and neck conformal radiotherapy.proposal for standarizing terminology and procedure based on the surgical experience *Radiotherapy and Oncology* **56** 135–150

Guchelaar HJ, Vermes A and Meerwaldt JH 1997 Radiation-induced xerostomia: pathophysiology, clinical course and supportive treatment.review. *Support Care Cancer.* **5** 281–8

Habermann CR, Cramer MC, Graessner J, Gossrau P, Reitmeier F, Fiehler J, Schoder V, Jaehne M and Adam G 2004 Functional imaging of parotid glands: diffusion-weighted echo-planar mri before and after stimulation. *Rofo* **176** 1385–9

Harrison L B, Zelefsky M J, Pfister D G, Capper E, Raden A *et al.* 1997 Detailed quality of life assesment in patients treated with primary radiotherapy for squamous cell cancer of the base of the tongue *Head Neck* **19** 169–175

Harvey CJ, Blomley MJ, Dawson P, Morgan JA, Dooher A, Deponte J, Vernon CC and Price P 2001 Functional ct imaging of the acute hyperemic response to radiation therapy of the prostate gland: early experience *J Comput Assist Tomogr* **25** 43–9

Henson B S, Inglehart MR, Eisbruch A and Ship J A 2001 Preserved salivary output and xerostomia-related quality of life in head and neck cancer patients receiving parotid-sparing radiotherapy *Oral Oncology* **37** 84–93

Huguenin P U, Taussky D, Moe K, Meister A, Baumert B, Lutolf U M and Glanzmann C 1999 Quality of life in patients cured from carcinomia of the head and neck by radiotherapy: the importance of the target volume *International Journal of Radiation Oncology, Biology and Physics* **45** 47–52

Hunt M A, Kutcher GJ, Burman C, Fass D, Harrison L, Leibel S and Fuks Z 1993 The effect of setup uncertainties on the treatment of nasopharynx cancer. *International Journal of Radiation Oncology, Biology and Physics* **27** 437–447

Hurkmans C W, Remeijer P, Lebesque J V and Mijnheer B J 2001 Set-up verification using portal imaging: review of current clinical practice *Radiotherapy and Oncology* **58** 105–120

ICRU Report No. 50 1993 *Prescribing, recording and reporting photon beam therapy* (ICRU Bethesda Maryland)

ICRU Report No. 62 1999 *Prescribing, recording and reporting photon beam therapy* (Bethesda, MD:ICRU Publications)

J Jansma 1991 *Oral sequale resulting from head-and-neck radiotherapy* Ph.D. thesis University of Groningen, The Netherlands

Jager L, Menauer F, Holzknecht N, Scholz V, Grevers G and Reiser M 2000 Sialolithiasis: MR sialography of the submandibular duct–an alternative to conventional sialography and US? *Radiology* **216** 665–671

Jensen SB, Pedersen AM, Reibel J and Nauntofte B. 2003 Xerostomia and hypofunction of the salivary glands in cancer therapy.review *Support Care Cancer* **11** 207–25

Kalinowski M, Heverhagen JT, Rehberg E, Klose KJ and Wagner HJ 2002 Comparative study of

mr sialography and digital subtraction sialography for benign salivary gland disorders *AJNR Am J Neuroradiol* **23** 1485–1492

Kashima HK, Kirkham WR and Andrews JR 1965 Postirradiation sialadenitis *Amer. J. of Roentgenology Radium therapy and Nuclear medicine.* **94** 271–91

Konings AW, Coppes RP and Vissink A 2005a On the mechanism of salivary gland radiosensitivity. *International Journal of Radiation Oncology, Biology and Physics* **62** 1187–94

Konings AW, Cotteleer F, Faber H, van Luijk P, Meertens H and Coppes RP. 2005b Volume effects and region-dependent radiosensitivity of the parotid gland. *International Journal of Radiation Oncology, Biology and Physics* **62** 1090–5

Konings AW, Faber H, Cotteleer F, Vissink A and Coppes RP. 2006 Secondary radiation damage as the main cause for unexpected volume effects: A histopathologic study of the parotid gland. *International Journal of Radiation Oncology, Biology and Physics* **64** 98–105

Konings AW, Faber H, Vissink A and Coppes RP. 2005c Radioprotective effect of amifostine on parotid gland functioning is region dependent. *International Journal of Radiation Oncology, Biology and Physics* **63** 1584–91

Kutcher GJ Burman C.K 1989 Calculation of complication probability factors for non-uniform normal tissue irradiation: the effective volume method. *International Journal of Radiation Oncology, Biology and Physics* **16** 1623–30

Lavelle C L 1988 *Saliva. Applied oral physiology* (London, Boston:Wright)

Leal SC, Toledo OA and Bezerra AC. 2003 Morphological alterations of the parotid gland of rats maintained on a liquid diet. *Braz Dent J.* **14** 172–6

Leong J 1987 Implementation of random positioning error in computerised radiation treatment planning systems as a result of fractionation *Physics in Medicine and Biology* **32** 327–334

Lof J, Lind B K and Brahme A 1998 An adaptive control algorithm for optimization of intensity modulated radiotherapy considering uncertainties in beam profiles, patient set-up and internal organ motion. *Physics in Medicine and Biology* **43** 1605–1628

Lomas DJ, Carroll NR, Johnson G, Antoun NM and Freer CE 1996 MR sialography. work in progress. *Radiology* **200** 129–133

Lujan AE, Ten Haken RK, Larsen EW and Balter JM 1999 Quantization of setup uncertainties in 3-d dose calculations. *Medical Physics* **26** 2397–2402

Mackie T R, Balog J, Ruchala K, Shepard D, Aldridge S, Fitchard R E, Reckwerdt P, Oliviera G, McNut T and Mehta M 1999 Tomotherapy *Seminars in Radiation Oncology* **9** 108–117

Maes A, Weltens C, Flamen P, Lambin P, Bogaerts R, Liu X *et al.* 2002 Preservation of parotid function with uncomplicated conformal radiotherapy *Radiotherapy and Oncology* **63** 203–211

Mageras GS, Fuks Z, Leibel SA, Ling CC, Zelefsky MJ, Kooy HM, van Herk M and Kutcher GJ 1999 Computerized design of target margins for treatment uncertainties in conformal radiotherapy *International Journal of Radiation Oncology, Biology and Physics* **43** 437–445

Mandel ID. 2002 Oral infections: impact on human health, well-being, and health-care costs. *Compend Contin Educ Dent.* **23** 403–6

Manning M A, Wu Q, Cardinale R M, Mohan R, Lauve A D, Kavanagh B D, Morris M M and Schmidt-Ullrich R K 2001 The effect of setup uncertainty on normal tissue sparing with imrt for head-and-neck cancer *International Journal of Radiation Oncology, Biology and Physics* **51** 1400–1409

McKenzie A, van Herk M and Mijnheer B 2000 The width of margins in radiotherapy treatment plans. *Physics in Medicine and Biology* **45** 3331–3342

McKenzie A, van Herk M and Mijnheer B 2002 Margins for geometric uncertainty around organs at risk in radiotherapy. *Radiotherapy and Oncology* **62** 299–307

Milne R W and Dawes C 1973 The relative contributions of different saliavry glands to the blood group activity of whole saliva in humans *Vox. Sang* **25** 298–307

Mizowaki T, Cohen GN, Fung AY and Zaider M. 2002 Towards integrating functional imaging in the treatment of prostate cancer with radiation: the registration of the mr spectroscopy imaging to ultrasound/ct images and its implementation in treatment planning. *International Journal of Radiation Oncology, Biology and Physics* **54** 1558–64

Mossman K 1994 Frequent short-term oral complications of head and neck radiotherapy. *Ear Nose Throat J.* **73** 316–320

Mossman K, Shatzman AR and Chencharick JD. 1981 Effects of radiotherapy on human parotid saliva. *ERadiat Res.* **88** 403–12

Mutic S, Dempsey JF, Bosch WR, Low DA, Drzymala RE, Chao KS, Goddu SM, Cutler PD and Purdy JA 2001 Multimodality image registration quality assurance for conformal three-dimensional treatment planning. *IJROBP* **51** 255–60

Nagler RM and Baum BJ 2003 Prophylactic treatment reduces the severity of xerostomia following radiation therapy for oral cavity cancer. *Arch Otolaryngol Head Neck Surg.* **129** 247–50

Nederveen A J, Lagendijk J J W and Hofman P 2000 Detection of fiducial gold markers for automatic on-line megavoltage position verification using a marker extraction kernel (MEK) *International Journal of Radiation Oncology, Biology and Physics* **47** 1435–1442

Nederveen A J, Lagendijk J J W and Hofman P 2001 Feasibility of automatic marker detection with an a-Si flat-panel imager *Physics in Medicine and Biology* **46** 1219–1230

Niemela RK, Takalo R, Paakko E, Suramo I, Paivansalo M, Salo T and Hakala M 2004 Ultrasonography of salivary glands in primary sjogren's syndrome. a comparison with magnetic resonance imaging and magnetic resonance sialography of parotid glands *Rheumatology* **43** 875–879

Nishioka T, Shiga T, Shirato H, Tsukamoto E, Tsuchiya K, Kato T, Ohmori K, Yamazaki A, Aoyama H, Hashimoto S, Chang T and Miyasaka K 2002 Image fusion between ^{18}FDG-PET and CT/MRI for radiotherapy planning of oropharyngeal and nasopharyngeal carcinomas *International Journal of Radiation Oncology, Biology and Physics* **53** 1051–1057

Nomayr A, Lell M, Sweeney R, Bautz W and Lukas P. 2001 Mri appearance of radiation-induced changes of normal cervical tissues. *Eur Radiol.* **11** 1807–17

Nowak P J C M, Wijers O B, Lagerwaard F J and Levendag P C 1999 A three-dimensional ct-based target definition for elective irradiation of the neck *International Journal of Radiation Oncology, Biology and Physics* **45** 33–39

O'Connell A C 2000 Natural history and prevention of radiation injury *Adv Dent Res* **14** 57–61

Pedersen AM, Bardow A, Jensen SB and Nauntofte B. 2002 Saliva and gastrointestinal functions of taste, mastication, swallowing and digestion.review *Oral Dis.* **8** 117–29

Pisani L, Lockman D, Jaffray D, Yan D, Martinez A and Wong J 2000 Setup error in radiotherapy: on-line correction using electronic kilovoltage and megavoltage radiographs. *International Journal of Radiation Oncology, Biology and Physics* **47** 825–839

Porter SR, Scully C and Hegarty AM. 2004 An update of the etiology and management of xerostomia. *Oral Surg Oral Med Oral Pathol Oral Radiol Endod.* **97** 28–46

Preiser K, Bortfeld T, Hartwig K, Schlegel W and Stein J 1997 A new program for inverse radiotherapy planning in *Proc. of XIIth ICCR*

Prins-Braam P, Raaijmakers C P J and Terhaard C H J 2004 Location of cervical lymph node metastasis in oropharyngeal or hypopharyngeal carcinoma:implications for cranial field borders *International Journal of Radiation Oncology, Biology and Physics* **58** 132–138

Raaijmakers A J E, Raaymakers B W and Lagendijk J J W 2005a Integrating a mri scanner with a 6 MV radiotherapy accelerator: Dose increase at tissue-air interfaces in a lateral magnetic field due to returning electrons *Physics in Medicine and Biology* **50** 1363–76

Raaijmakers A J E, Raaymakers B W and W Lagendijk J J 2005b Simulations for the virtual prototyping of a radiotherapy MRI-linear accelerator system: Linear accelerator output, CT-data implementation, dose deposition in the presence of a 1.5 T magnetic field *10th GEANT4 User Conference, Bordeaux, France, http://geant4.in2p3.fr/2005/*

Robbins K T 1999 Integrating radiological criteria into the classification of cervical lymph node disease. *Arch Otolaryngol Head Neck Surg* **125** 385–7

Robbins K T, Atkinson J L D, Byers M R, Cohen J I, Lavertu P and Pellitteri P 2001 The use and misuse of neck dissection for head and neck cancer *J Am Coll Surg* **193** 91–102

Robbins K T, Medina J E, Wolfe G T, Levine P A, Sessions R B and Pruet C W. 1991 Standardizing neck dissection terminology. official report of the academy's committee for head and neck surgery and oncology. *Arch Otolaryngol Head Neck Surg* **117** 601–5

Roesink J 2005 *Parotid gland function after radiotherapy* Ph.D. thesis Utrecht University

Roesink J M, Konings AW, Terhaard CH, Battermann JJ, Kampinga HH and Coppes RP. 1999 Preservation of the rat parotid gland function after radiation by prophylactic pilocarpine treatment: radiation dose dependency and compensatory mechanisms. *International Journal of Radiation Oncology, Biology and Physics* **45** 483–9

Roesink J M, Moerland M A, Battermann J J, Hordijk G J and Terhaard C H J 2001 Quantitative dose-volume response analysis of changes in parotid gland function after radiotherapy in the head-and-neck region *International Journal of Radiation Oncology, Biology and Physics* **51** 938–946

Roesink J M, Moerland M A, Hoekstra A, Van Rijk PP and Terhaard C H J 2004 Scintigraphic assessment of early and late parotid gland function after radiotherapy for head-and-neck cancer: a prospective study of dose-volume response relationships. *International Journal of Radiation Oncology, Biology and Physics* **58** 1451–1460

Roesink J M, Schipper M, Busschers W, Raaijmakers C P J and Terhaard C H 2005 A comparison of mean parotid gland dose with measures of parotid gland function after radiotherapy for head-and-neck cancer: implications for future trials *International Journal of Radiation Oncology, Biology and Physics*

Roesink J M, Terhaard C H J, Moerland M A, van Iersel F and Battermann J J 2000 CT-based parotid gland location: implications for preservation of parotid function *Radiotherapy and Oncology* **55** 131–133

Rostron J, Rogers S, Longman L, Kaney S and Field EA. 2002 Health-related quality of life in patients with primary sjogren's syndrome and xerostomia: a comparative study. *Gerontology* **19** 53–9

Saito M, Umeda M, Fujiwara K, Kakimoto N, Tanaka C, Murakami S and Furukawa S 2002 Functional analysis of human parotid gland in vivo using the (1)h mrs mt effect *NMR Biomed.* **15** 416–21

Samuelsson A, Mercke C and Johansson KA 2003 Systematic set-up errors for IMRT in the head and neck region: effect on dose distribution. *Radiotherapy and Oncology* **66** 303–311

Sartoretti-Schefer S, Kollias S, Wichmann W and Valavanis A. 1999 3d t2-weighted fast spin-echo mri sialography of the parotid gland. *Neuroradiology* **41** 46–51

Seikaly H, Jha N, McGaw T, Coulter L, Liu R and Oldring D. 2001 Submandibular gland transfer: a new method of preventing radiation-induced xerostomia. *Laryngoscope* **111** 347–52

Shah J P, Medina J E, Shaha A R, Schantz S P and Marti J R 1993 Cervical lymph node metastasis *Curr Probl Surg* **30** 1–335

Smitsmans MH, de Bois J, Sonke JJ, Betgen A, Zijp LJ, Jaffray DA, Lebesque JV and van Herk M. 2005 Automatic prostate localization on cone-beam ct scans for high precision image-guided radiotherapy *IJROBP* **63** 975–84

Stein J, Mohan R, Wang X, Bortfeld T, Wu Q, Preiser K, Ling C C and Schlegel W 1997 Number and orientations of beams in intersity-modulated radiation treatments *Medical Physics* **24** 149–159

Stephens LC, King GK, Peters LJ, Ang KK, Schultheiss TE and Jardine JH. 1896 Unique radiosensitivity of serous cells in rhesus monkey submandibular glands. *Am J Pathol* **124** 479–87

Stroom J C, de Boer J C J, Huizenga H and Visser A G 1999 Inclusion of geometrical uncertainties in radiotherapy treatment planning by means of coverage probability *International Journal of Radiation Oncology, Biology and Physics* **43** 905–919

Stroom J C and Heijmen B J M 2002 Geometrical uncertainties, radiotherapy planning margins, and the ICRU-62 report *Radiotherapy and Oncology* **64** 75–83

Stuchell RN and Mandel ID. 1988 Salivary gland dysfunction and swallowing disorders. *Otolaryngol Clin North Am.* **21** 649–61

Takagi Y, Sumi M, Sumi T, Ichikawa Y and Nakamura T. 2005 Mr microscopy of the parotid glands in patients with sjogren's syndrome: Quantitative mr diagnostic criteria. *AJNR Am J Neuroradiol.* **26** 1207–1214

Tonami H, Higashi K, Matoba M, Yokota H, Yamamoto I and Sugai S 2001 A comparative study between mr sialography and salivary gland scintigraphy in the diagnosis of sjogren syndrome. *J Comput Assist Tomogr* **25** 262–268

Valdez IH, Atkinson JC, Ship JA and Fox PC. 1993 Major salivary gland function in patients with radiation-induced xerostomia: flow rates and sialochemistry. *International Journal of Radiation Oncology, Biology and Physics* **25** 47–7

Van Asselen B, Dehnad H, Raaijmakers C P J, Lagendijk J J W and Terhaard C H J 2003 Implanted gold markers for positioning verification during irradiation of head-and-neck cancers: a feasibility study *International Journal of Radiation Oncology, Biology and Physics* **59** 1011–1017

Van Asselen B, Dehnad H, Raaijmakers C P J, Roesink J M, Lagendijk J J W and Terhaard C H J 2002 The dose to the parotid glands with IMRT for oropharyngeal tumors: the effect of reduction of positioning margins *Radiotherapy and Oncology* **64** 197–204

van Dieren E B, Nowak P J C M, Wijers O B, Sörensen de Koste J R, van der Est H, Binnekamp D P, Heijmen B J M and Levendag P C 2000 Beam intensity modulation using tissue compensators or dynamic multileaf collimation in three-dimensional conformal radiotherapy of primary cancers of the oropharynx and larynx, including the elective neck *International Journal of Radiation Oncology, Biology and Physics* **47** 1299–1309

Van Herk M 2004 Errors and margins in radiotherapy *Semin Radiat Oncol.* **14** 52–64

Van Herk M, Remeijer P, Rasch C and Lebesque J V 2000 The probability of correct target dosage: dose-population histograms for deriving treatment margins in radiotherapy *International Journal of Radiation Oncology, Biology and Physics* **47** 1121–1135

Van Herk M, Witte M, van der Geer J, Schneider C and Lebesque J V 2003 Biologic and physical fractionation effects of random geometric errors *International Journal of Radiation Oncology, Biology and Physics* **57** 1460–1471

van Lin E N, van der Vight L, Huizenga H, Kaanders J H and Visser A G 2003 Set-up improvement in head and neck radiotherapy using a 3D off-line EPID-based correction protocol and a customised head and neck support. *Radiotherapy and Oncology* **68** 137–148

Vieira SC, Dirkx ML, Pasma KL and Heijmen BJ. 2002 Fast and accurate leaf verification for dynamic multileaf collimation using an electronic portal imaging device. *Med Phys.* **29** 2034–40

Vineberg K A, Eisbruch A, Coselmon M M, McShan D L, Kessler M L and Fraass B A 2002 Is uniform target dose possible in imrt plans in the head and neck? *International Journal of Radiation Oncology, Biology and Physics* **52** 1159–1172

Vissink A, Panders A K, 's Gravenmade E J and Vermey A 1988 The causes and consequences of hyposalivation *Ear Nose Throat* **67** 166–176

Vissink A, PJansma J, Spijkervet FK, Burlage FR and Coppes RP 2003 Oral sequelae of head and neck radiotherapy *Crit Rev Oral Biol Med.* **14** 199–212

Warde P, O'Sullivan B, Aslanidis J, Kroll B, Lockwood G, Kim J, Liu FF, Maxymiw W, Sprague S and Cummings B. 2003 A phase iii placebo-controlled trial of oral pilocarpine in patients undergoing radiotherapy for head-and-neck cancer. *International Journal of Radiation Oncology, Biology and Physics* **54** 9–13

Webb S 2001 *Intensity-modulated radiation therapy* Medical Sience Series (Bristol, UK: IOP Publishing Ltd)

Weiss M H, Harrison L B and Isaacs R S 1994 Use of decision analysis in planning a management strategy for the stage N0 neck *Arch Otolaryngol Head Neck Surg* **120** 699–702

Wendling M, Louwe RJ, McDermott LN, Sonke JJ, van Herk M and Mijnheer BJ. 2006 Accurate two-dimensional imrt verification using a back-projection epid dosimetry method. *Med.Phys* **33** 259–73

Wijers O B, Levendag P C, Braaksma M M, Boonzaaijer M, Visch L L and Schmitz PI 2002 Patients with head and neck cancer cured by radiation therapy: a survey of the dry mouth syndrome in long-term survivors. *Head Neck* **24** 737–47

Wijers O B, Levendag P C, Tan T, van Dieren E B, van Sörnsen de Koste J, van der Est H, Senan S and Nowak P J C M 1999 A simplified ct-based definition of the lymph node levels in the node negative neck *Radiotherapy and Oncology* **52** 35–42

Withers H R, Peters L J and Taylor J M G 1995 Dose-response relationship for radiation therapy of subclinical disease *International Journal of Radiation Oncology, Biology and Physics* **31** 353–359

Wu Q, Manning M, Schmidt-Ullrich R and Mohan R 2000 The potential for sparing of parotids and escalation of biologically effective dose with intensity -modulated radiation treatments of head and neck cancers: a treatment design study *International Journal of Radiation Oncology, Biology and Physics* **46** 195–205

Wu Q J, Chankong V, Jitprapaikulsarn S, Wessels B W, Einstein D B, Mathayomchan B and Kinsella T J 2003 Real-time inverse planning for gamma knife radiosurgery *Medical Physics* **30** 2988–95

Wyman D R, Ostapiak OZ and Gamble LM 2002 Analysis of mechanical sources of patient alignment errors in radiation therapy. *Medical Physics* **29** 2698–2704

Xing L, Lin Z, Donaldson SS, Le QT, Tate D, Goffinet DR, Wolden S, Ma L and Boyer AL. 2000 Dosimetric effects of patient displacement and collimator and gantry angle misalignment on intensity modulated radiation therapy. *Radiotherapy and Oncology* **56** 97–108

Yu C X and Wong J W 1993 Implementation of the ETAR method for 3D inhomogeneity correction using FFT *Medical Physics* **20** 627–632

Publications

Peer reviewed journals

1. 3D MR sialography protocol for post-radiotherapy follow up of the salivary duct system. E. Astreinidou, J.J.W. Lagendijk, C.P.J. Raaijmakers, J. Roesink, C.H.J.Terhaard, and W. Bartels. 2006 J. of Magnetic Resonance Imaging In press.

2. Adequate margins for random set-up uncertainties in head-and-neck IMRT. E. Astreinidou, A.Bel, C.P..J. Raaijmakers, C.H.J.Terhaard, and J.J.W. Lagendijk. 2005 Int. J. of Radiation Oncology, Biology and Physics Mar 1;61(3):938-44

3. Level II Lymph Nodes and radiation-induced xerostomia. E. Astreinidou, H. Dehnad, C.H.J.Terhaard, and C.P.J. Raaijmakers. 2004 Int. J. of Radiation Oncology, Biology and Physics Jan 1;58(1)124-31

4. Monte Carlo simulation of possible conversion processes with respect to soft error generation in a dynamic RAM based neutron detector. D.G Darambara, S.W. Harvey, E. Astreinidou, N.M. Spyrou. 1997 J. of Radioanalytical and Nuclear Chemistry, Vol 215, No2, 287-294.

Submitted manuscripts

1. 3D MR sialography as a tool to investigate radiation-induced xerostomia: Feasibility study. E. Astreinidou, J. Roesink, W. Bartels, C.P.J Raaijmakers, T.Witkamp, H Dehnad, J.J.W Lagendijk and C.H.J Terhaard. 2006 Int. J. of Radiation Oncology, Biology and Physics.

2. Parotid volume reduction after head-and-neck radiotherapy. E. Astreinidou, J. Roesink, C.P.J Raaijmakers, T. Witkamp, H. Dehnad, W. Bartels, and C.H.J Terhaard. Int. J. of Radiation Oncology, Biology and Physics. 2006.

Proceedings and Abstracts

1. The potential of using MRI to obtain spatial information about the salivary gland function. E. Astreinidou, J. Roesink, M. Moerland, C.H.J.Terhaard, and CP.J. Raaijmakers. Radiotherapy and Oncology, Sep 2005, vol 76, supplement 2, S145.

2. MR image guided evaluation and quantification of complications to the salivary glands and ducts after head-and-neck irradiation. E. Astreinidou, J. Roesink, W. Bartels, C.H.J.Terhaard and C.P.J. Raaijmakers. Radiotherapy and Oncology, Sep 2005, vol 76, supplement 2, S61

3. Clinical relevance of FDG-PET scanning for image guided RT in head-and-neck cancer. C.H.J.Terhaard, M.G.G Hobbelink, U.A. van der Heide, G.M. Verduijn, A.N.T.J. Kotte, E. Astreinidou and P.P van Rijk . Radiotherapy and Oncology, Oct 2004, vol 73, supplement 1, S226

4. The dosimetric accuracy of step-and-shoot IMRT for head-and-neck cancer patients in clinical routine. C.P.J. Raaijmakers, E. Astreinidou, J.J.Welleweerd and C.H.J.Terhaard. Radiotherapy and Oncology, Oct 2004, vol 73, supplement 1, S33

5. Development and evaluation of an MRI protocol to investigate radiation-induced changes to the parotid glands and the salivary gland system. E. Astreinidou, W. Bartels, C.P.J. Raaijmakers, J. Roesink, H. Denhnad, C.H.J.Terhaard, and J. Lagendijk. Radiotherapy and Oncology Oct 2004, vol 73, supplement 1, S375

6. Adequate margins in head-and-neck IMRT irradiation by incorporating the random set-up uncertainties in the dose calculation. E.Astreinidou, A.Bel, and C.P.J. Raaijmakers. Medical Physics, Vol 30 No.6 June 2003 p.1385.

7. On line position verification. J. Lagendijk, U.A. van der Heide, B.W. Raaymakers, C.P.J. Raaijmakers , B. van Asselen, H. Denhnad, E. Astreinidou, C.H.J.Terhaard. Radiotherapy and Oncology Sep 2003, vol 68, supplement 1, S41.

8.Evaluation of the effect of geometric uncertainties on IMRT plans for head-and-neck treatments. A.Bel, E.Astreinidou, H. Denhnad and C.P.J. Raaijmakers. Radiotherapy and Oncology. Sep 2002, vol 64, supplement 1, S213.

9. The influence of the cranial border of the level II lymph node regions on xerostomia for conformal and intensity-modulated irradiation of oropharyngeal cancer. E.Astreinidou, H. Denhnad C.H.J.Terhaard and C.P.J. Raaijmakers. Radiotherapy and Oncology Sep 2002, vol 64, supplement 1, S243.

Acknowledgments

The marvelous journey has come to an end. Over recent years I have come to realize that doing a PhD is the best job one can have, and that the Netherlands is actually the best place for doing it. I consider myself lucky that I have been given the opportunity to do my PhD here, at the radiotherapy department in the UMC, both for professional and social reasons. The atmosphere at the department was, as the Dutch say, *gezellig*, not only during work, but also during the "obligatory" coffee breaks, *borrels*, dinners, and evenings out until late (or early morning).
I would like to thank all of my colleagues for the great time I have had here, and I am surely going to miss you (once I actually leave, that is...). In particular I would like to express my gratitude to the colleagues that have contributed to this thesis in one way or another.
First of all professor Lagendijk, beste Jan, you have been like a *Θεός από μηχανής, deus ex machina* to me. Whenever I was in need of your divine intervention, I found that the climb up your mount Olympus was only a short one. I consider your scientific attitude, not being afraid to take risks, as very stimulating.
Dear Niels, during my PhD I always found your door open for me, even though we may not always have agreed on which direction to take the research. I appreciate that a lot, and I want to thank you for that. Also I have regarded you optimistic and positive attitude as very encouraging. *"Het komt goed, Eleftheria"*, you always said with your big smile, and you were right.
The foundation of this thesis was formed by work done in the head-and-neck group. They make up a strong team, with a wealth of knowledge and experience from which I have benefited much.
Dear Chris, you are the walking encyclopedia of head-and-neck radiotherapy. Thank you for your patience, even when I came to your office asking if you had time to answer one question, when in fact I was holding a list of 21 questions behind my back.
Dear Judith, everything I know about the salivary gland function I have learnt from you. And thanks once more for waiting for me when I was lagging behind during my first time riding a *step* in Rotterdam.
Dear Homan, thank you for providing me with patients for my study and always being available to answer any of my questions. I have much enjoyed our scientific

discussions, but our philosophical discussions I will never forget.
Dear Bram, thank you for all your help and specifically for your IMRT class solution, which formed the basis of my IMRT studies.
Lieve Pètra, you are the sunshine in the group, I wish you good luck with the completion of your *boekje*.
The last three chapters of my thesis are the result of a close collaboration with the radiology department, and in particular with the Image Science Institute, and even more in particular with dr. Wilbert Bartels.
Dear Wilbert, I am very much indebted to you for developing the MR sialography protocols. You, and your friends Wat Sels en Fat Sels were both pleasant and instructive company during the long evenings developing the protocols at the MR scanner. Your comprehensive knowledge of MRI and your scientific instinct have been of great value to me. Without you there would not be a single spitting image in my thesis.
Also invaluable in this regard were the volunteers that were so kind to allow me to image their spit: Jeroen Hendrikse with his *paprika chips*, Astrid, Alexander, Hugo, Kees, Cecile, Martijn, Pètra, and in particular those who had to endure the swallowing of citric acid: Jeroen, Nico, Martijn Bom, and Bas Gobets.
I am grateful to dr. Witkamp for allotting us the protocol development time on the MRI scanner, and for his constructive comments on the MRI images.
I would like to thank Jan Stout for planning the scantime of the patients, which I know was not always easy.
Furthermore I would like to thank all *laboranten*, both from the radiology and the radiotherapy department, for putting into practice a new protocol.
Dear Arjan, it was an honor to work with you, and I am very happy that our *gezellige* evenings on the Utrechtse Heuvelrug and on the tennis court have culminated in a "shaking" publication.
Also I would like to thank everybody who participated in the annual workshop in Groningen (which I always referred to as *de spuugdag*). These meetings have been very inspiring for my research.
I would like to thank professor Konings for the spontaneous and stimulating email discussions regarding the problem of xerostomia.
The analysis of the data I gathered in my studies would have been impossible without the software developed by Alexis and Gijs. Without you, C^{++}-illiterate PhD students like me would not be able to do research. Many thanks, you have been amazing. Bas, thank you for your always to the point comments.
Alexander, I am amazed with your *kennis* in histoty.
My dear Jeroen, thank you for all you have done for me, thanks for being a friend, and for being my paranimf.
Dear Theo, thank you for opening some secret doors in PLATO for me.
Dear Hugo, special thanks for helping me in organizing the final stages of my thesis, and for setting up the much-needed latex files in which this text is contained.

The ICT support has always been spotless, thanks Ric, Kees and Rob.
Also I would like to thank my roommates, Marion, Cecile, and Irene for the good time and for putting up with my Greek temper(ament).
Dear Uulke and Hans, thank you for the *gezelligheid* in California and in Iceland.
Dear Hans, special thanks to you for the confidence you have shown in me, for allowing me to finish my clinical physicist training here in the UMC, and finally for introducing me to the noble art of *klaverjassen*.
I would like to thank the nuclear medicine department in Utrecht for helping me when I needed it. Dear Jaap, I want to thank you in particular for your friendship and the book on salivary gland function and scintigraphy, which was very useful to me.
My dear Nico, first and foremost you are my friend, and you just happen to be a collegue as well. I have no doubt that your *boekje* will be a huge success.
Guapa Maria, you are full of life and your positive energy radiates out to everybody around you.
My dear fellow-*levensgenieters* Jochen en Paula, Smita en Michiel, Iemy, Hugo and of course Uulke. You are all divine chefs. And my dear Jochen, no news is good news, indeed.
All my friends have at some point lent me an ear to listen to the frustrations of my PhD and personal life. A special thank to all of you. Βάλλυ μου φιλούρες.
Dear Ietske, Klairh, Kosta, Astrid, Paul, and Femke, thank you for your friendship.
My dear Aussie friends, Jean Paul and Simon, you both have a special place in my heart. Agtrium, I am very happy that you will be in Holland on the 30th of May.
Marina and Eise-Jan, I can always rely on you. Thank you for that. Cara Marina you have introduced an additional dimension to my life.
"Super-women" Annette, Kristien, and Nelleke, you have always been the example to me that everything is possible with hard work. Lieve Nel, the beginning of the end of this thesis started that week at your beautiful house in the Ardennes, one year ago. Thanks to you and Leen for that.
Dear Arthur thank you for lending me a laptop during the last stage of my thesis. It has been of great value to me.
Nina, thank you very much for creating the fantastic (and personal) cover of my thesis. Manoli, thank you for being patient with us and for correcting the last errors.
My dear Jos, nobody has ever been so close to me as you are. Thank you for everything.
Caroline, γλυκιά μου Caroline, you are more than a friend to me, you are family. And I know Utrecht is not friendly to cars, in particular not to *paardenwagens*, but you made it happen.

Αγαπημένέ μου Bas, you have made the final stage of my journey a little more exciting than necessary, but I would not have reached my destination without you.

My dear family, I owe everything to you. Μπαμπάκα μου και μητέρα μου, σας ευχαριστώ πολύ για όλα και πάνω από ολα για την ελευθερία που μου δώσατε. Αδελφή μου, λατρεμένη μου Νατάσσα, συγνώμη που έφυγα. Δημήτρη, σε ευχαριστώ που φρόντιζες πάντα να έχω φέτα στην Ολλανδία. Γιαγιάκα μου, Ορφέα και Φοίβο σας φιλώ.

Curriculum Vitae

Born in Thessaloniki, Greece, Eleftheria studied physics at the Aristotle University of Thessaloniki. Then ventured to UK to follow an MSc course in Medical Physics at the University of Surrey. After completing her studies she returned to Greece, where she worked as clinical physicist in training at the cancer institute of Thessaloniki, *Theagenio*. She was certified as clinical physicist by the Greek ministry of Health a year and a half later, after succeeding in national exams on the following subjects: radiation therapy, nuclear medicine, radiation protection and diagnostic radiology. During this period she started gaining some other work experience. She worked part time for the Greek ministry of Defence, teaching electronics and telecommunications to air force defence students. Then the distributor of Mallinkrodt Medical BV, Petten, the Netherlands, in Greece appointed her as sales manager in N.Greece. Her tasks were to set up the branch office and to provide clinical support. Having moved to the Netherlands she was employed by Nucletron BV, Veenendaal, the Netherlands, as international application specialist for a radiotherapy treatment planning system. Having gained significant work experience Eleftheria was faced with the choice of pursuing her career or following her dream of doing research. Fortunately, she got the opportunity to do her PhD at the University Medical Center Utrecht, where she worked with world experts in the field of head-and-neck radiotherapy and xerostomia. The results of this research, which was supported by the Dutch Cancer Society, are presented in this thesis.